AD-A129 716 REDUCED EXPERIMENTAL STRESS-STRAIN RESULTS FOR A LOW-STRENGTH CONCRETE UN..(U) NEW MEXICO ENGINEERING RESEARCH INST ALBUQUERQUE L A TRAINA ET AL. MAY 83 1/2

UNCLASSIFIED AFWL-TR-83-3 F29601-81-C-0013 F/G 11/2 NL

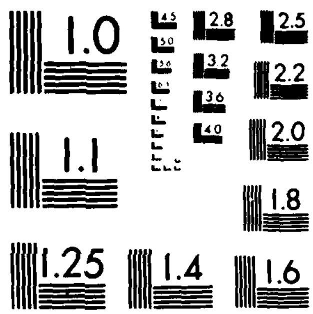

MICROCOPY RESOLUTION TEST CHART
NATIONAL BUREAU OF STANDARDS 1963 A

AFWL-TR-83-3

AFWL-TR-83-3

REDUCED EXPERIMENTAL STRESS-STRAIN RESULTS FOR A LOW-STRENGTH CONCRETE UNDER MULTIAXIAL STATES OF STRESS

L. A. Traina
S. M. Babcock
H. L. Schreyer

New Mexico Engineering Research Institute
University of New Mexico
Albuquerque, New Mexico 87131

May 1983

Final Report

Approved for public release; distribution unlimited.

AIR FORCE WEAPONS LABORATORY
Air Force Systems Command
Kirtland Air Force Base, NM 87117

AFWL-TR-83-3

This final report was prepared by the New Mexico Engineering Institute Albuquerque, New Mexico, under Contract F29601-81-C-0013, Job Order 88091354 with the Air Force Weapons Laboratory, Kirtland Air Force Base, New Mexico. Rodney G. Galloway (NTES) was the Laboratory Project Officer-in-Charge.

When Government drawings, specifications, or other data are used for any purpose other than in connection with a definitely Government-related procurement, the United States Government incurs no responsibility or any obligation whatsoever. The fact that the Government may have formulated or in any way supplied the said drawings, specifications, or other data, is not to be regarded by implication, or otherwise in any manner construed, as licensing the holder, or any other person or corporation; or as conveying any rights or permission to manufacture, use, or sell any patented invention that may in any way be related thereto.

This report has been authored by a contractor of the United States Government. Accordingly, the United States Government retains a nonexclusive, royalty-free license to publish or reproduce the material contained herein, or allow others to do so, for the United States Government purposes.

This report has been reviewed by the Public Affairs Office and is releasable to the National Technical Information Services (NTIS). At NTIS, it will be available to the general public, including foreign nations.

If your address has changed, if you wish to be removed from our mailing list, or if your organization no longer employs the addressee, please notify AFWL/NTES, Kirtland AFB, NM 87117 to help us maintain a current mailing list.

This technical report has been reviewed and is approved for publication.

Rodney G. Galloway

RODNEY G. GALLOWAY
Project Officer

FOR THE COMMANDER

Paul E. Minto

PAUL E. MINTO
Capt, USAF
Chief, Applications Branch

John H. Storm

JOHN H. STORM
Col, USAF
Chief, Civil Engrg Rsch Division

DO NOT RETURN COPIES OF THIS REPORT UNLESS CONTRACTUAL OBLIGATIONS OR NOTICE ON A SPECIFIC DOCUMENT REQUIRES THAT IT BE RETURNED.

UNCLASSIFIED

SECURITY CLASSIFICATION OF THIS PAGE (When Data Entered)

REPORT DOCUMENTATION PAGE		READ INSTRUCTIONS BEFORE COMPLETING FORM
1. REPORT NUMBER AFWL-TR-83-3	2. GOVT ACCESSION NO. AD-A129716	3. RECIPIENT'S CATALOG NUMBER
4. TITLE (and Subtitle) REDUCED EXPERIMENTAL STRESS-STRAIN RESULTS FOR A LOW-STRENGTH CONCRETE UNDER MULTIAXIAL STATES OF STRESS		5. TYPE OF REPORT & PERIOD COVERED Final Report 6. PERFORMING ORG. REPORT NUMBER
7. AUTHOR(s) L. A. Traina S. M. Babcock H. L. Schreyer		8. CONTRACT OR GRANT NUMBER(s) F29601-81-C-0013
9. PERFORMING ORGANIZATION NAME AND ADDRESS New Mexico Engineering Research Institute University of New Mexico, Box 25, University Station, Albuquerque, New Mexico 87131		10. PROGRAM ELEMENT, PROJECT, TASK AREA & WORK UNIT NUMBERS 62601F/88091354
11. CONTROLLING OFFICE NAME AND ADDRESS Air Force Weapons Laboratory (NTES) Kirtland Air Force Base, NM 87117		12. REPORT DATE May 1983 13. NUMBER OF PAGES 134
14. MONITORING AGENCY NAME & ADDRESS(if different from Controlling Office)		15. SECURITY CLASS. (of this report) Unclassified 15a. DECLASSIFICATION DOWNGRADING SCHEDULE

16. DISTRIBUTION STATEMENT (of this Report)

Approved for public release; distribution unlimited.

17. DISTRIBUTION STATEMENT (of the abstract entered in Block 20, if different from Report)

18. SUPPLEMENTARY NOTES

19. KEY WORDS (Continue on reverse side if necessary and identify by block number)

Stress Invariants
Strain Invariants
Concrete
Concrete Experimental Data

20. ABSTRACT (Continue on reverse side if necessary and identify by block number)

Results of an experimental program on low-strength concrete under multiaxial states of stress were evaluated for consistency and for baseline shifts. After adjustments to the data had been made, various plots of the experimental results were prepared. Loading paths and limit points are shown in plots of stress and strain, pressure and volumetric strain, three stress invariants, and three inelastic strain invariants. The result is a set of curves that are beneficial for developing and evaluating constitutive models.

DD FORM 1 JAN 73 1473 EDITION OF 1 NOV 65 IS OBSOLETE

UNCLASSIFIED

SECURITY CLASSIFICATION OF THIS PAGE (When Data Entered)

UNCLASSIFIED

SECURITY CLASSIFICATION OF THIS PAGE(When Data Entered)

UNCLASSIFIED

SECURITY CLASSIFICATION OF THIS PAGE(When Data Entered)

CONTENTS

ILLUSTRATIONS

TABLES

I. INTRODUCTION

An experimental program on the three-dimensional response of concrete cubes (Ref. 1) was recently completed at New Mexico State University (NMSU). The results were presented as plots of stress versus strain for each concrete specimen tested. No in-depth evaluation of the quality and consistency of the data was performed by NMSU. The New Mexico Engineering Research Institute (NMERI) subsequently evaluated the data obtained by NMSU. This report presents revised results based on that evaluation.

In the NMSU experiments, each concrete cube specimen was subjected to a prescribed stress path test until the specimen failed. Each type of stress path test was performed on two or three concrete specimens. Because multiple runs had been performed for each path, it was possible for NMERI to inspect the data for apparent discrepancies and baseline shifts. The data were then adjusted, and composite stress-strain curves were developed. These curves should prove to be invaluable for the development and evaluation of constitutive models for plain concrete.

In Sections II and III of this report, the stress paths on which the NMSU experimental program was based are described, and experimental values for limit states are presented. The paths and limit points are given in the two stress-invariant spaces that are used for constitutive modeling.

The actual corrections made by NMERI in the stress-strain data and the reasoning on which the changes were based are summarized in Section IV. Plots of both the original and the adjusted data are given so that a reader who interprets the results differently from the authors can apply independent judgment. Composite stress-strain curves are given for each stress path in Section V.

---

1. Traina, L. A., Experimental Stress-Strain Behavior of a Low Strength Concrete Under Multiaxial States of Stress, AFWL-TR-82-92, Air Force Weapons Laboratory, Kirtland Air Force Base, New Mexico, December 1982.

Invariants of inelastic strain are used in most constitutive models. These invariants can also be used to provide an alternate check on the adequacy of the composite stress-strain curves. The check consists of illustrating each path in a strain-invariant space. If the strain-invariant curves obtained by using the composite stress-strain data provide a reasonable representation of the strain-invariant curves obtained by using corrected stress-strain data, the indication is that the composite stress-strain data points have been chosen in a consistent manner. The results of this check are discussed in Section VI. Limit states in terms of strain invariants are also given. The conclusions drawn as a result of the evaluation program are presented in Section VII.

II. STRESS PATHS AND LIMIT STATES INVOLVING FIRST AND SECOND INVARIANTS

In most of the engineering literature concerned with the testing of concrete, first and second invariants of stress are used. These invariants are the mean pressure (P) and the second invariant of the stress deviator, $(\sqrt{J_2'})$, defined as follows:

$$P = -\frac{1}{3}(\sigma_1 + \sigma_2 + \sigma_3)$$

$$\sqrt{J_2'} = \left\{ \frac{1}{6} \left[(\sigma_1 - \sigma_2)^2 + (\sigma_2 - \sigma_3)^2 + (\sigma_3 - \sigma_1)^2 \right] \right\}^{1/2}$$

where σ_1, σ_2, and σ_3 denote principal stresses positive in tension. These parameters are used to define the stress paths that were employed in the NMSU experimental program.

The tests were divided into three sets. Each of the first set of eight stress path tests was performed on two specimens. The set consisted primarily of conventional uniaxial, biaxial, triaxial, and shear tests with all stress components in compression. The second set of nine tests involved more complicated paths in the compressive regime; consequently, each type of test in this set was performed on three specimens. The last set consisted of ten tests in which one component of stress was in the tensile region for at least some portion of each path. Again, each type of test in this set was performed on three specimens.

To perform each experiment, it was necessary to give the stress paths in incremental form. This is also a convenient way to describe the paths analytically. Tables 1, 2, and 3 provide a complete description of the paths in terms of a positive increment in stress, Δs. Each path is identified with a number and the set to which it belongs, and each segment of the path is described briefly. Terms are defined in the tables as needed. In particular, f_c' and f_b' denote the limit stress in uniaxial compression and biaxial stress. The corresponding limit stress in uniaxial tension is f_t'.

TABLE 1. SET 1: STRESS PATHS IN COMPRESSION

Path	Description
1	Uniaxial stress to failure $\Delta\sigma_1 = \Delta\sigma_2 = 0$; $\Delta\sigma_3 = -\Delta s$ Limit stress $f'_c = (-\sigma_3)_{max}$
2	Uniaxial stress to failure. This and path 1 give an initial test for anisotropy. $\Delta\sigma_1 = -\Delta s$; $\Delta\sigma_2 = -\Delta\sigma_3 = 0$.
3	Biaxial stress to failure with $\sigma_2/\sigma_1 = 1.0$; $\sigma_3 = 0$ $\Delta\sigma_1 = -\Delta s$; $\Delta\sigma_2 = -\Delta s$; $\Delta\sigma_3 = 0$ Limit stress $f'_b = (-\sigma_1)_{max} = (-\sigma_2)_{max}$
4	Hydrostatic loading to C; uniaxial loading to failure (i) $\Delta\sigma_1 = \Delta\sigma_2 = \Delta\sigma_3 = -\Delta s$ to the point $\sigma_1 = \sigma_2 = \sigma_3 = -f'_b/3$ (ii) $\Delta\sigma_1 = -\Delta s$; $\Delta\sigma_2 = \Delta\sigma_3 = 0$
5	Hydrostatic loading to 2/3 f'_b; shear loading to failure (i) $\Delta\sigma_1 = \Delta\sigma_2 = \Delta\sigma_3 = -\Delta s$ to the point $\sigma_1 = \sigma_2 = \sigma_3 = -2/3\ f'_b$ (ii) $\Delta\sigma_1 = -\Delta s$; $\Delta\sigma_2 = \Delta s$; $\Delta\sigma_3 = 0$
6	3-D stress to failure (subject to extensometer capability) with $\sigma_2/\sigma_1 = 1.0$; $\sigma_3/\sigma_1 = 0.1$ $\Delta\sigma_1 = -\Delta s$; $\Delta\sigma_2 = -\Delta s$; $\Delta\sigma_3 = -0.1\ \Delta s$

TABLE 1. CONCLUDED

Path	Description
7	Biaxial stress to failure with $\sigma_2/\sigma_1 = 0.5$; $\sigma_3 = 0$ $\Delta\sigma_1 = -\Delta s$; $\Delta\sigma_2 = -0.5\ \Delta s$; $\Delta\sigma_3 = 0$
8	3-D stress to failure (subject to extensometer capability) with $\sigma_2/\sigma_1 = 0.5$; $\sigma_3/\sigma_1 = 0.1$ $\Delta\sigma_1 = -\Delta s$; $\Delta\sigma_2 = -0.5\ \Delta s$; $\Delta\sigma_3 = -0.1\ \Delta s$

TABLE 2. SET 2: ADDITIONAL STRESS PATHS IN COMPRESSION

Path	Description
1	(i) Load hydrostatically to $\sigma_1 = \sigma_2 = \sigma_3 = -0.1\ f'_c$; $\Delta\sigma_1 = \Delta\sigma_2 = \Delta\sigma_3 = -\Delta s$ (ii) Load uniaxially to $\bar{\sigma} = \alpha\ f'_c$ ($\sigma_1 = -0.85\ f'_c$; $\sigma_2 = \sigma_3 = -0.1\ f'_c$) $\Delta\sigma_1 = -\Delta s$; $\Delta\sigma_2 = \Delta\sigma_3 = 0$ (iii) Unload to $\sigma_1 = \sigma_2 = \sigma_3 = -0.1\ f'_c$; $\Delta\sigma_1 = \Delta s$; $\Delta\sigma_2 = \Delta\sigma_3 = 0$ (iv) Load biaxially in x_1-x_2 plane to failure with $\sigma_2/\sigma_1 = 1.0$; $\sigma_3 = -0.1\ f'_c$ $\Delta\sigma_1 = \Delta\sigma_2 = -\Delta s$; $\Delta\sigma_3 = 0$
2	(i) Load hydrostatically to $\sigma_1 = \sigma_2 = \sigma_3 = -0.1\ f'_c$; $\Delta\sigma_1 = \Delta\sigma_2 = \Delta\sigma_3 = -\Delta s$ (ii) Load biaxially in x_1-x_2 plane to failure with $\sigma_1/\sigma_2 = 1.0$; $\sigma_3 = -0.1\ f'_c$ (Check on stress-induced anisotropy) $\Delta\sigma_1 = \Delta\sigma_2 = -\Delta s$; $\Delta\sigma_3 = 0$
3	(i) Load hydrostatically to $\sigma_1 = \sigma_2 = \sigma_3 = -0.1\ f'_c$; $\Delta\sigma_1 = \Delta\sigma_2 = \Delta\sigma_3 = -\Delta s$ (ii) Biaxial stress in x_1-x_2 plane to $\bar{\sigma} = \alpha\ f'_b$ ($\sigma_1 = \sigma_2 = -0.85\ f'_b$; $\sigma_3 = -0.1\ f'_c$) $\Delta\sigma_1 = \Delta\sigma_2 = -\Delta s$; $\Delta\sigma_3 = 0$ (iii) Unload to $\sigma_1 = \sigma_2 = \sigma_3 = -0.1\ f'_c$; $\sigma_1 = \Delta\sigma_2 = \Delta s$; $\Delta\sigma_3 = 0$ (iv) Load uniaxially in x_1-direction to failure $\Delta\sigma_1 = -\Delta s$; $\Delta\sigma_2 = \Delta\sigma_3 = 0$

TABLE 2. CONTINUED

Path	Description
4	(i) Load hydrostatically to $\sigma_1 = \sigma_2 = \sigma_3 = -0.1\ f'_c$; $\Delta\sigma_1 = \Delta\sigma_2 = \Delta\sigma_3 = -\Delta s$ (ii) Load uniaxially in x_1-direction to failure (test of stress-induced anisotropy) $\Delta\sigma_1 = \Delta s$; $\Delta\sigma_2 = \Delta\sigma_3 = 0$
5	(i) Load hydrostatically to $\sigma_1 = \sigma_2 = \sigma_3 = -f'_b$ $\Delta\sigma_1 = \Delta\sigma_2 = \Delta\sigma_3 = -\Delta s$ (ii) Unload hydrostatically to $\sigma_1 = \sigma_2 = \sigma_3 = -2/3\ f'_b$ $\Delta\sigma_1 = \Delta\sigma_2 = \Delta\sigma_3 = \Delta s$ (iii) Load in shear to failure $\Delta\sigma_1 = -\Delta s$; $\Delta\sigma_2 = \Delta s$; $\Delta\sigma_3 = 0$
6	(i) Load hydrostatically to $\sigma_1 = \sigma_2 = \sigma_3 = -2\ f'_c$ $\Delta\sigma_1 = \Delta\sigma_2 = \Delta\sigma_3 = -\Delta s$ (ii) Unload hydrostatically to $\sigma_1 = \sigma_2 = \sigma_3 = -0.1\ f'_c$ $\Delta\sigma_1 = \Delta\sigma_2 = \Delta\sigma_3 = \Delta s$ (iii) Load biaxially to failure $\Delta\sigma_1 = \Delta\sigma_2 = -\Delta s$; $\Delta\sigma_3 = 0$
7	(i) Load hydrostatically to $\sigma_1 = \sigma_2 = \sigma_3 = -0.1\ f'_c$ $\Delta\sigma_1 = \Delta\sigma_2 = \Delta\sigma_3 = -\Delta s$ (ii) Load uniaxially to $\sigma_1 = -0.75\ f'_c$; $\sigma_2 = \sigma_3 = 0$ $\Delta\sigma_1 = -\Delta s$; $\Delta\sigma_2 = \Delta\sigma_3 = 0$ (iii) Load to a biaxial state $\sigma_1 = \sigma_2 = -0.75\ f'_c$; $\sigma_3 = 0$ $\Delta\sigma_1 = \Delta\sigma_3 = 0$; $\Delta\sigma_2 = -\Delta s$ (iv) Load biaxially to failure $\Delta\sigma_1 = \Delta\sigma_2 = -\Delta s$; $\Delta\sigma_3 = 0$

TABLE 2. CONCLUDED

Path	Description
8	(i) Load hydrostatically to $\sigma_1 = \sigma_2 = \sigma_3 = -0.1\ f'_c$ $\Delta\sigma_1 = \Delta\sigma_2 = \Delta\sigma_3 = -\Delta s$ (ii) Load uniaxially to $\sigma_1 = -0.85\ f'_c$ $\Delta\sigma_1 = -\Delta s;\ \Delta\sigma_2 = \Delta\sigma_3 = 0$ (iii) Trace a path to $\sigma_1 = -0.1\ f'_c;\ \sigma_2 = -0.85\ f'_c$ $\sigma_3 = -0.1\ f'_c$ $\Delta\sigma_1 = \Delta s;\ \Delta\sigma_2 = -\Delta s;\ \Delta\sigma_3 = 0$ (iv) Load uniaxially to failure $\Delta\sigma_1 = \Delta\sigma_3 = 0;\ \Delta\sigma_2 = -\Delta s$
9	(i) Load hydrostatically to $\sigma_1 = \sigma_2 = \sigma_3 = -2\ f'_c$ $\Delta\sigma_1 = \Delta\sigma_2 = \Delta\sigma_3 = -\Delta s$ (ii) One cycle in shear (a) $\Delta\sigma_1 = \Delta s;\ \Delta\sigma_2 = -\Delta s;\ \Delta\sigma_3 = 0$ to $\sigma_1 = -f'_c;$ $\sigma_2 = -3\ f'_c;\ \sigma_3 = -2\ f'_c$ (b) $\Delta\sigma_1 = -\Delta s;\ \Delta\sigma_2 = \Delta s;\ \Delta\sigma_3 = 0$ to $\sigma_1 = \sigma_2 = \sigma_3 = -2\ f'_c$ (iii) Unload hydrostatically to $\sigma_1 = \sigma_2 = \sigma_3 = -0.1\ f'_c$ $\Delta\sigma_1 = \Delta\sigma_2 = \Delta\sigma_3 = \Delta s$ (iv) Load biaxially to failure $\Delta\sigma_1 = \Delta\sigma_2 = -\Delta s;\ \Delta\sigma_3 = 0$

TABLE 3. SET 3: STRESS PATHS INVOLVING TENSION

Path	Description
1	Uniaxial stress to failure $\sigma_1 = f'_t$; $\sigma_2 = \sigma_3 = 0$ $\Delta\sigma_1 = \Delta s$; $\Delta\sigma_2 = \Delta\sigma_3 = 0$
2	Uniaxial stress to failure $\sigma_1 = \sigma_2 = 0$; $\sigma_3 = f'_t$ (test for anisotropy) $\Delta\sigma_1 = \Delta\sigma_2 = 0$; $\Delta\sigma_3 = \Delta s$
3	Biaxial stress to failure $\Delta\sigma_1 = \Delta s$, $\Delta\sigma_2 = -0.5\ \Delta s$; $\Delta\sigma_3 = 0$
4	Shear to failure $\sigma_1 = f'_s$; $\sigma_2 = -f'_s$; $\sigma_3 = 0$ $\Delta\sigma_1 = \Delta s$; $\Delta\sigma_2 = -\Delta s$; $\Delta\sigma_3 = 0$
5	(i) Uniaxial stress to $\sigma_1 = 0.5\ f'_t$; $\sigma_2 = \sigma_3 = 0$ $\Delta\sigma_1 = \Delta s$; $\Delta\sigma_2 = \Delta\sigma_3 = 0$ (ii) Shear to failure $\Delta\sigma_1 = \Delta s$; $\Delta\sigma_2 = -\Delta s$; $\Delta\sigma_3 = 0$
6	(i) Shear to $\sigma_1 = 0.5\ f'_s$; $\sigma_2 = -0.5\ f'_s$; $\sigma_3 = 0$ $\Delta\sigma_1 = \Delta s$; $\Delta\sigma_2 = -\Delta s$; $\Delta\sigma_3 = 0$ (ii) Uniaxial stress to failure $\Delta\sigma_1 = \Delta s$; $\Delta\sigma_2 = 0$; $\Delta\sigma_3 = 0$
7	Curved path to failure (i) $\Delta\sigma_1 = \Delta s$ $\Delta\sigma_2 = -0.2\ \Delta s$ $\Delta\sigma_3 = 0$ (to $\sigma_1 = 0.5\ f'_t$) (ii) $\Delta\sigma_1 = \Delta s$ $\Delta\sigma_2 = -0.4\ \Delta s$ $\Delta\sigma_3 = 0$ (to failure)
8	Curved path to failure (i) $\Delta\sigma_1 = \Delta s$ $\Delta\sigma_2 = -0.3\ \Delta s$ $\Delta\sigma_3 = 0$ (to $\sigma_1 = 0.5\ f'_s$) (ii) $\Delta\sigma_1 = \Delta s$ $\Delta\sigma_2 = -0.6\ \Delta s$ $\Delta\sigma_3 = 0$ (to failure)

TABLE 3. CONCLUDED

Path		Description
9	(i)	Initial compressive state $\sigma_2 = \sigma_3 = -f'_t$
		$\Delta\sigma_1 = 0$; $\Delta\sigma_2 = \Delta\sigma_3 = -\Delta s$
	(ii)	Uniaxial stress to failure
		$\Delta\sigma_1 = \Delta s$; $\Delta\sigma_2 = \Delta\sigma_3 = 0$
10	(i)	Initial compressive state $\sigma_3 = -f'_t$
		$\Delta\sigma_1 = \Delta\sigma_2 = 0$; $\Delta\sigma_3 = -\Delta s$
	(ii)	Shear to failure
		$\Delta\sigma_1 = \Delta s$; $\Delta\sigma_2 = -\Delta s$; $\Delta\sigma_3 = 0$

The paths are also shown in Figure 1 for the $\sqrt{J_2'}$-P plane. As these plots demonstrate rather vividly, the paths cover a large spectrum of possible load so the resulting stress-deformation relations should provide a comprehensive test for a constitutive model.

Of particular significance is the limit state; that is, the state at which an incremental increase in deformation ceases to yield a corresponding incremental increase in stress. Historically, this state has been called failure, but structural failure will occur only if the structure is statically determinant and a limit state is reached. For many materials, this limit state is described by a line in the $\sqrt{J_2'}$-P plane. The limit points for all paths considered in this study are shown in Figure 2. This plot demonstrates that the use of a straight line for a limit surface is a poor fit for these data.

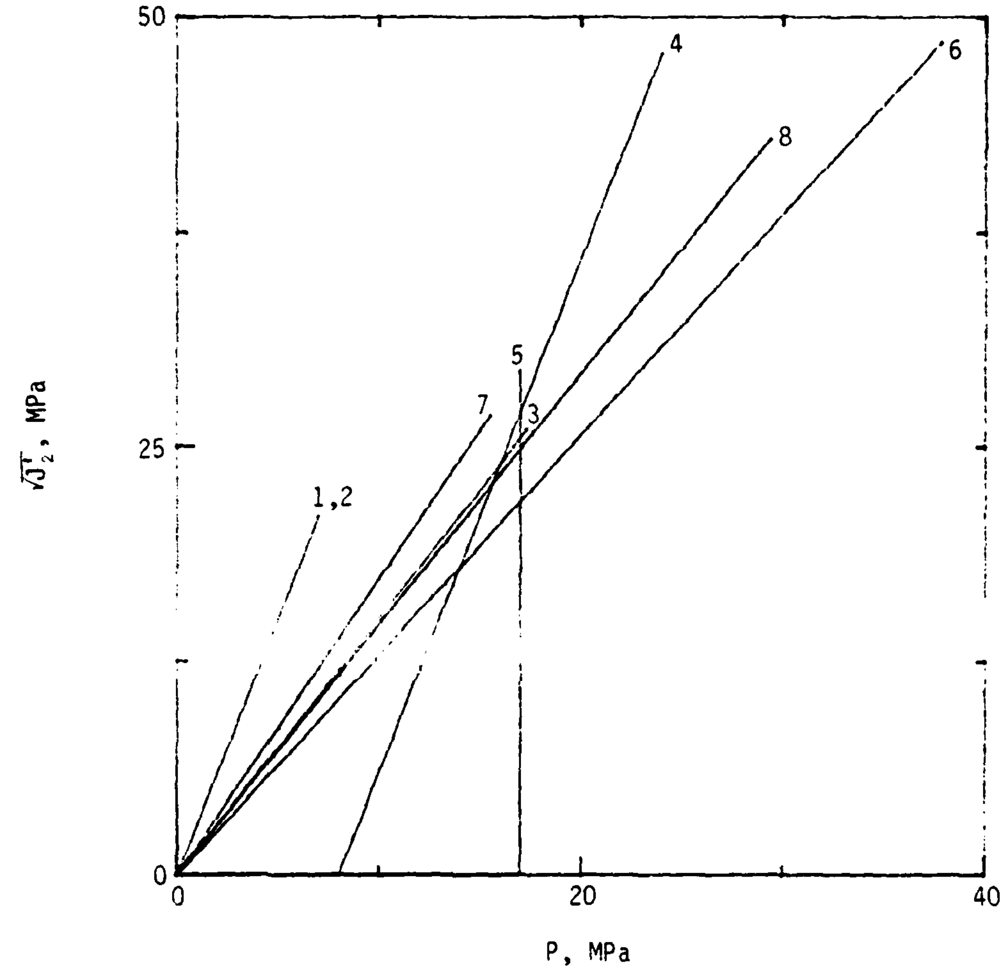

(a) Set 1.

Figure 1. Stress paths in $\sqrt{J'_2}$-P plane.

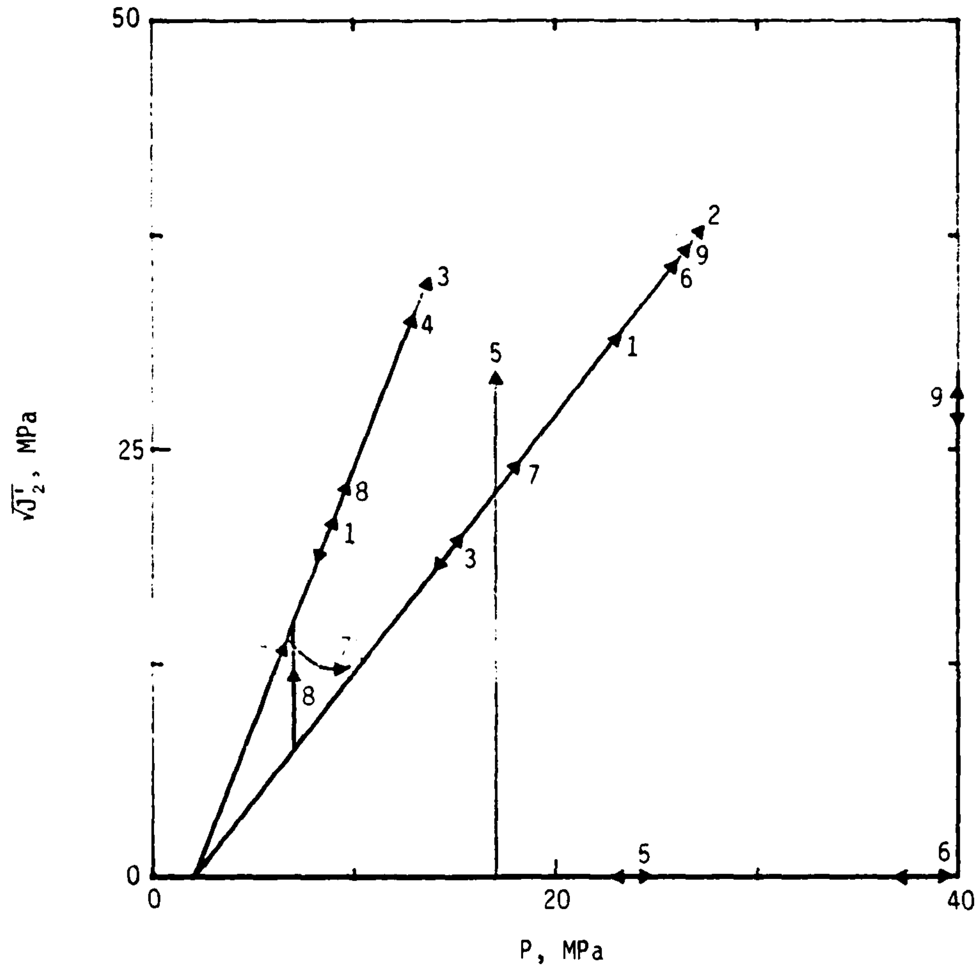

(b) Set 2.

Figure 1. Continued.

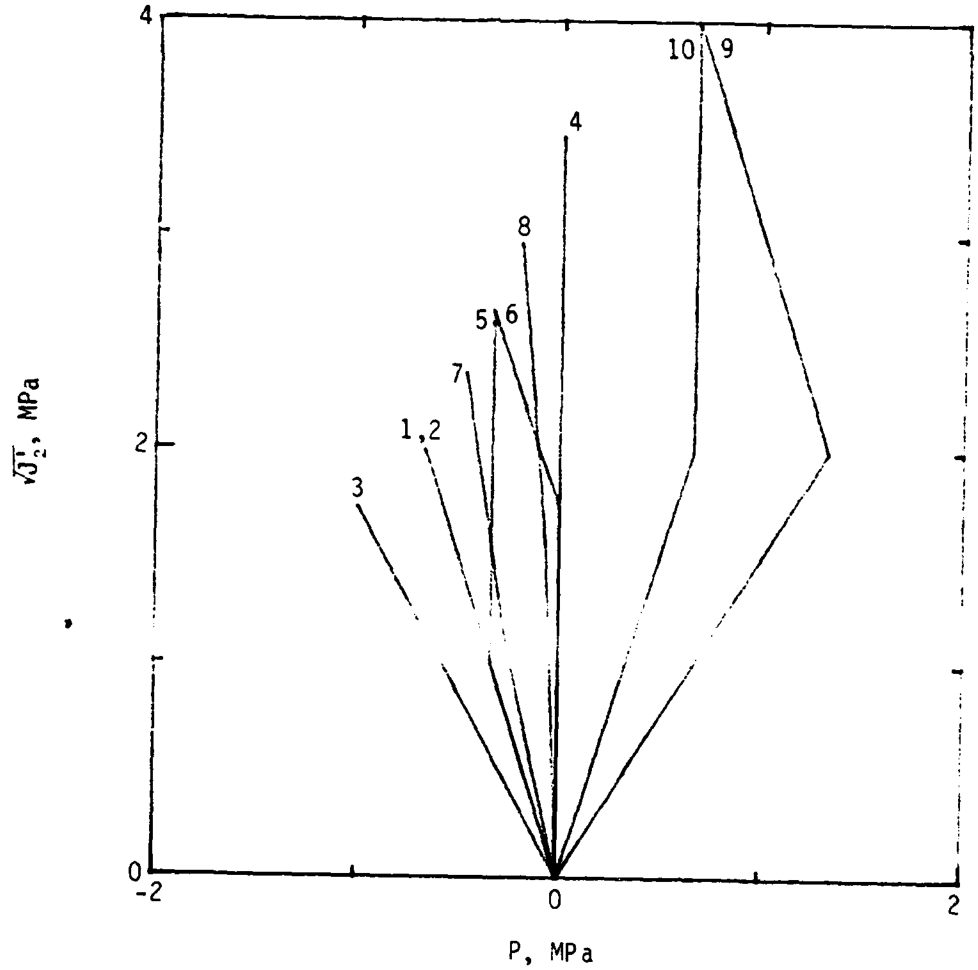

(c) Set 3.

Figure 1. Concluded.

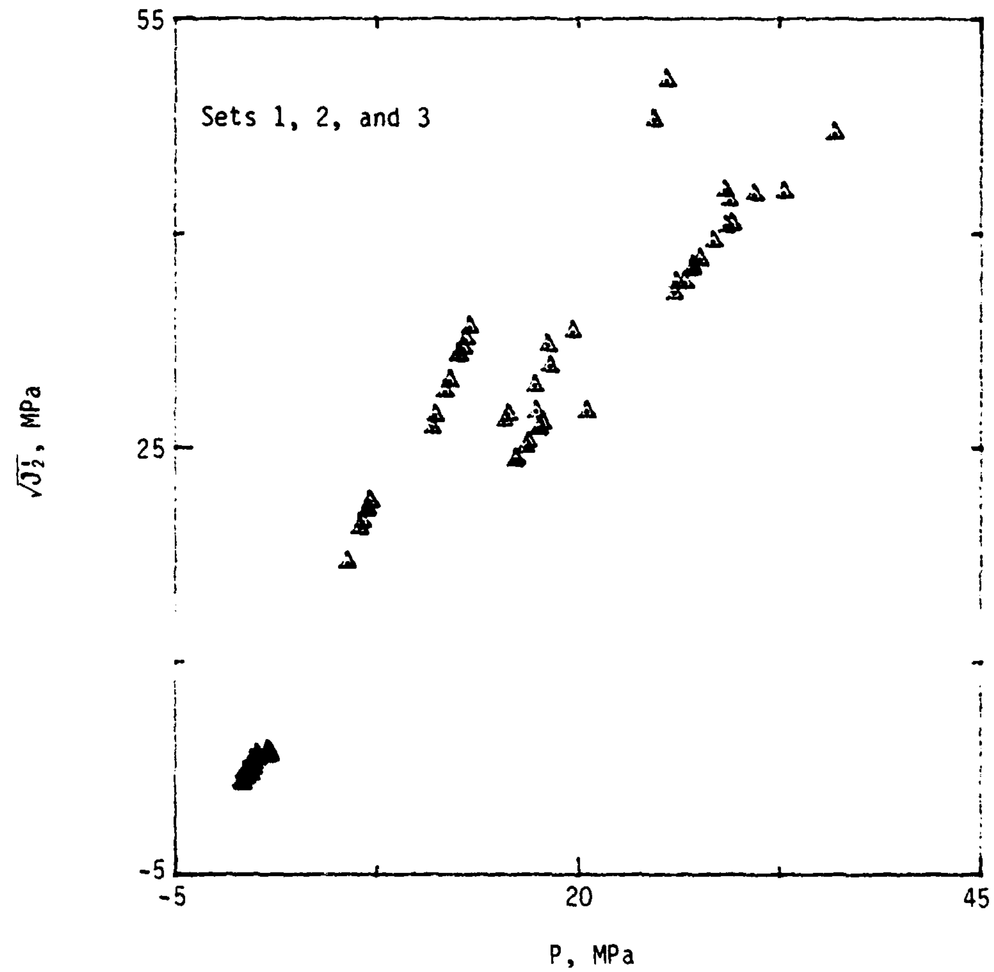

Figure 2. Limit states in $\sqrt{J_2'}$-P plane for all paths.

III. LIMIT STATES AND STRESS PATHS INVOLVING FIRST AND THIRD INVARIANTS

Lade (Ref. 2) suggested that a better fit to limit data would be obtained if a third invariant of stress were used instead of the second invariant. This suggestion has been investigated (Ref. 3) for a third invariant, L, defined by

$$L = -\left[(\sigma_1 - \sigma_s)(\sigma_2 - \sigma_s)(\sigma_3 - \sigma_s) + \sigma_s^3\right]^{1/3}$$

where σ_s is a parameter that can be interpreted as the shear strength of the material under zero mean pressure. Limit points in the L-P space are shown in Figure 3. It is evident that a straight line in this space is a much better fit to these data than is a straight line in the $\sqrt{J_2'}$-P space.

These results suggest that for the formulation and evaluation of constitutive models, the use of the L-P space may be preferable to the use of the $\sqrt{J_2'}$-P space. Thus, for the sake of completeness, stress paths in the L-P space are shown in Figure 4 for each of the three sets of tests. The hydrostatic compression path is included as a reference curve because L is not independent of P. All paths involving compression lie in the small sector between the hydrostatic compression curve and the limit line. The advantage of this presentation is that it shows the similarities of many of the conventional testing paths used for concrete. A disadvantage is that some resolution is lost in comparison to that obtained in plots in the space of $\sqrt{J_2'}$-P or in plots in the space of two principal stresses.

---

2. Lade, P. V., "Three-Parameter Failure Criterion for Concrete," Journal of the Engineering Mechanics Division, ASE, 108:850-863, 1982.

3. Schreyer, H. L., "A Third-Invariant Plasticity Theory for Frictional Materials," Journal of Structural Mechanics, June 1983.

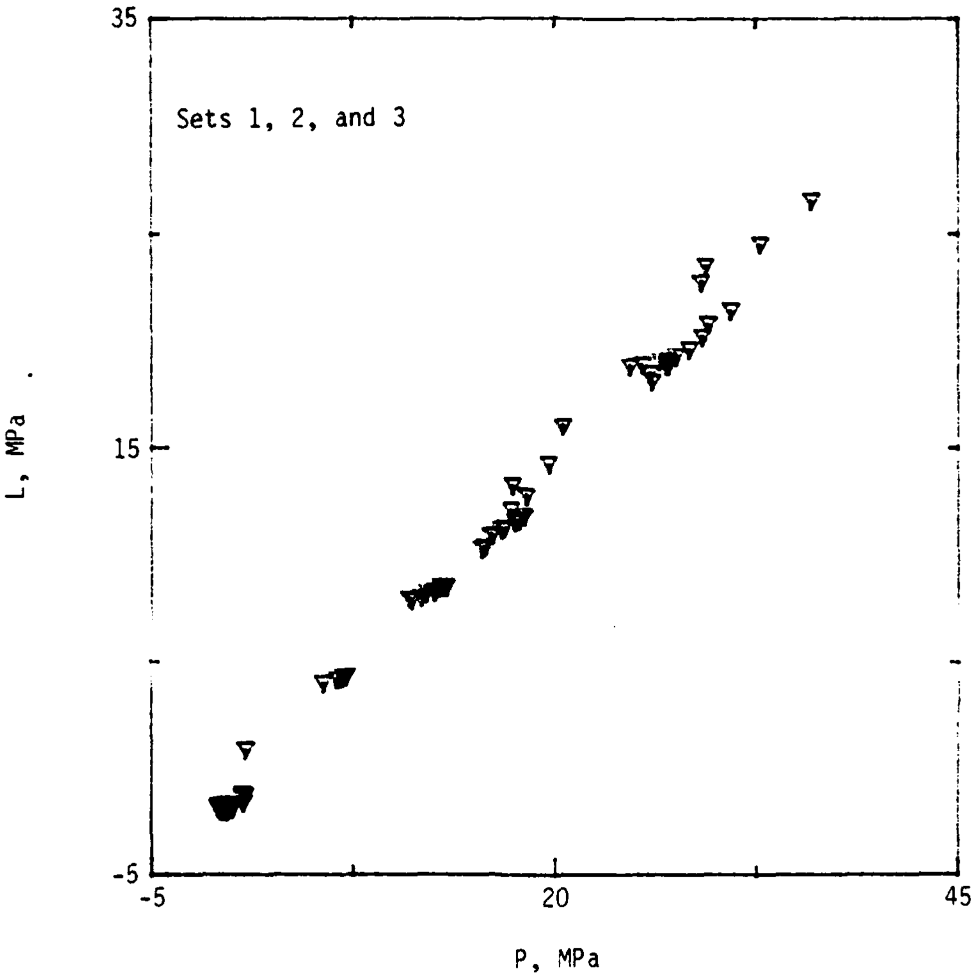

Figure 3. Limit states in L-P plane for all paths.

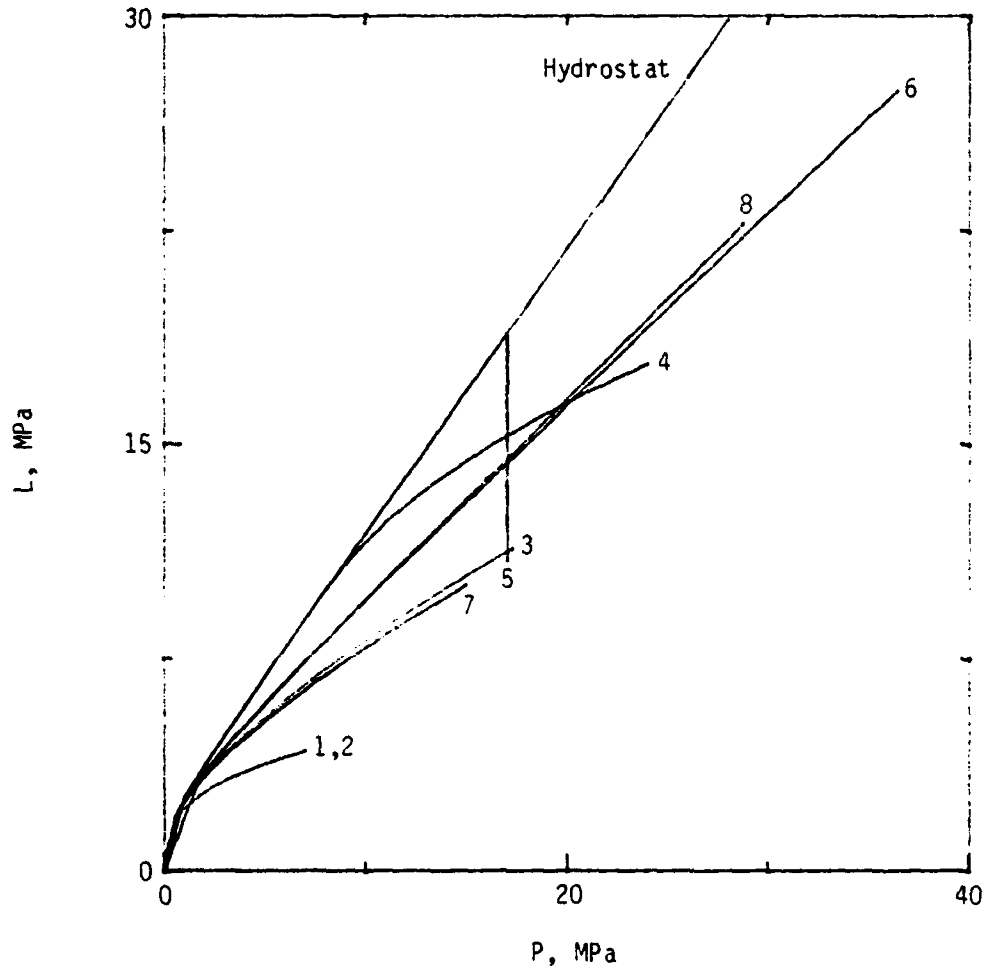

(a) Set 1.

Figure 4. Stress paths in L-P plane.

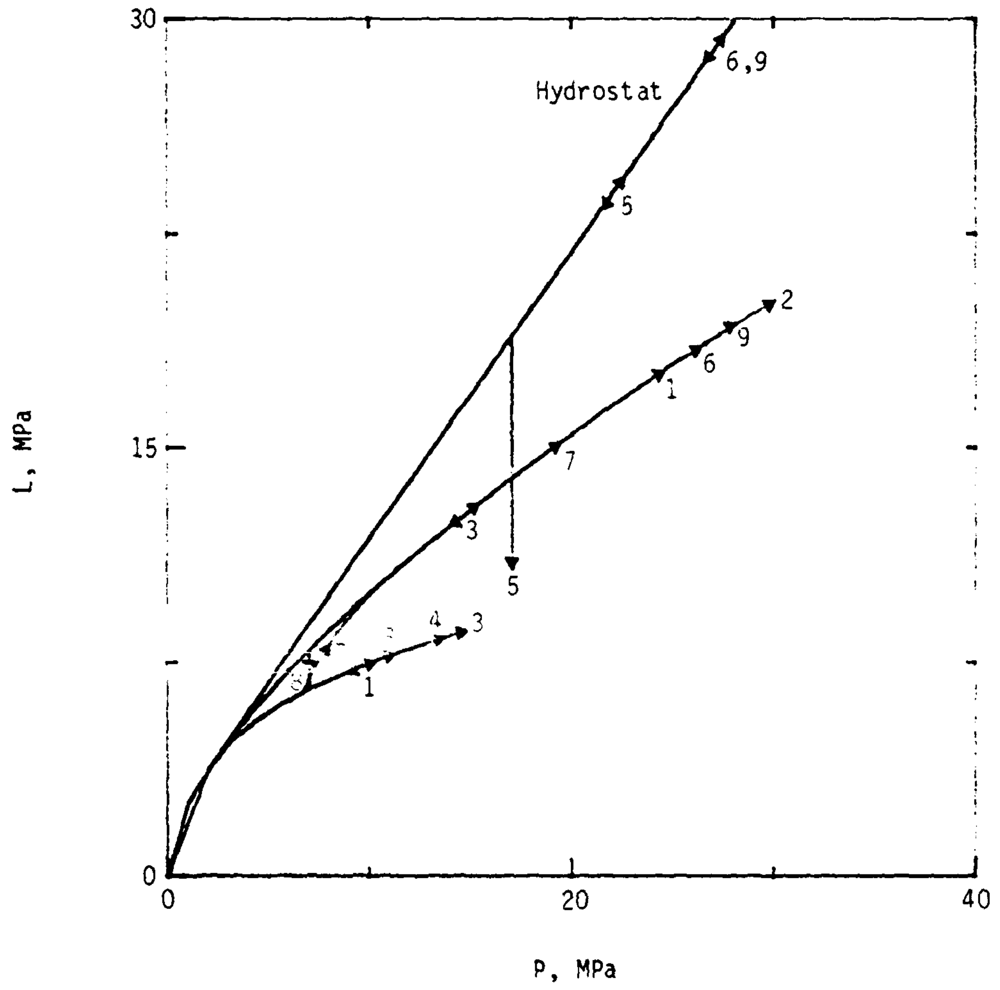

(b) Set 2.

Figure 4. Continued.

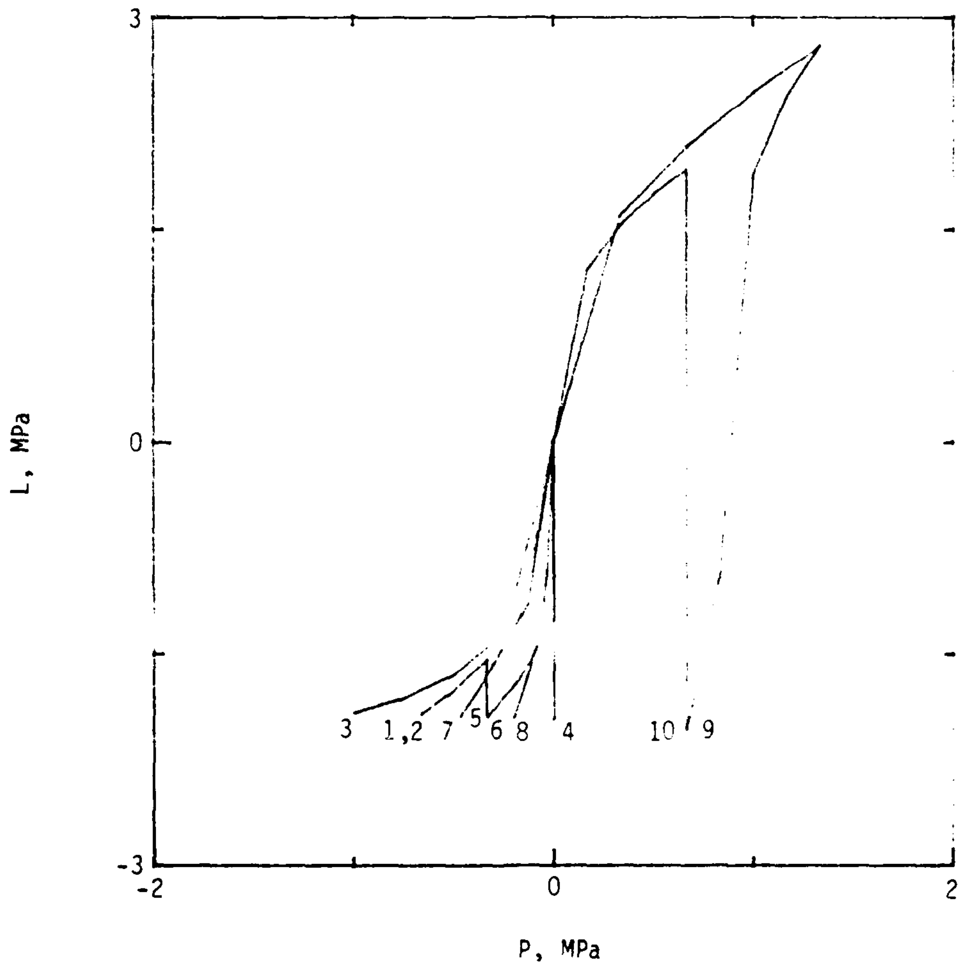

(c) Set 3.

Figure 4. Concluded.

IV. ADJUSTMENTS TO STRESS-STRAIN DATA

PRELIMINARY COMMENTS

The data obtained from Reference 1 were digitized for processing and plotting on a Tektronix miniprocessor system. These data are given in Appendix A. Multiple runs for a given stress path are shown on one plot. The stresses are positive in compression (negative in tension); the strains are positive in contraction (negative in extension). The data have been plotted so that the scale for contractive strains appears along the bottom, and curves of contractive strain start at the lower left corner. The scale for extensive strains appears along the top, and curves of extension start at the lower right corner. The use of two scales yields a higher resolution of the strain data than is available with a single scale.

The same data are given in plots of pressure versus volumetric strain, e_v, where

$$e_v = -(\varepsilon_1 + \varepsilon_2 + \varepsilon_3)$$

With this sign convention, the volumetric strain is positive for compaction and negative for dilatation. These plots also appear in Appendix A.

From a survey of all the uniaxial stress path data, which included four concrete specimens from set 1 and an additional four specimens from the concrete batches used in set 2, the elastic constants were determined. The Young's modulus suggested by these data was 21 GPa, and the Poisson's ratio was about 0.25. These values were used when the need for data adjustments on each plot was considered. Adjustments to the data were based only on the linear elastic regime of the data. Linear elasticity and the aforementioned elastic constants were used to determine the strains from the given stresses. These calculated strains were then compared with strains obtained experimentally, and a baseline-type shift was made in the experimental strains for data that were significantly different from the calculated strains. Some subjectivity was involved in these adjustments, so all changes were recorded. The reasoning behind the alterations is explained in the succeeding paragraphs.

ADJUSTMENTS TO SET 1

Some anomalies and missing data points were found in several of the sets of strain data. The first correction of the data was made to compensate for mechanical difficulties attendant upon the measurement of small strains. For this purpose the elastic portion of each set of data was compared to the calculated theoretical strains, and a strain correction was added to or subtracted from all of the strains (except the initial zero strain).

To correct for anomalous data found for strain in the 1-direction of path 1, specimen B-6, ε_1 was set equal to ε_2 because this specimen had been uniaxially loaded in the σ_3 direction, and therefore ε_1 should equal ε_2. For the missing seven data points for ε_2 of path 4, specimen D-2, the values of ε_3 were used because this test theoretically produces strains of $\varepsilon_2 = \varepsilon_3$, and the available data points from the other run confirmed these values. This data set and the data set for path 1, specimen B-6, remain inconsistent. For five other specimens, one or two data points were missing from one axis of principal stress at the limit state. For these points, the given stress data were used to find the estimated volumetric strain, and the volumetric strain versus mean pressure curves were extrapolated. The two known strains were subtracted, which left a relatively reliable value for the missing strain. The data corrected in this manner were path 3, specimen B-3, ε_3; path 3, specimen C-3, ε_3; path 5, specimen D-5, ε_3; path 6, specimen C-1, ε_3; and path 8, specimen D-4, ε_3.

All the corrections are summarized in Table 4.

ADJUSTMENTS TO SET 2 (NONSTANDARD COMPRESSION DATA)

Corrections to the data for set 2 consisted only of adjusting the initial strain data to make them consistent with linear elasticity. The corrections are listed for each path and concrete specimen in Table 5. The inconsistencies in the data that made the corrections necessary were caused primarily by the same mechanical difficulties in measuring strain as were encountered in the data for set 1.

TABLE 4. MODIFICATIONS TO SET 1

Path	Specimen	Adjustment to strain measurement, $\mu\varepsilon$		
		ε_1	ε_2	ε_3
1	C-6	+100	-70	0
1	B-6	$\varepsilon_1 = \varepsilon_2$	0	0
2	C-2	0	0	0
2	B-2	0	0	0
3	C-3	0	0	0
3	B-3	0	0	0
4	D-2	-40	+300	0
4	A-2	0	+160 (n = 2,3) +300 ($n > 3$)	-20 (n = 2) -200 (n = 3) -700 (n = 4)
5	A-5	0	0	0
5	D-5	0	+100	+170
6	C-1	-100	-50	0
6	B-5	-100	-50	0
7	B-4	0	+100 (n = 2) +250 ($n > 2$)	0
7	C-4	0	0	+150
8	D-4	-200	-80	-200
8	A-6	-150 (n = 2) -300 ($n > 2$)	-30	+50

Note: n represents the number of the data point in a run where $n = 1$ corresponds to $\varepsilon = 0$ and $\sigma = 0$.

TABLE 5. MODIFICATIONS TO SET 2

Path	Specimen	n	Adjustment to strain measurement, $\mu\varepsilon$		
			ε_1	ε_2	ε_3
1	A-2	= 2	-40	0	-30
		> 2	-40	0	+80
1	B-2	= 2	-100	-70	+50
		= 3	-100	-70	+15
		> 3	-100	-70	-25
1	C-2	> 2	-80	-95	+25
2	A-1	> 2	+40	+40	-50
2	B-1	= 2	0	+40	+35
		> 2	0	+40	+90
2	C-1	= 2	-30	0	+20
		= 3	-30	0	+95
		> 3	-30	0	+160
3	A-4	= 2	+30	+40	0
		= 3	+30	-30	0
		> 3	+30	-85	+50
3	B-4	= 2	+30	+40	+100
		= 3	+30	+80	+25
		> 3	+30	+150	+25
3	C-4	= 2	+30	0	+80
		> 2	+30	0	+125
4	B-5	> 2	+80	+80	+90
4	C-5	= 2	+60	+80	+60
		= 3	+200	+80	+40
		> 3	+200	+80	+20
4	A-5	= 2	+40	0	+20
		= 3	+40	-20	-120
		= 4	+40	-80	-120
		> 4	+40	-90	-120
5	D-1	= 2	+40	0	0
		> 2	-70	-55	-30

Note: n represents the number of the data point in a run where $n = 1$ corresponds to $\varepsilon = 0$ and $\sigma = 0$.

TABLE 5. CONTINUED.

Path	Specimen	n	Adjustment to strain measurement, $\mu\varepsilon$		
			ε_1	ε_2	ε_3
5	D-2	= 2	+90	+80	+30
		= 3	+25	+80	+30
		= 4	+115	+50	+50
		> 4	+5	0	+100
5	D-4	= 2	+100	+100	+430
		= 3	+125	+200	+170
		= 4	+150	+230	-250
		> 4	+200	+230	-660
6	B-2	= 2	0	0	+280
		= 3	0	0	+470
		= 4	0	0	+518
		> 4	0	0	+630
6	C-2	= 2	+30	0	+160
		= 3	+45	-30	+40
		= 4	+60	-100	-40
		= 5	+80	-150	-60
		> 5	+90	-275	-60
6	D-2	= 2	-20	+30	[illegible]
		= 3	+50	0	+120
		= 4	+50	0	+100
		= 5	+40	+40	+190
		> 5	+70	+40	+220
7	A-1	= 2	+50	+20	0
		= 3	+50	+50	0
		= 4	+130	+50	0
		> 4	+150	+30	+40
7	B-1	= 2	+40	-90	0
		= 3	+40	+130	+40
		= 4	+20	+120	+20
		> 4	+20	+110	+60
7	C-1	= 2	+30	+30	+30
		= 3	+30	+60	+30
		= 4	+40	+75	+40
		> 4	+35	+75	+60

Note: n represents the number of the data point in a run where $n = 1$ corresponds to $\varepsilon = 0$ and $\sigma = 0$.

TABLE 5. CONCLUDED.

Path	Specimen	n	Adjustment to strain measurement, $\mu\varepsilon$		
			ε_1	ε_2	ε_3
8	A-3	= 2	+120	+80	+150
		= 3	+110	+80	+105
		= 4	+190	+100	-50
		> 4	+290	+30	-110
8	B-3	= 2	+90	0	+50
		= 3	+160	0	+35
		= 4	+150	+40	-30
		> 4	+300	+40	-150
8	C-3	= 2	+70	+60	+150
		= 3	+125	+70	+135
		= 4	+80	+70	+170
		> 4	+180	+70	+70
9	B-4	= 2	+170	+130	+100
		= 3	+260	+210	+80
		= 4	+380	+230	+140
		> 4	+480	+400	+130
9	C-4	= 2	0	+100	+110
		= 3	[illegible]	[illegible]	[illegible]
		= 4	[illegible]	[illegible]	[illegible]
		> 4	+180	+50	+200
9	D-4	> 4	0	0	+200

Note: n represents the number of the data point in a run where $n = 1$ corresponds to $\varepsilon = 0$ and $\sigma = 0$.

ADJUSTMENTS TO SET 3

Typically, very small strains are recorded for concrete in tension (on the order of 100 $\mu\varepsilon$ at failure, compared to several thousand $\mu\varepsilon$ at compression failure). The small strains are difficult to measure accurately with the extensometers that were used in these tests. The tensile data, therefore, are less reliable than the compression data. For this reason, no attempt was made to shift anomalous data. Instead, where data obtained for one of the three specimens were inconsistent with data obtained for the other two specimens, the inconsistent data were neglected. These deletions are noted in the strain-stress plots in Appendix B, where all the data are shown; the inconsistent sets are marked with an x. The deletions were based on the strain-stress plots as well as on the plots of pressure versus volumetric strain and plots involving strain invariants.

REVISED PLOTS

After the adjustments had been made, the data shown in Appendix A were plotted again. The results are shown in Appendix B. Thus, the reader can observe the effects of any adjustment by comparing corresponding figures.

Most of the tests for a given path had good repeatability. As expected, the concrete material was not ideally isotropic. This is noticeable in the difference between the uniaxial tests in which σ_3 was the uniaxial direction (set 1, path 1) and those in which σ_1 was the uniaxial direction (set 1, path 2). The compression path for which repeatability was probably least successful was path 9 of set 2. This path started with a large hydrostatic load followed by a shear cycle, hydrostatic unload, and then biaxial loading to failure. The loading and unloading did not produce completely repeatable strains.

For the P-e_v graphs, large dilatation is evident in the uniaxial (set 1, paths 1 and 2), biaxial (set 1, path 3), and triaxial (set 1, path 8) test data as well as in most of the data paths for set 2. The large

dilatation is particular to this low-strength concrete; higher strength concretes exhibit much less dilatation. (For example, see Reference 4.) Even though the triaxial data for set 1, path 8, exhibited a fair amount of dilatation, the triaxial data for set 1, path 6, exhibited almost none. Another interesting comparison can be made of the path 4 data for sets 1 and 2. In both cases, the specimens were subjected to a hydrostatic load and then a uniaxial load to failure. Set 1, path 4, had a larger hydrostatic load and exhibits almost no dilatation, while set 2, path 4, with the small hydrostatic load, has a large amount of dilatation. The behavior of the concrete specimens depended upon the amounts of hydrostatic pressure applied in these two stress path tests. The material behavior changed from a uniaxially loaded response to something more like a triaxially loaded response.

---

4. Green, S. J., and Swanson, S. R., Static Constitutive Relations for Concrete, AFWL-TR-72-244, Air Force Weapons Laboratory, Kirtland Air Force Base, New Mexico, 1973.

V. COMPOSITE STRESS-STRAIN CURVES

The adjusted strain-stress data are given in Appendix B. Each stress path test was executed on two or three different concrete specimens, and the data for all specimens have been plotted on one graph for each stress path. From these sets of data, average, or composite, strain-stress curves were developed for each stress path. The repeatability of the test data was considered. When the results of one test were very different from those of the other two tests in a series, the anomalous test data were eliminated from the development of the composite curve. In the nonstandard compression test series (set 2), one of the sets of strain-stress curves sometimes differed only slightly from the other two sets of curves for a particular stress path. In such cases, the two similar sets of data were given more consideration, and were weighted more heavily, than was the slightly anomalous curve. The more inconsistent data occurred in the tension test series.

The composite curves were overlaid on the experimental data curves as shown in Appendix B. The curves are presented separately for stress versus strain in Figures 5, 6, and 7 and for pressure versus volumetric strain in Figures 8, 9, and 10. Scatter bars are given to indicate the bounds of the experimental data. These curves, which show both the deformation and limit features of the material, are generally most useful in the development of constitutive models.

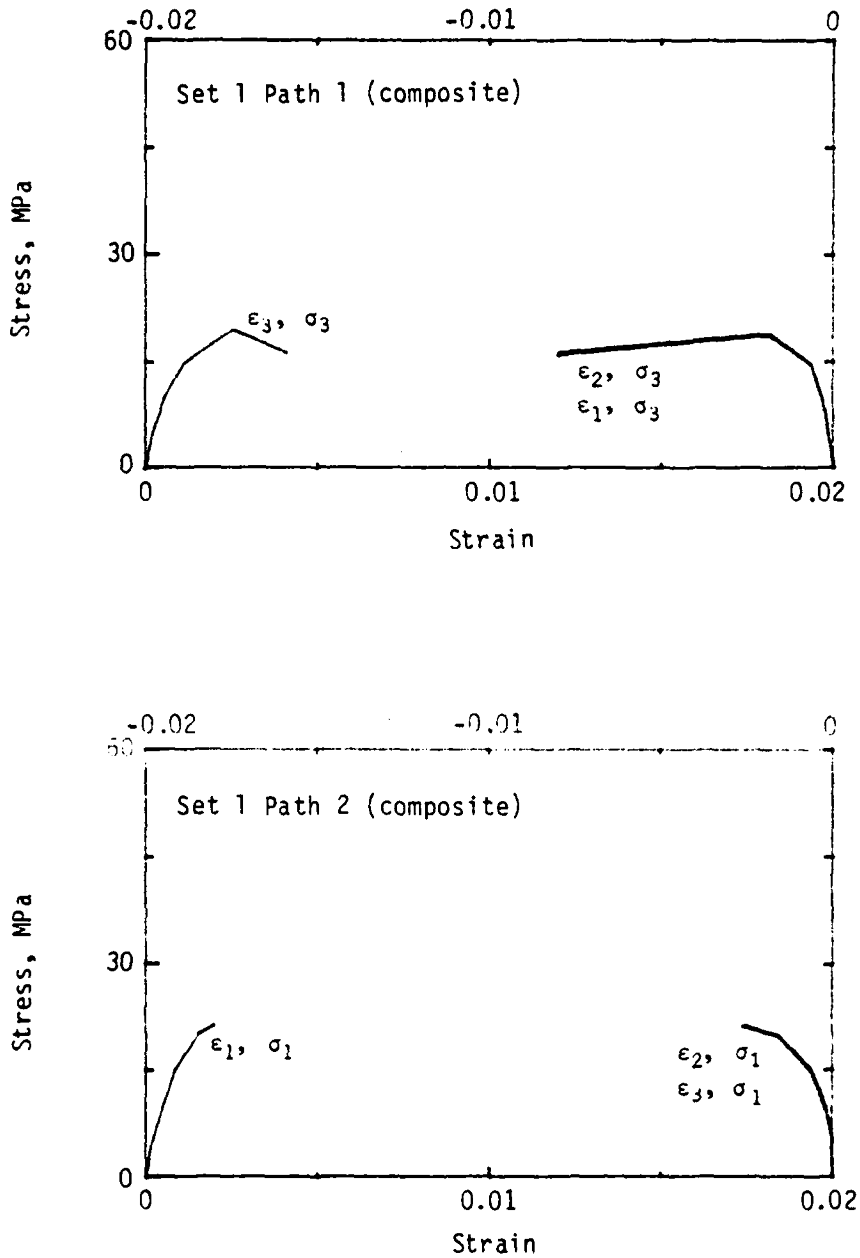

(a) Paths 1 and 2.

Figure 5. Composite stress-strain curves, set 1.

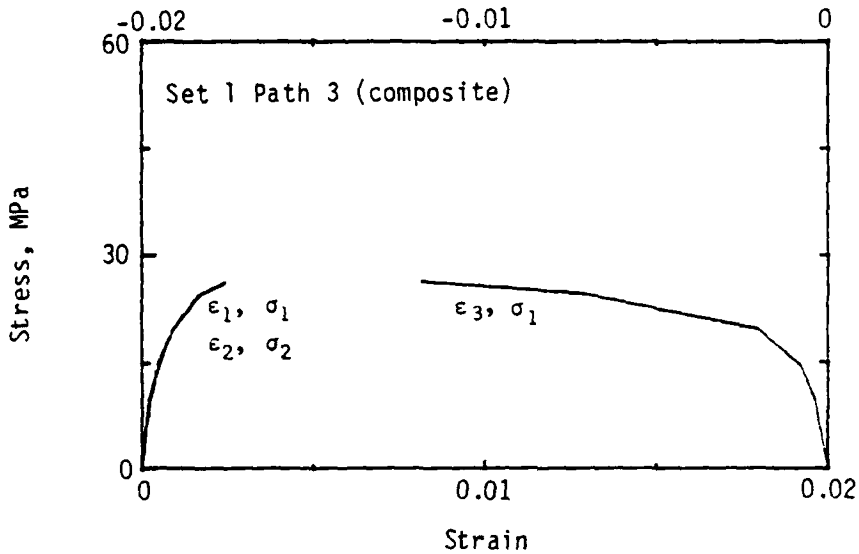

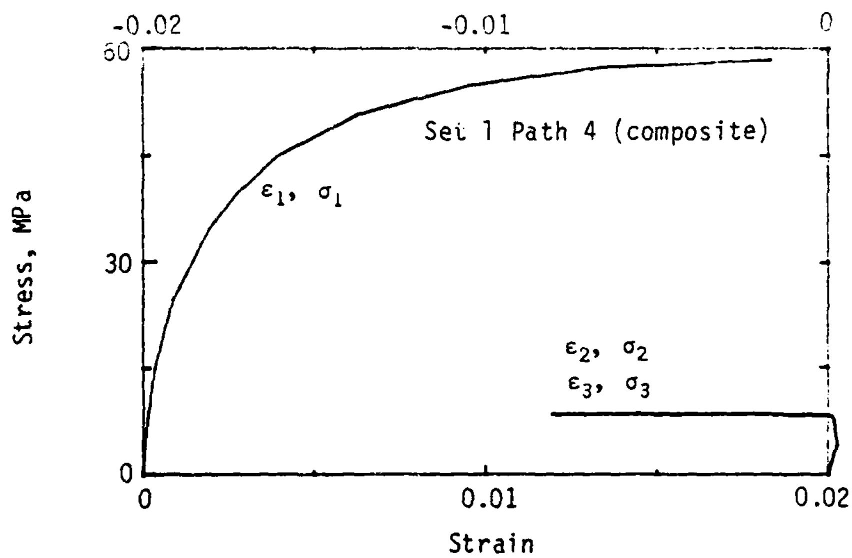

(b) Paths 3 and 4.

Figure 5. Continued.

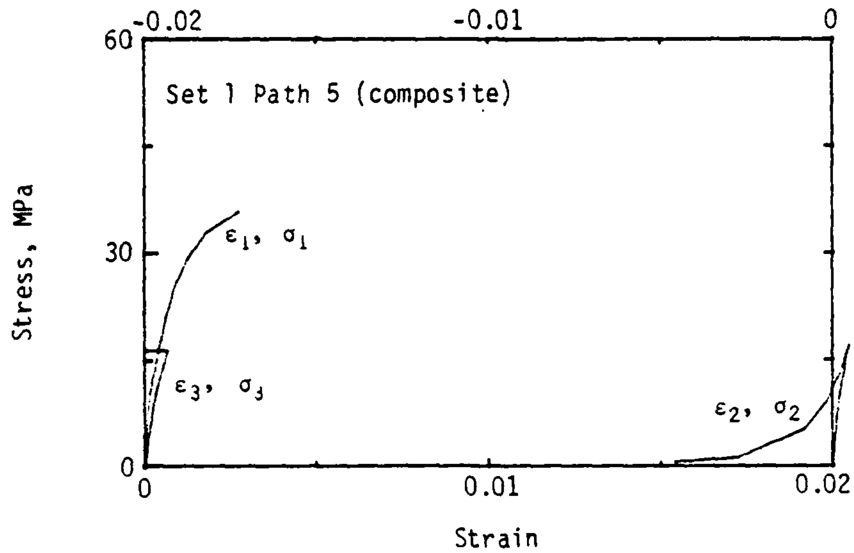

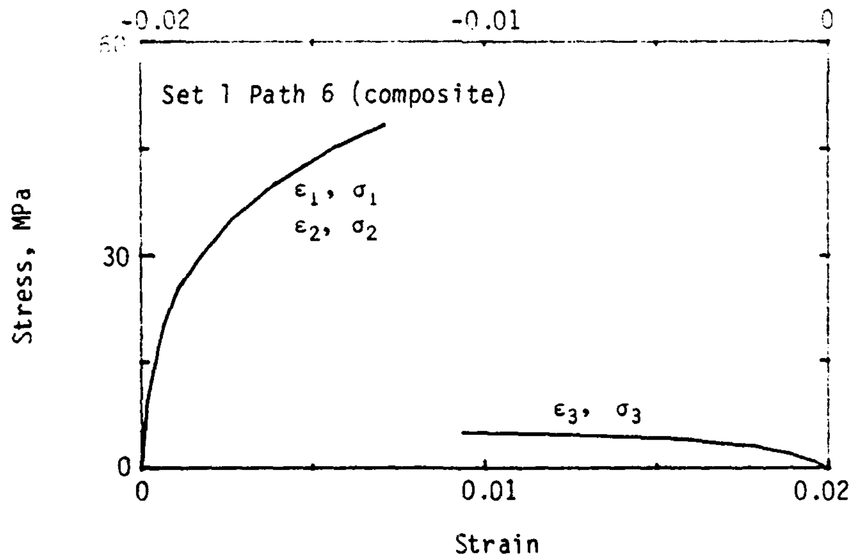

(c) Paths 5 and 6.

Figure 5. Continued.

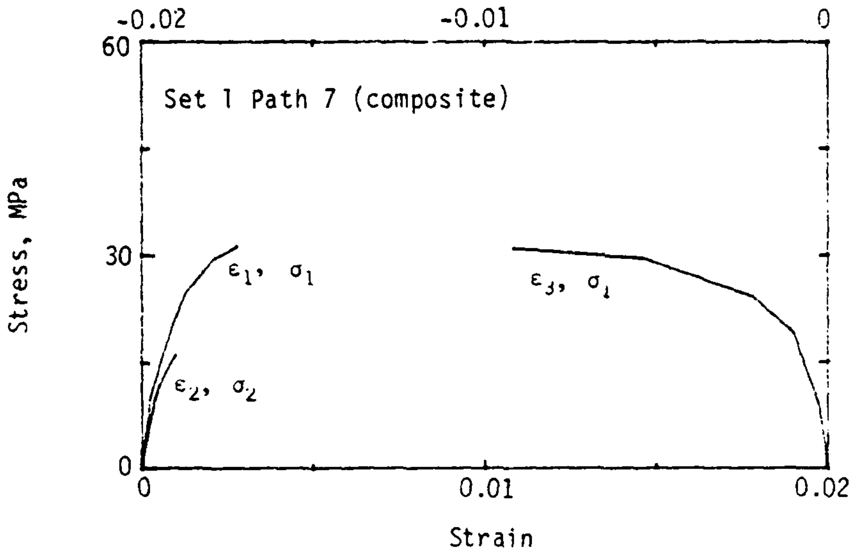

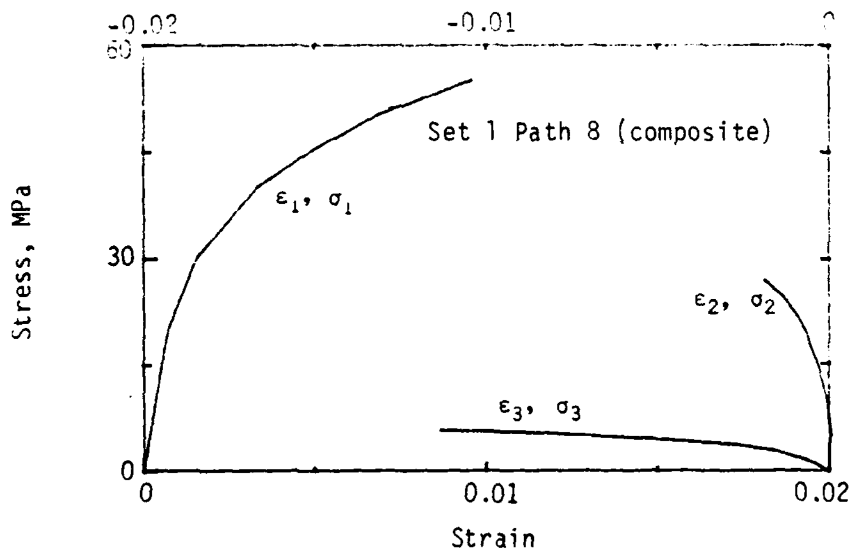

(d) Paths 7 and 8.

Figure 5. Concluded.

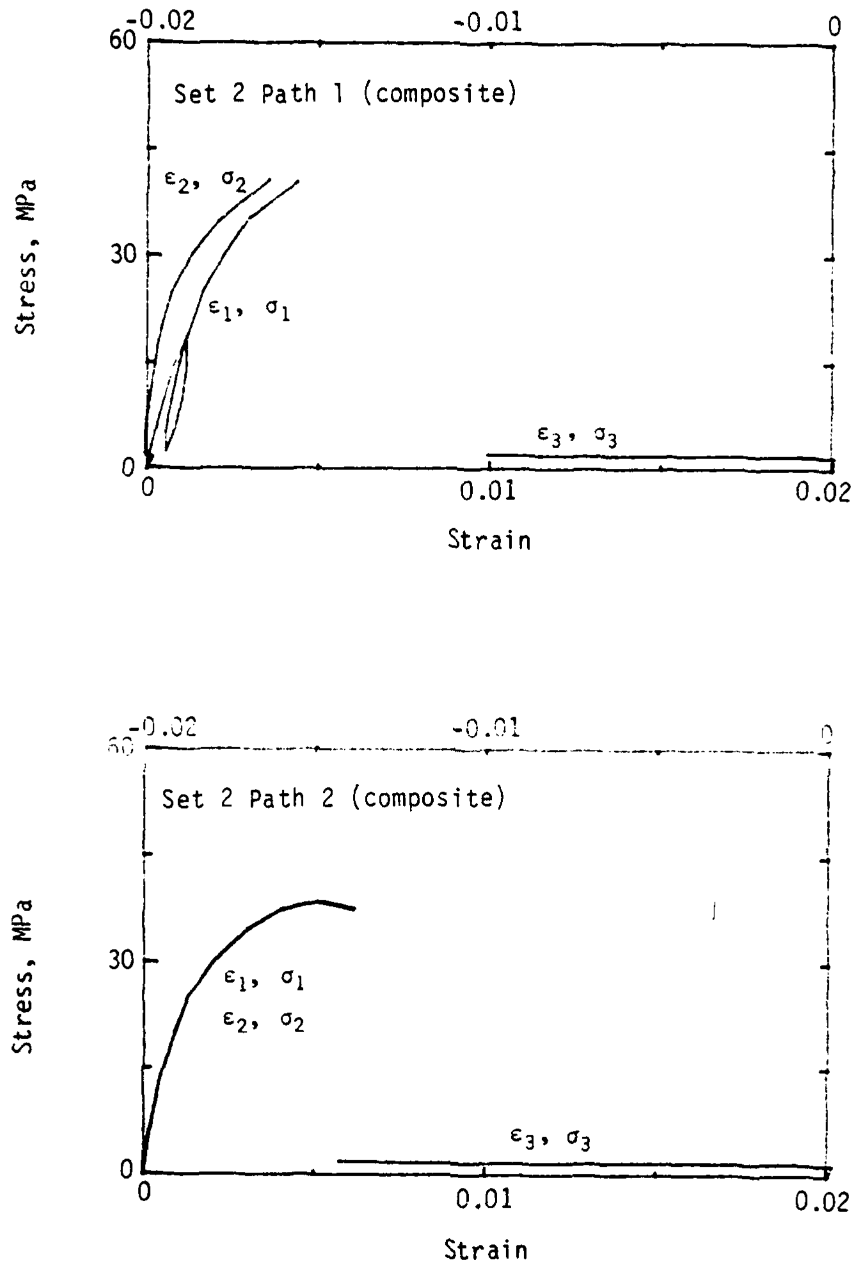

(a) Paths 1 and 2.

Figure 6. Composite stress-strain curves, set 2.

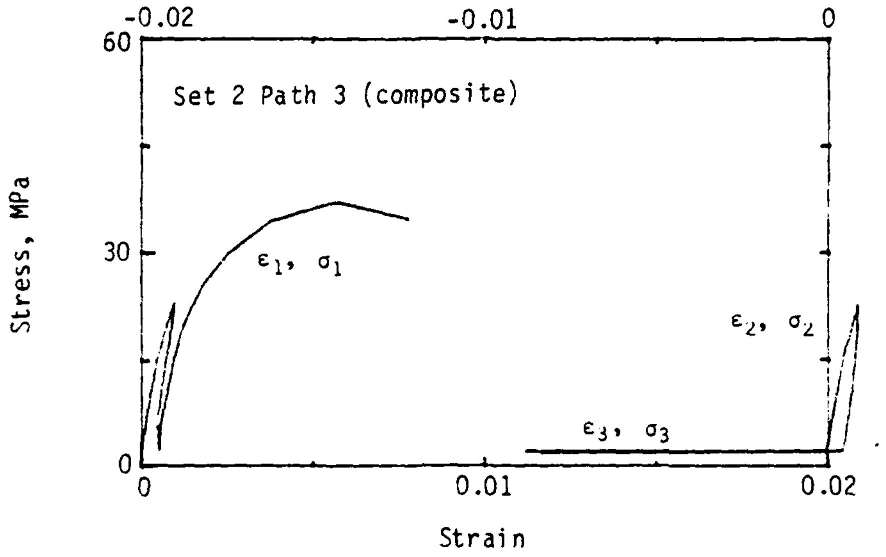

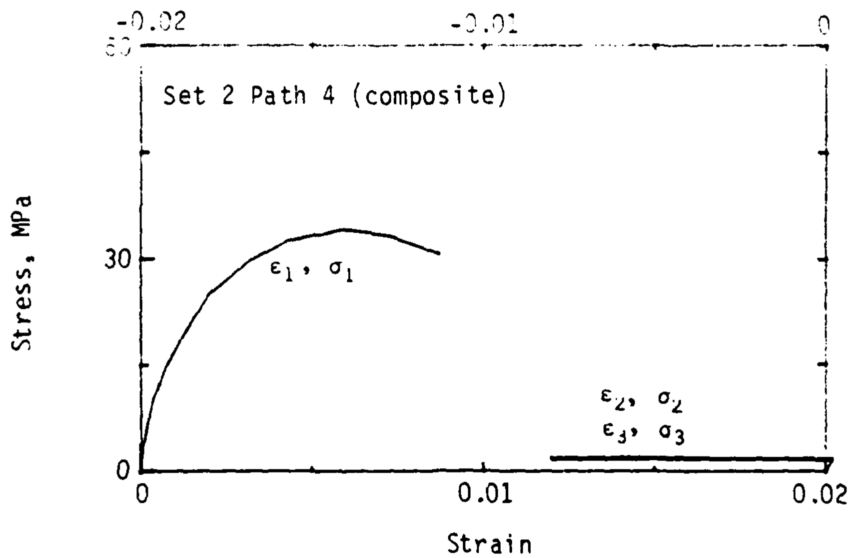

(b) Paths 3 and 4.

Figure 6. Continued.

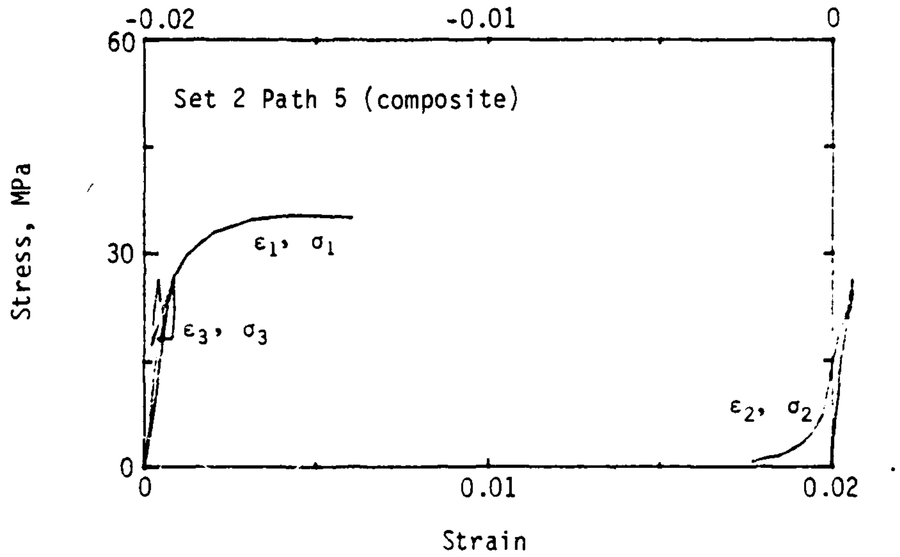

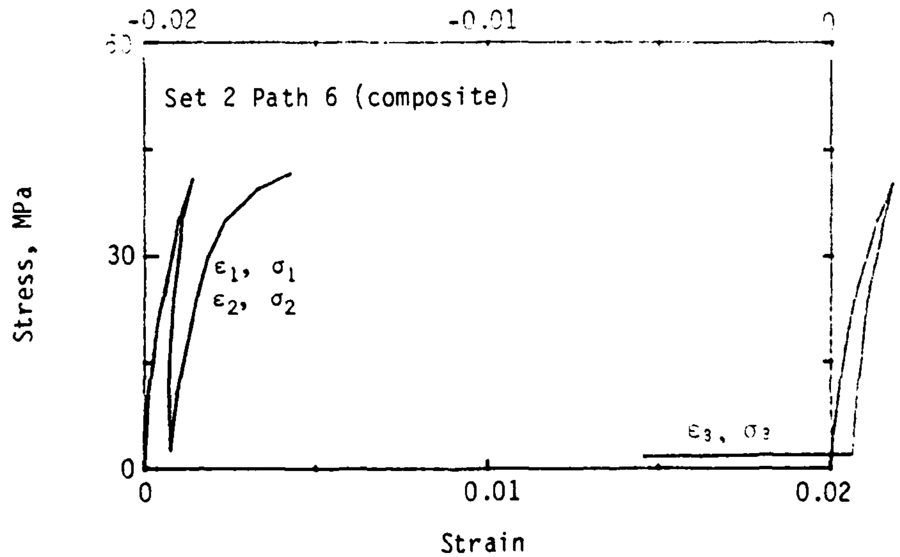

(c) Paths 5 and 6.

Figure 6. Continued.

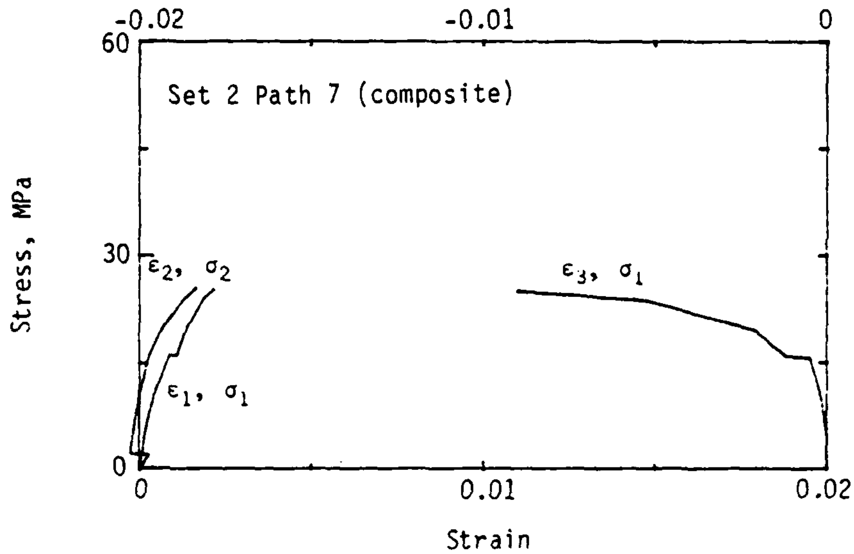

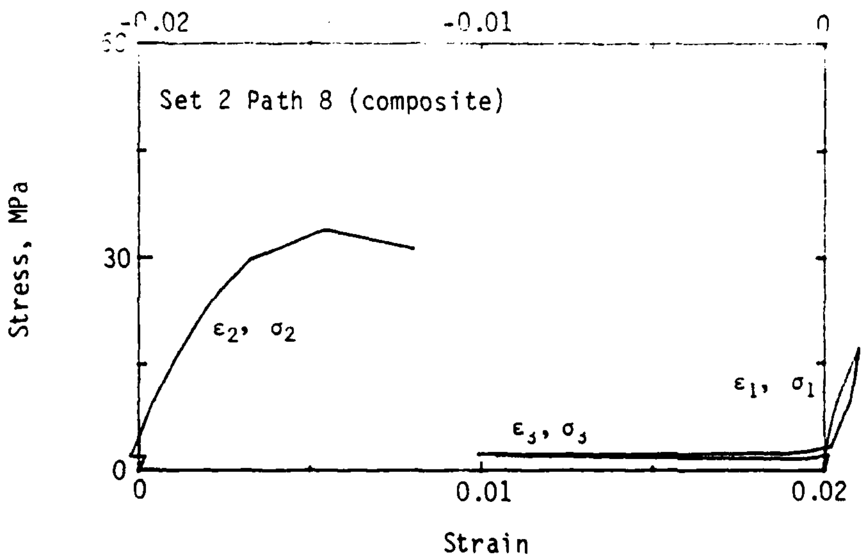

(d) Paths 7 and 8.

Figure 6. Continued.

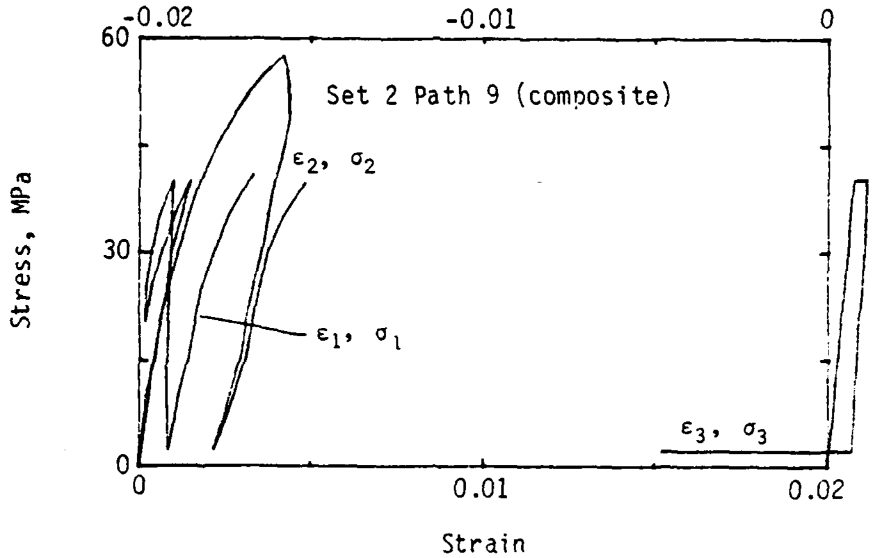

(e) Path 9.

Figure 6. Concluded.

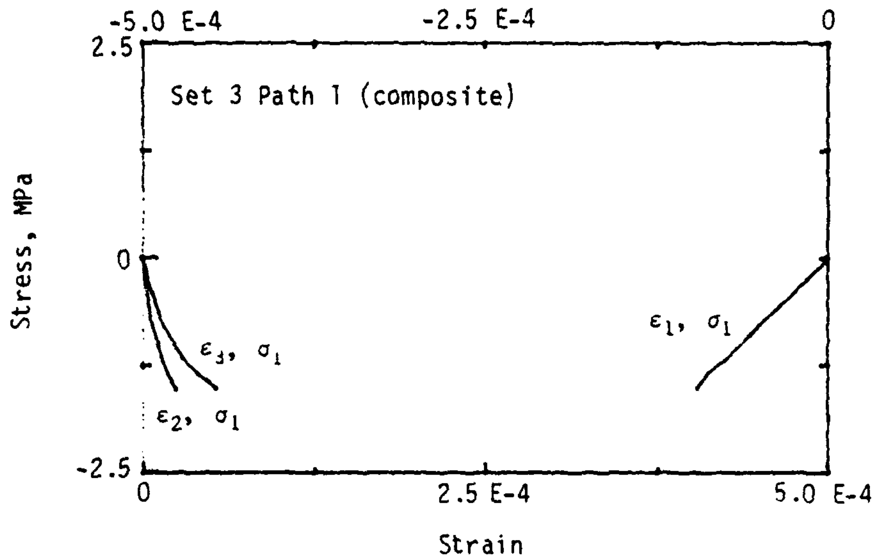

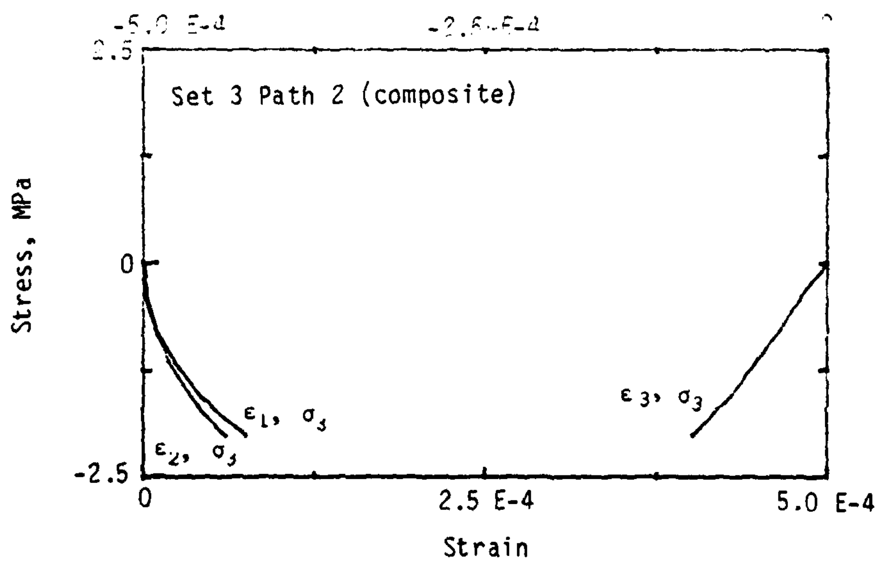

(a) Paths 1 and 2.

Figure 7. Composite stress-strain curves, set 3.

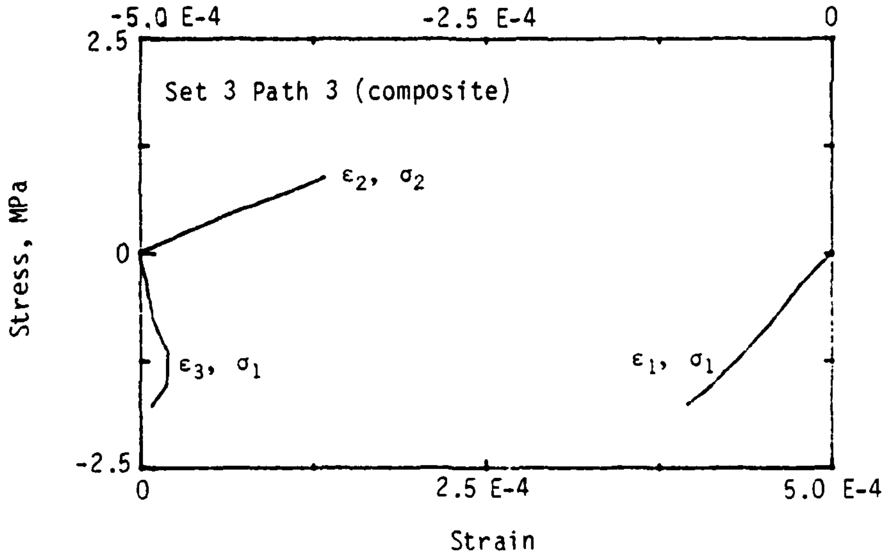

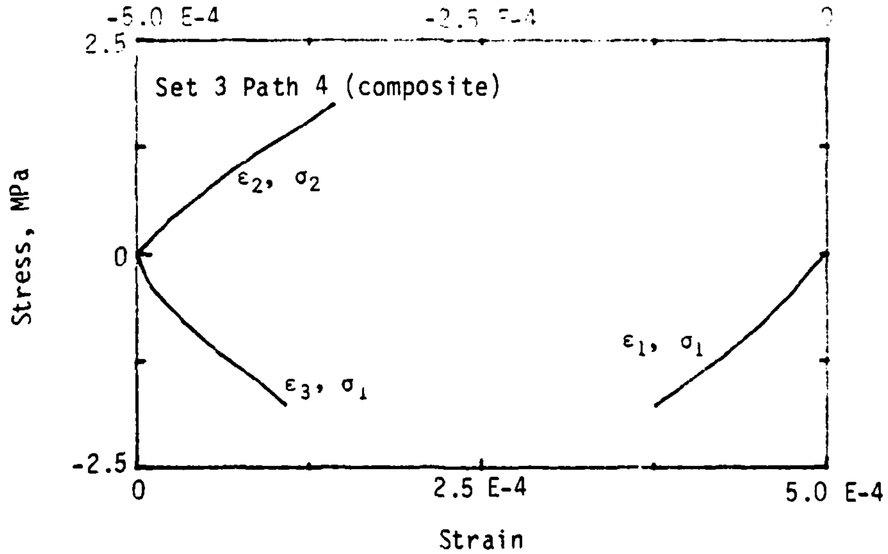

(b) Paths 3 and 4.

Figure 7. Continued.

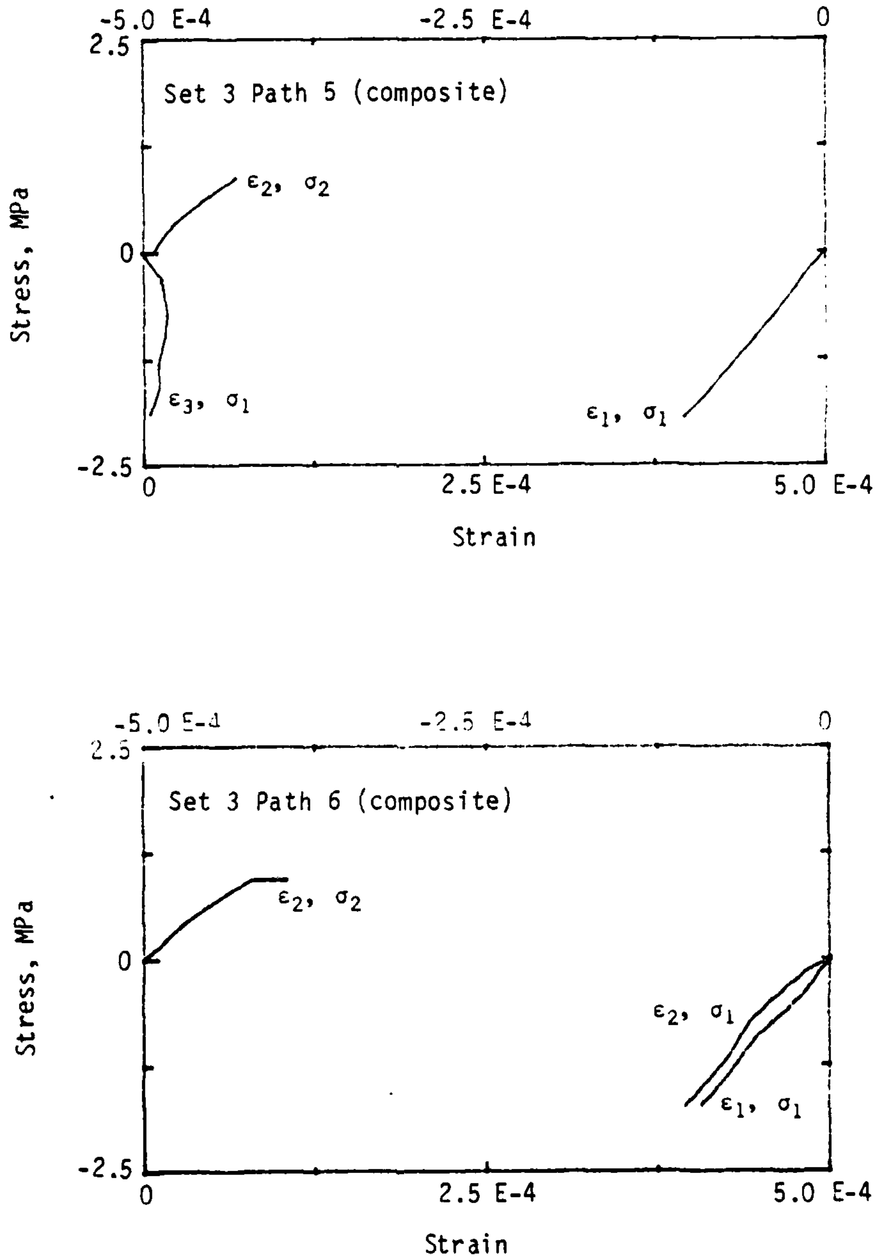

(c) Paths 5 and 6.

Figure 7. Continued.

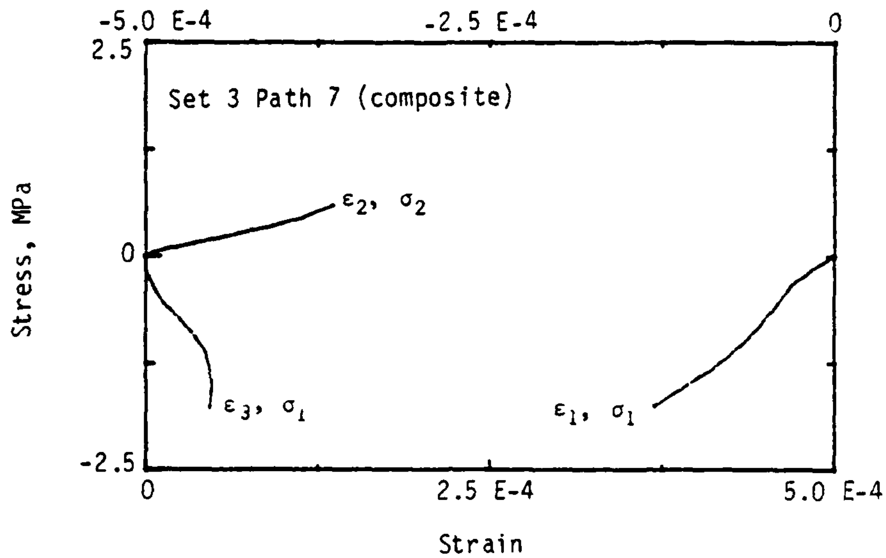

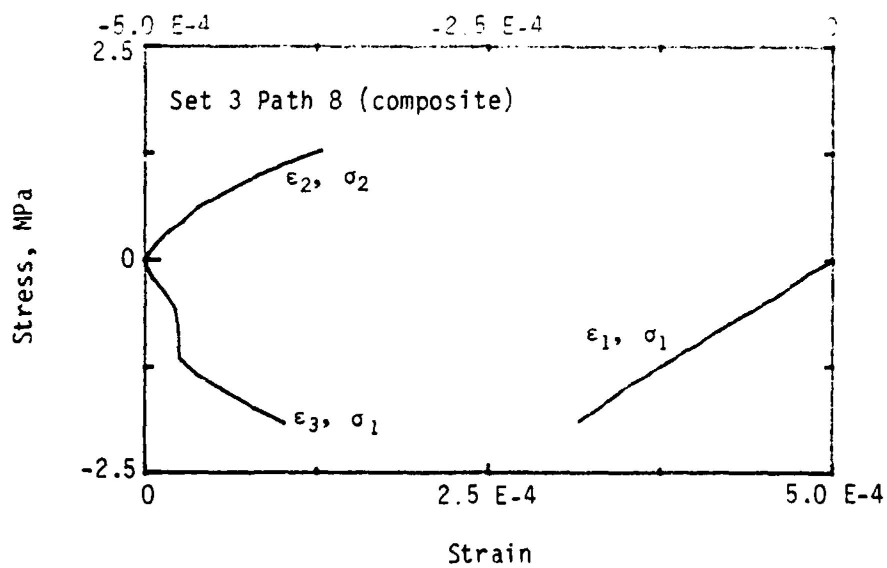

(d) Paths 7 and 8.

Figure 7. Concluded.

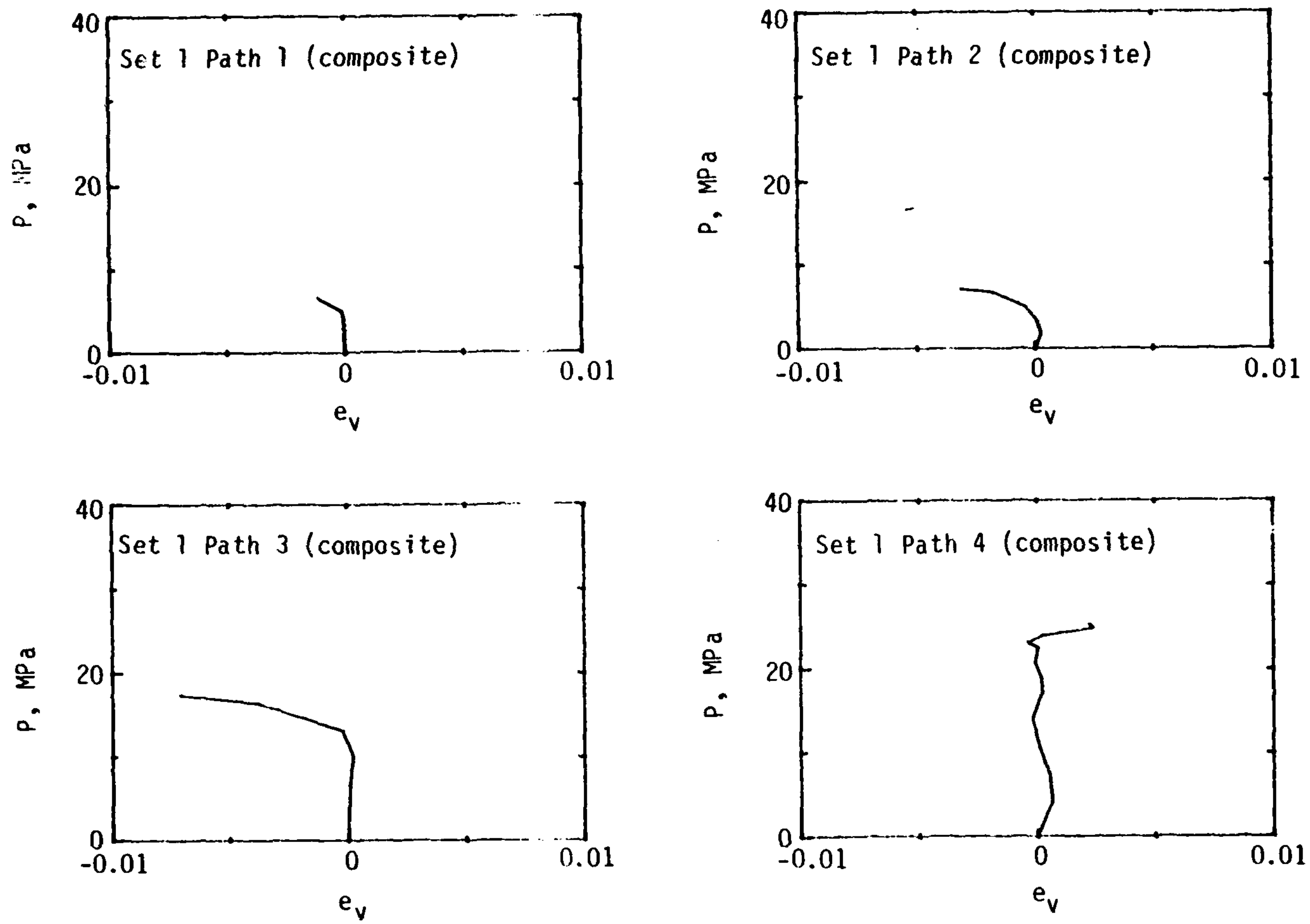

(a) Paths 1 through 4.

Figure 8. Composite pressure-volumetric strain curves, set 1.

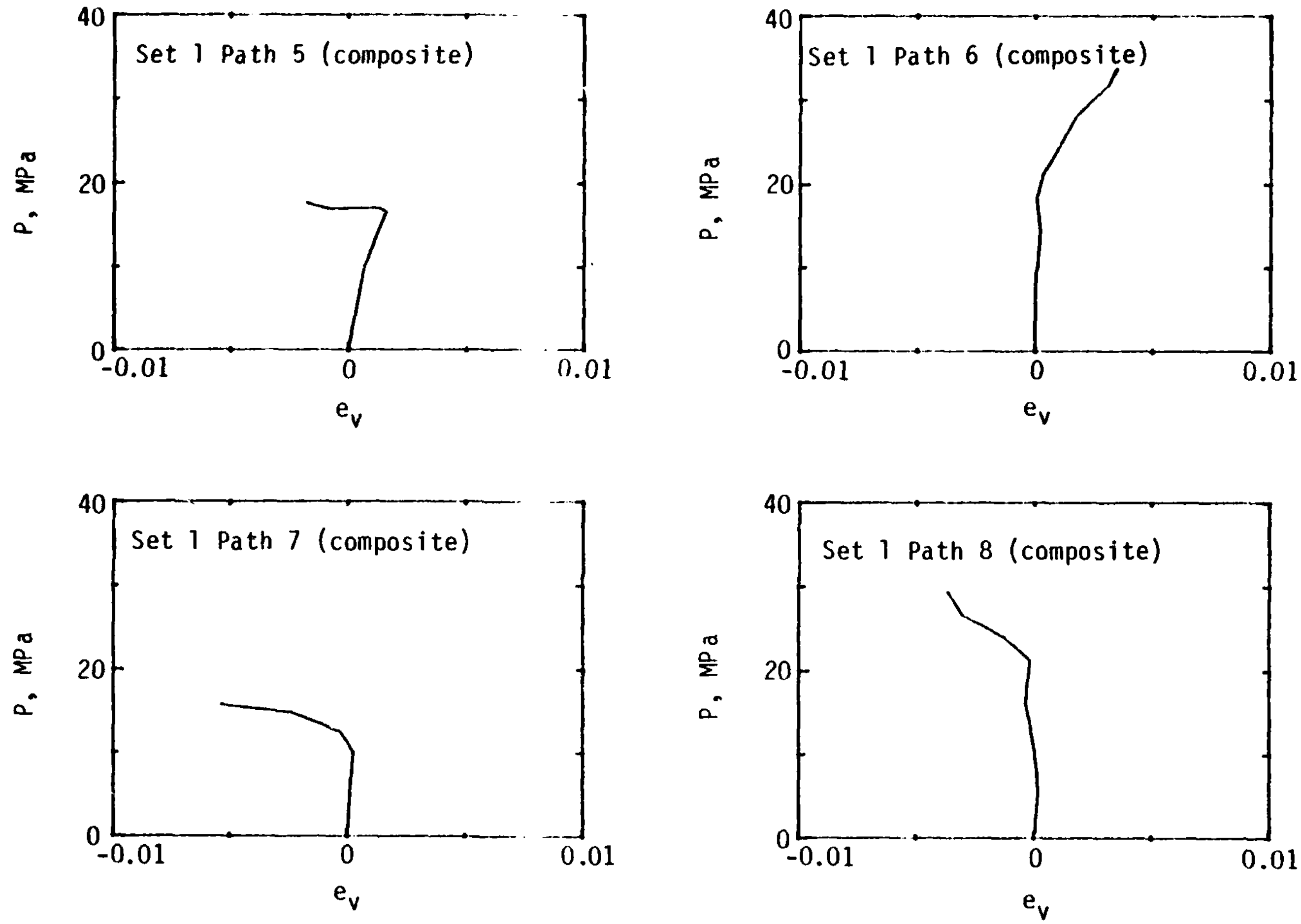

(b) Paths 5 through 8.

Figure 8. Concluded.

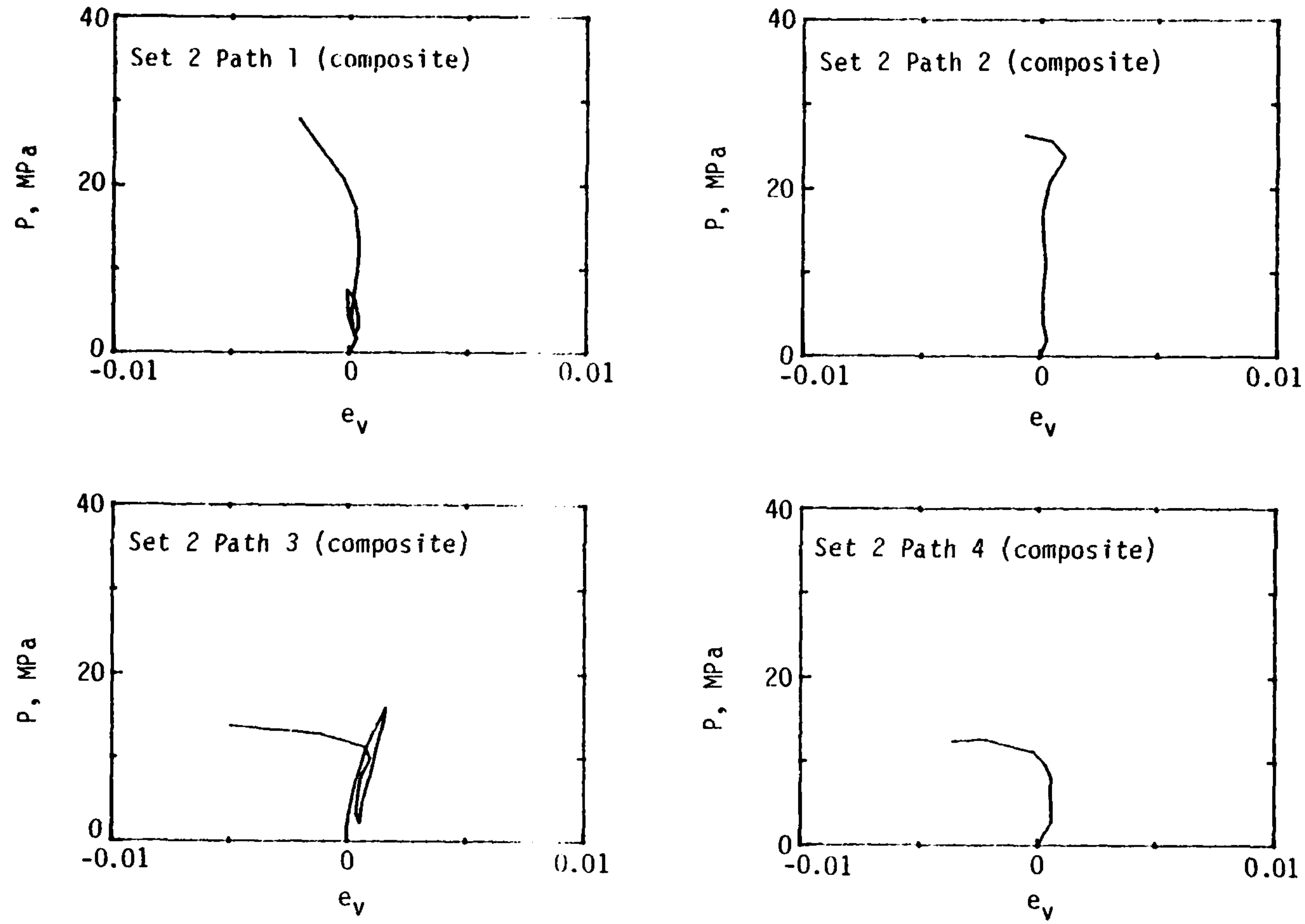

(a) Paths 1 through 4.

Figure 9. Composite pressure-volumetric strain curves, set 2.

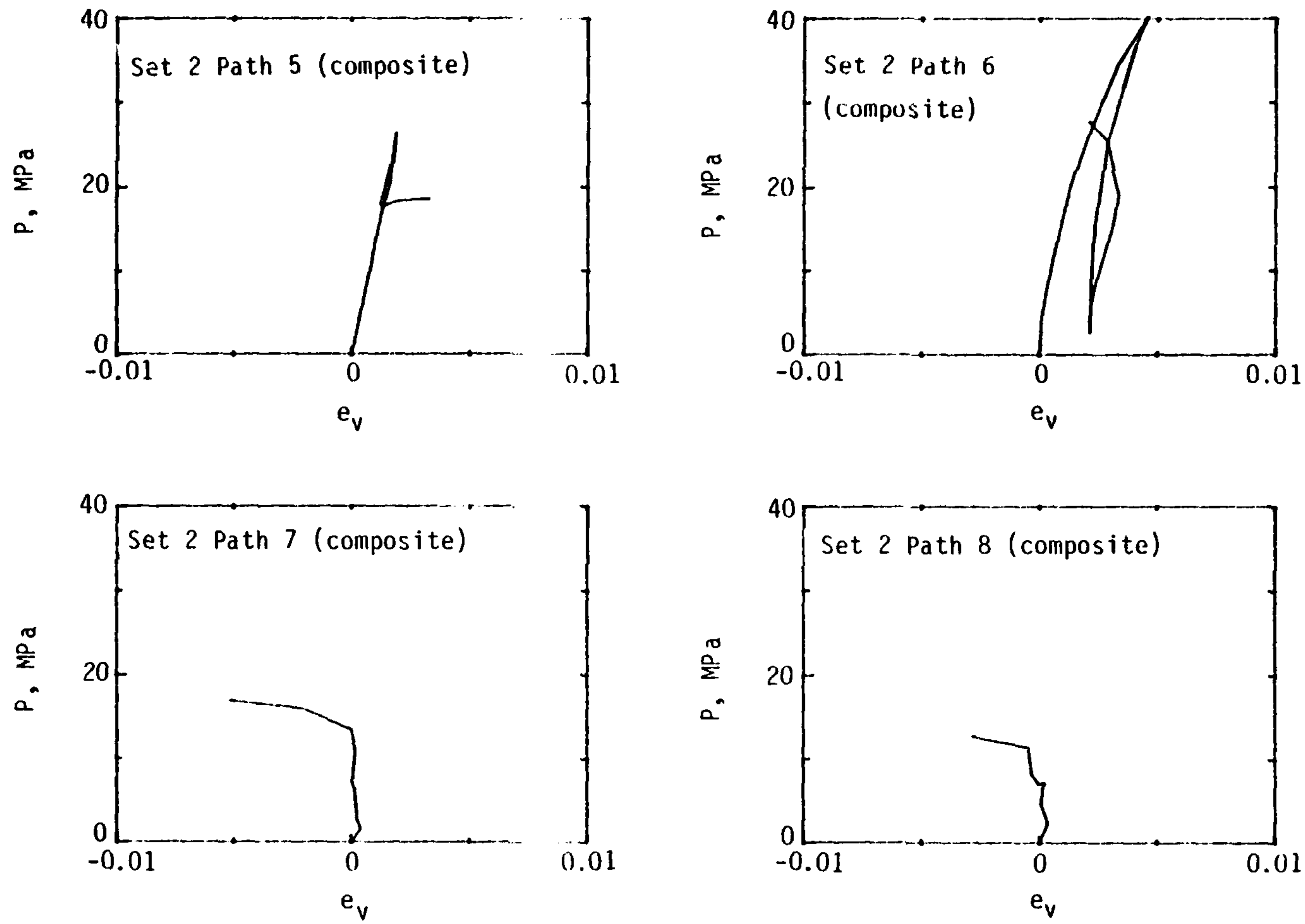

(b) Paths 5 through 8.

Figure 9. Continued.

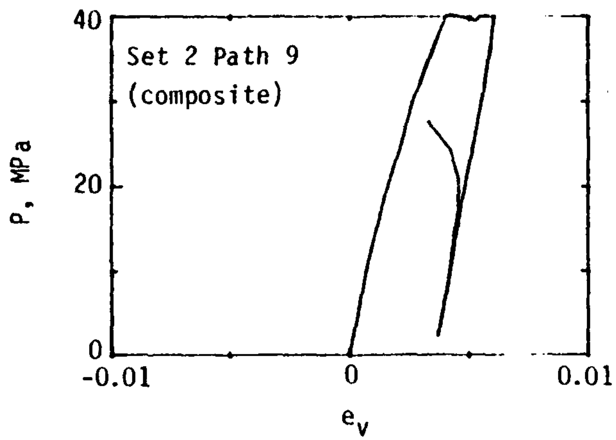

(c) Path 9.

Figure 9. Concluded.

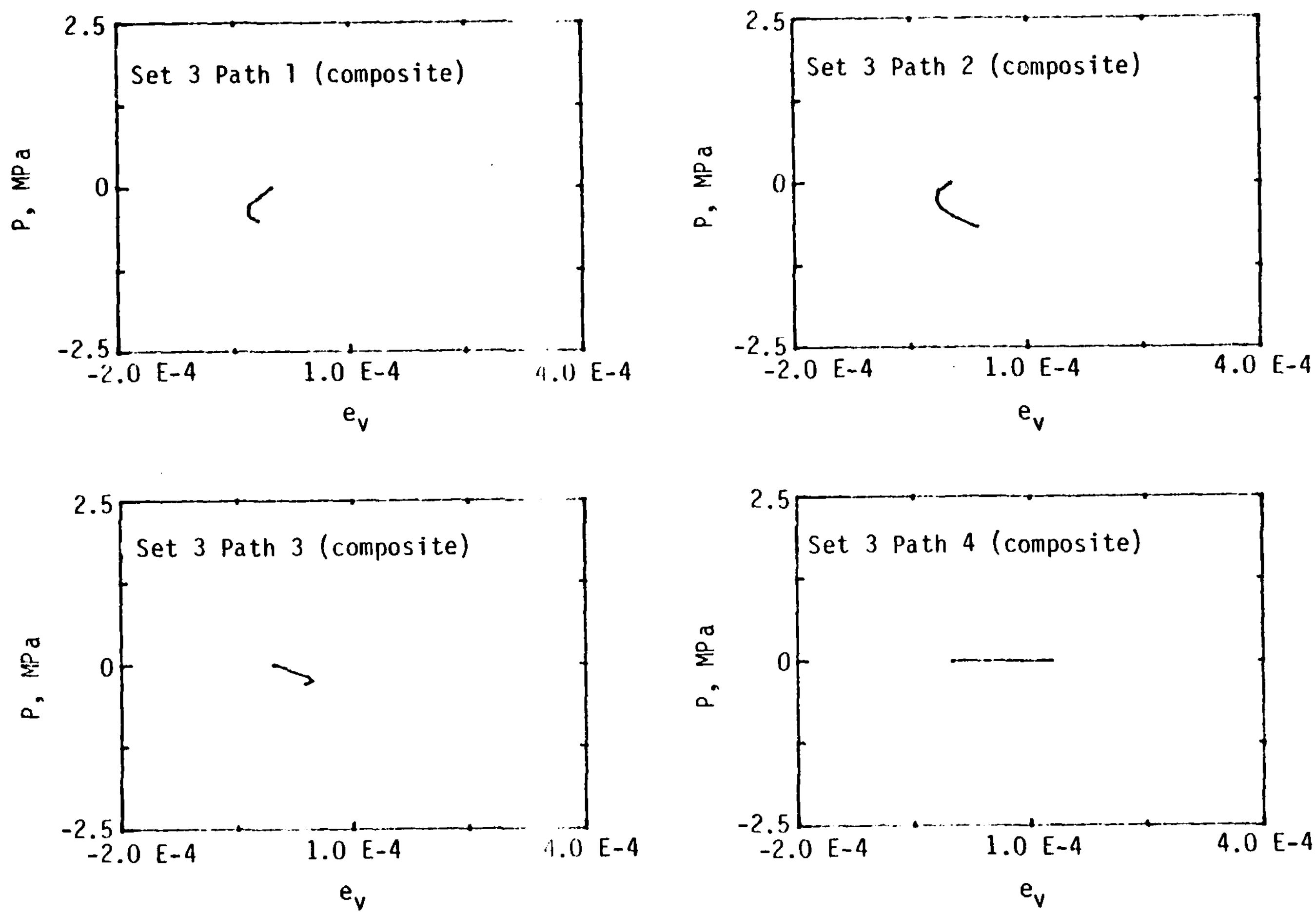

(a) Paths 1 through 4.

Figure 10. Composite pressure-volumetric strain curves, set 3.

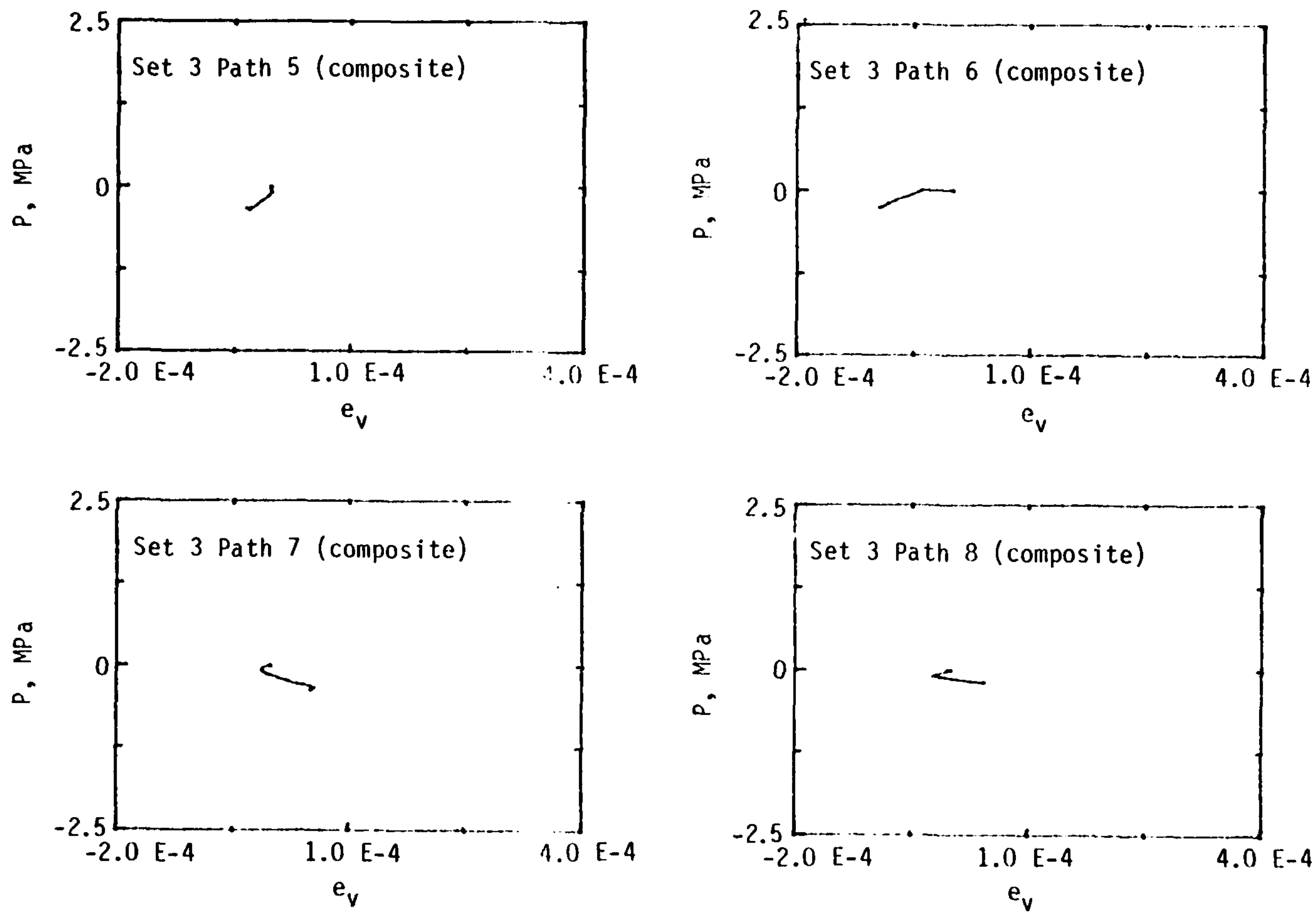

(b) Paths 5 through 8.

Figure 10. Continued.

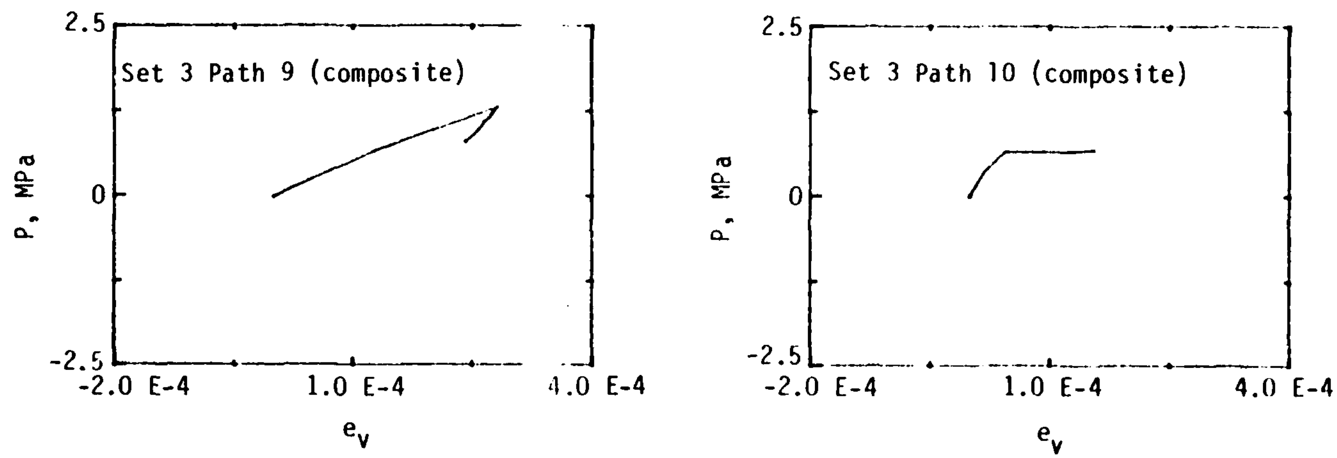

(c) Paths 9 and 10.

Figure 10. Concluded.

VI. DEFORMATION PATHS AND LIMIT STATES INVOLVING STRAIN PATH INVARIANTS

Strain path invariants comprise an important part of the theory of plasticity if such a model is used to predict the hardening and softening behavior of a material. To adequately predict the limit state in terms of strain, a relationship involving strain invariants is needed. No completely reliable relationship has been defined, but approximate relationships based on some form of the strain invariants have been used with adequate results. Because the strain invariants are central to algorithms used in the attempt to predict the behavior of materials, three strain path invariants are considered here. These invariants are defined as follows:

$$e_v^i = \int tr\left(d\underset{\sim}{e}^i\right)$$

$$e_s^i = \int \left(tr\ d\underset{\sim}{e}^{id} d\underset{\sim}{e}^{id}\right)^{1/2}$$

$$e_3^i = \int \left|\det\ d\underset{\sim}{e}^i\right|^{1/3}$$

where $\underset{\sim}{e}^i$ is the inelastic strain $(\underset{\sim}{e}^i = \underset{\sim}{e}^t - \underset{\sim}{e}^e)$, $\underset{\sim}{e}^{id}$ is the inelastic strain deviator, $\underset{\sim}{e}^t$ is the total (measured) strain, and $\underset{\sim}{e}^e$ is the elastic strain.

Plots of e_s^i versus e_v^i and of e_3^i versus e_v^i for the adjusted stress-strain data are given in Appendix C. Corresponding curves based on the composite stress-strain data are overlaid on the plots in the appendix and are shown separately in Figures 11 through 16. The correlation between the overlaid or composite curve and the curves based on adjusted data represents a measure of how well the composite curves were chosen in the first place. Overall, the results shown in Appendix C attest to the reasonability of the composite curves.

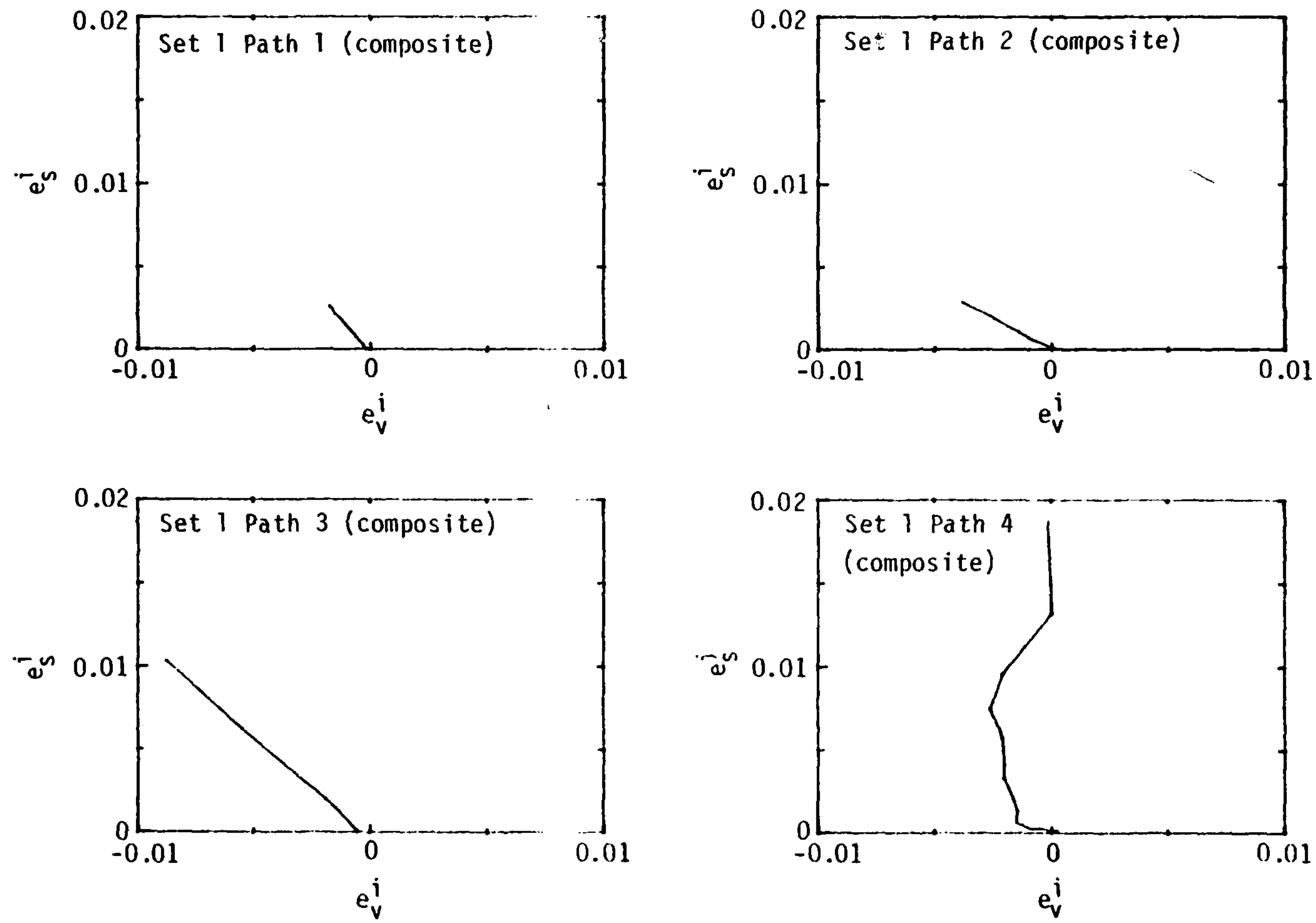

(a) Paths 1 through 4.

Figure 11. e_s^i versus e_v^i, set 1.

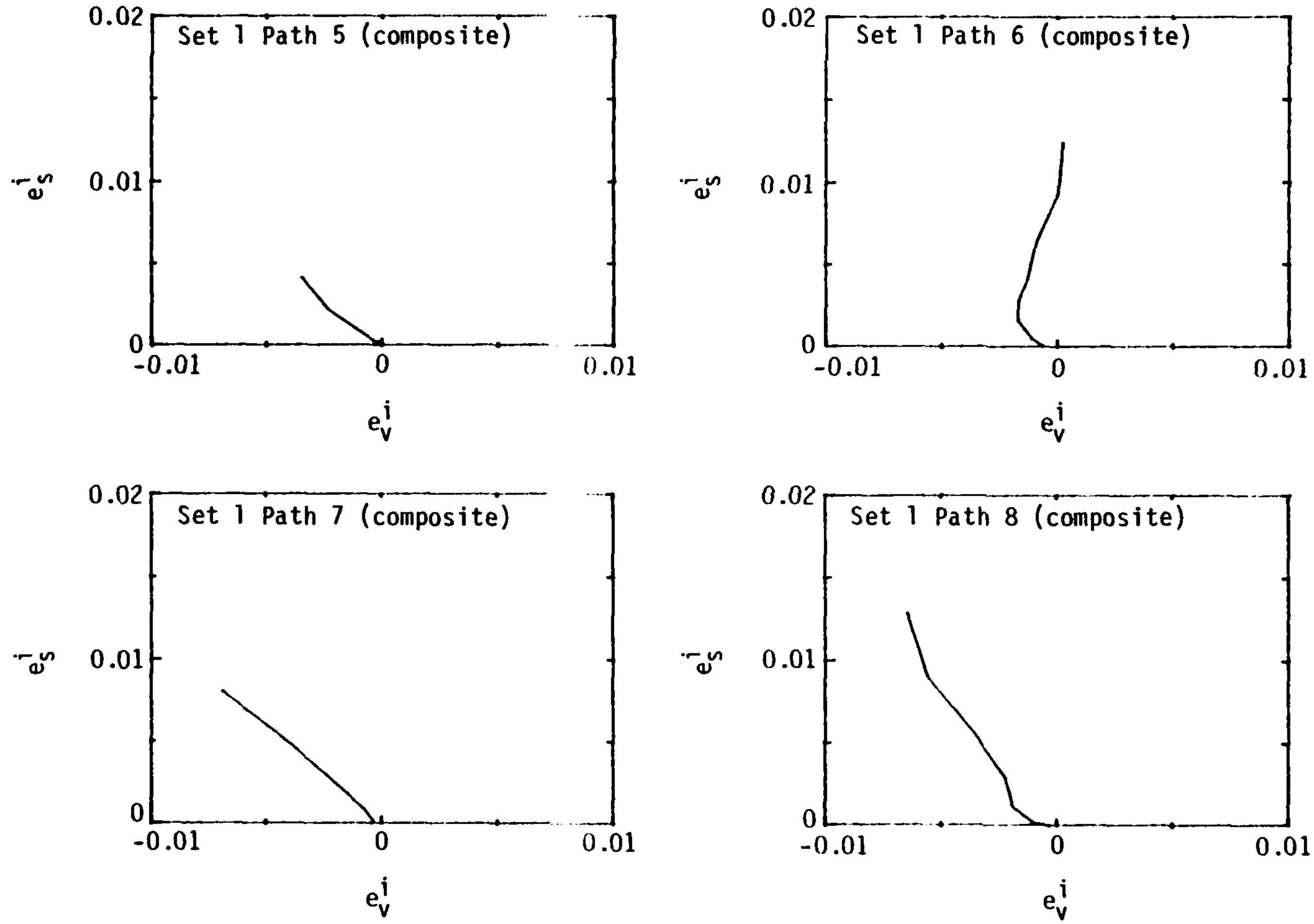

(b) Paths 5 through 8.

Figure 11. Concluded.

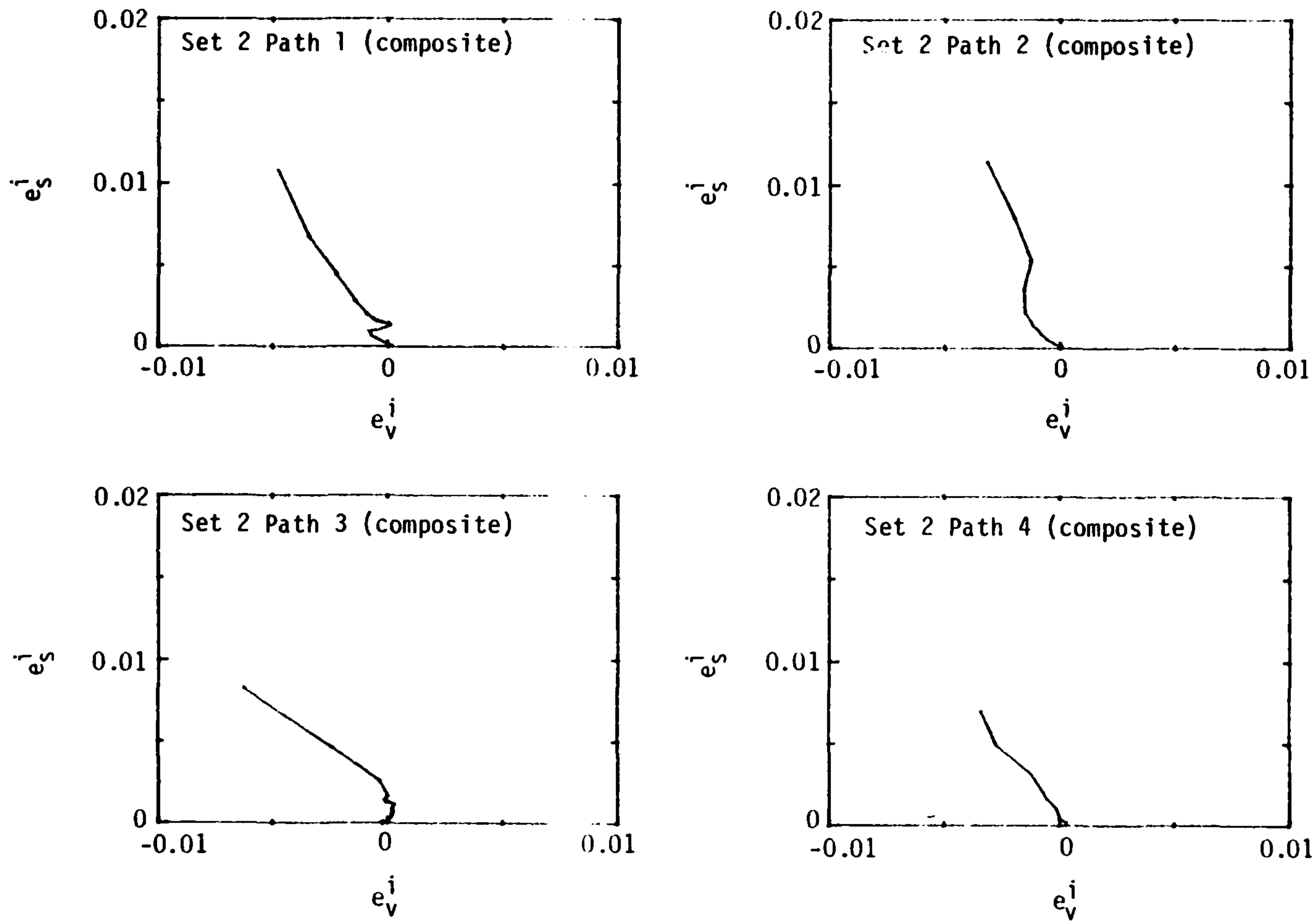

(a) Paths 1 through 4.

Figure 12. e_s^i versus e_v^i, set 2.

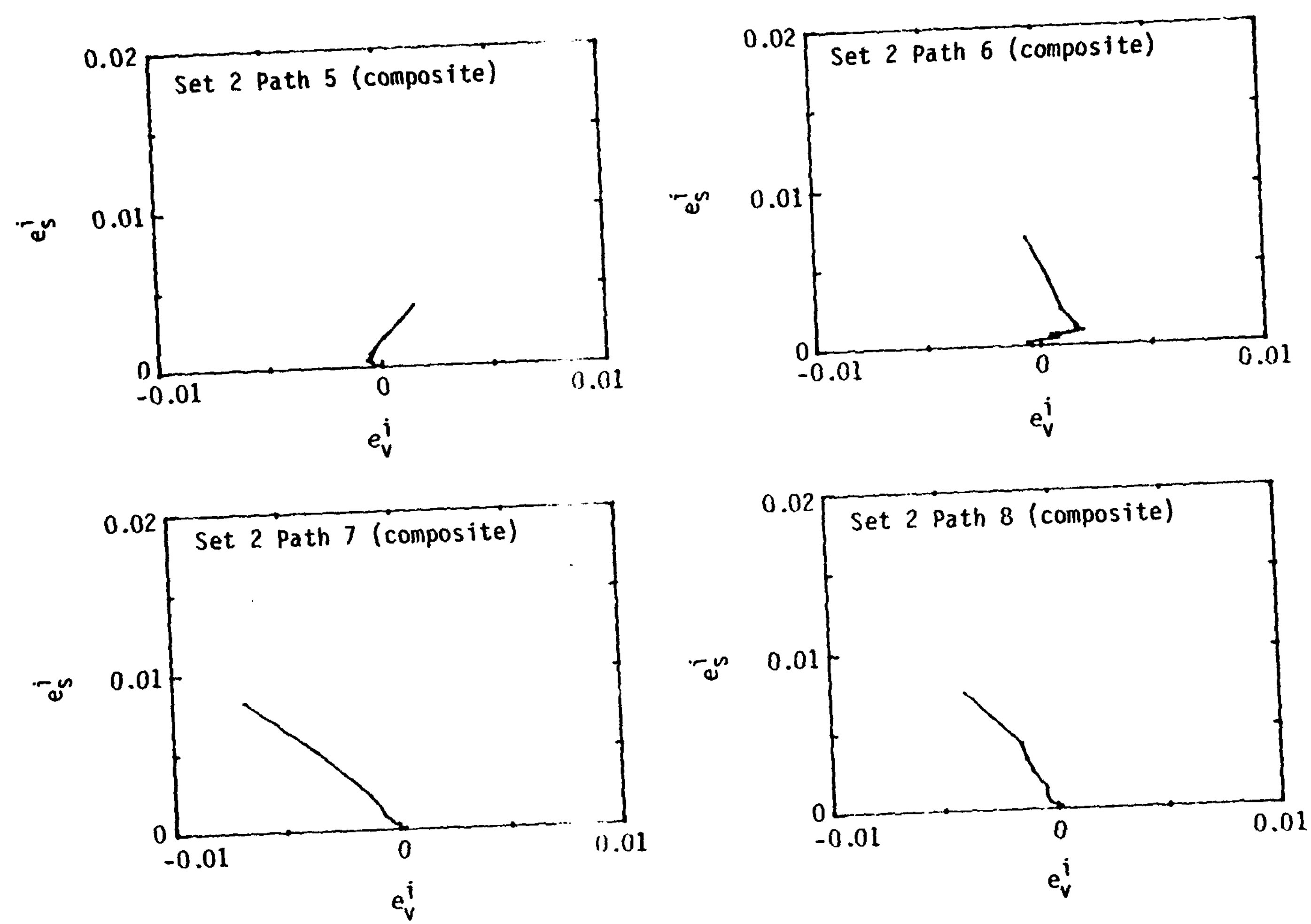

(b) Paths 5 through 8.

Figure 12. Continued.

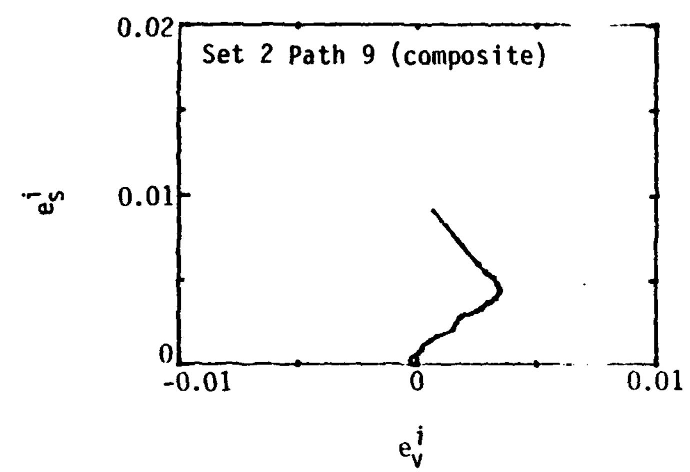

(c) Path 9.

Figure 12. Concluded.

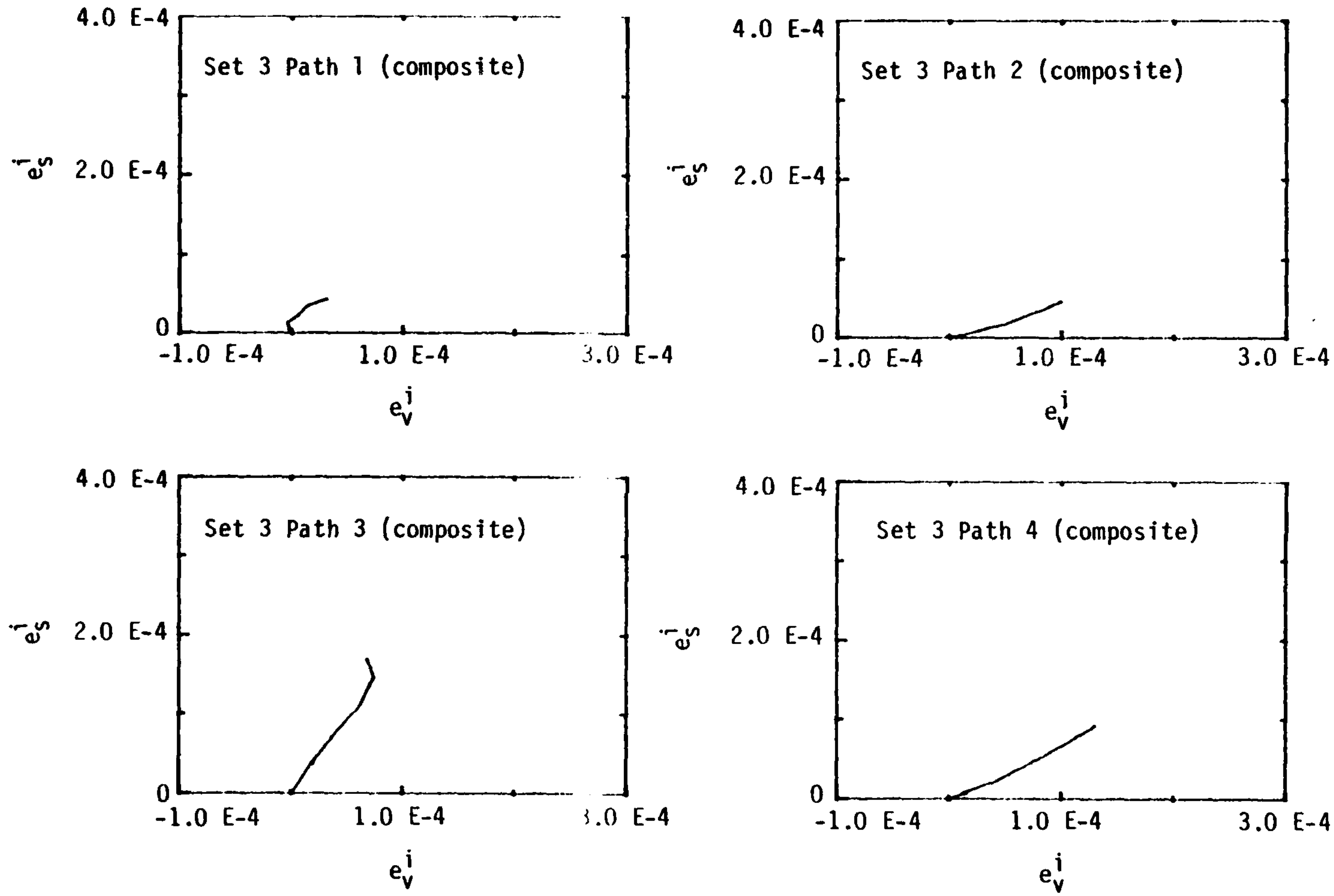

(a) Paths 1 through 4.

Figure 13. e_s^i versus e_v^i, set 3.

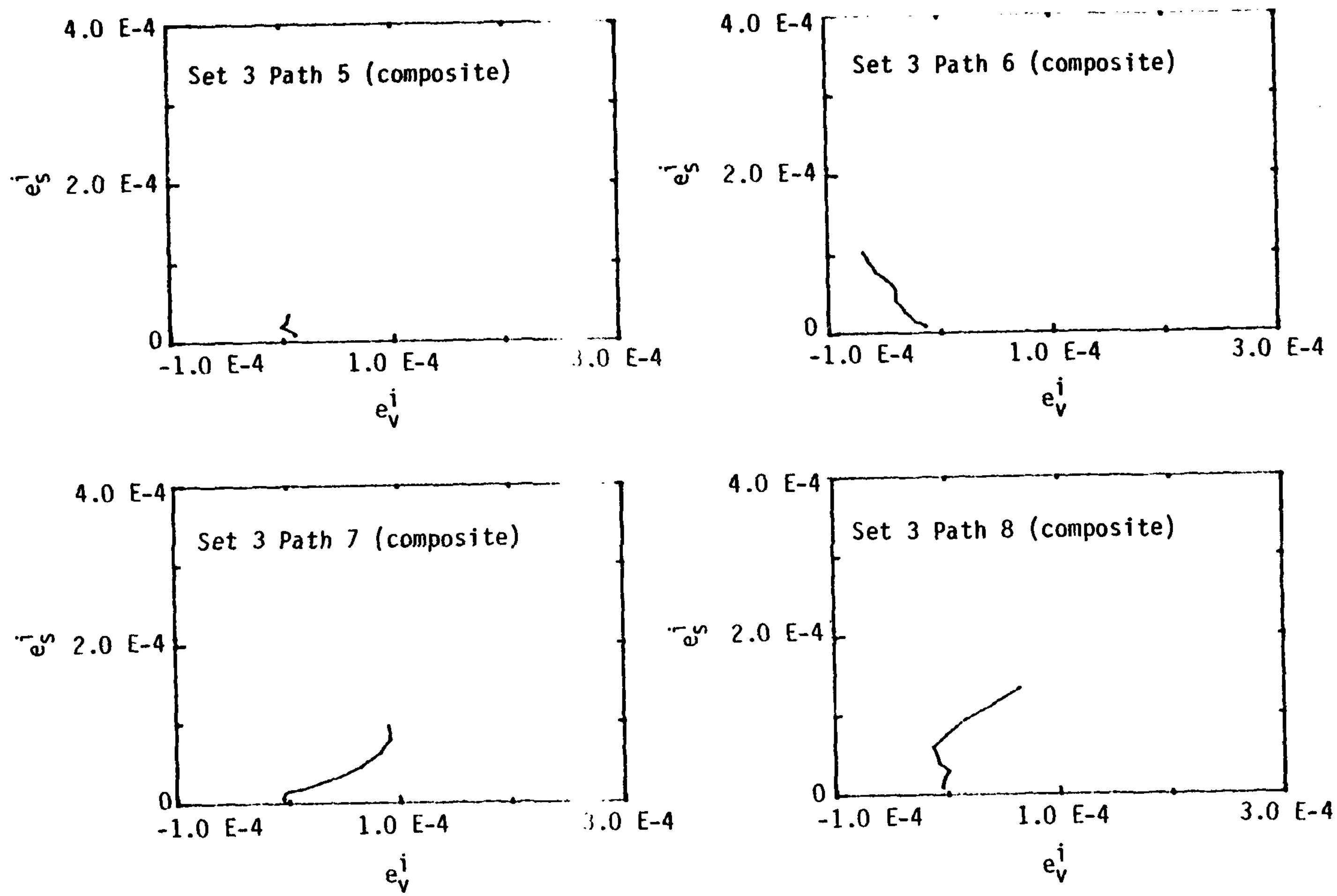

(b) Paths 5 through 8.

Figure 13. Continued.

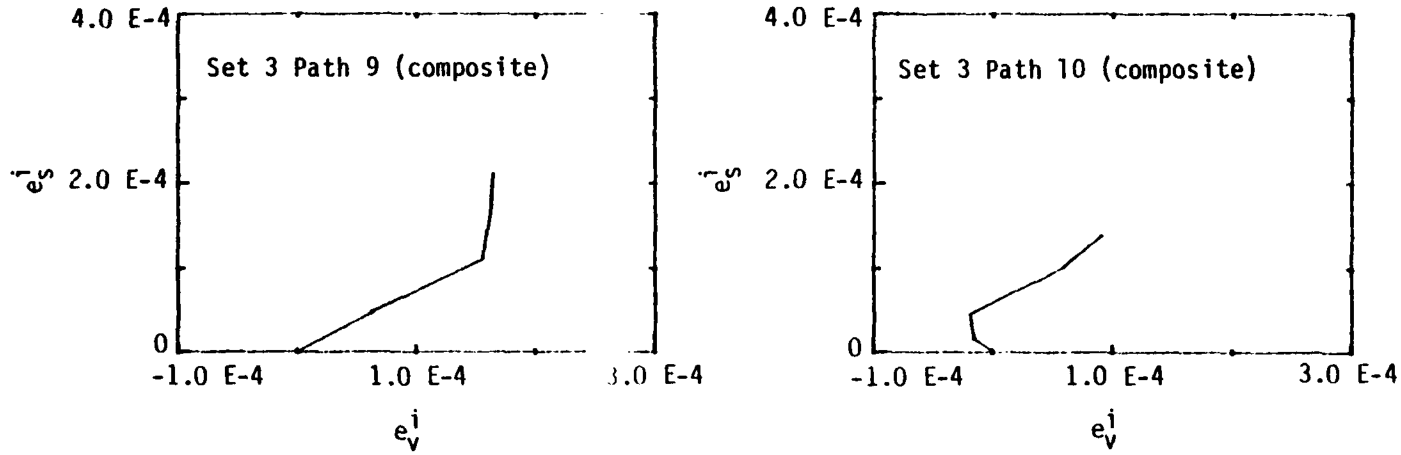

(c) Paths 9 and 10.

Figure 13. Concluded.

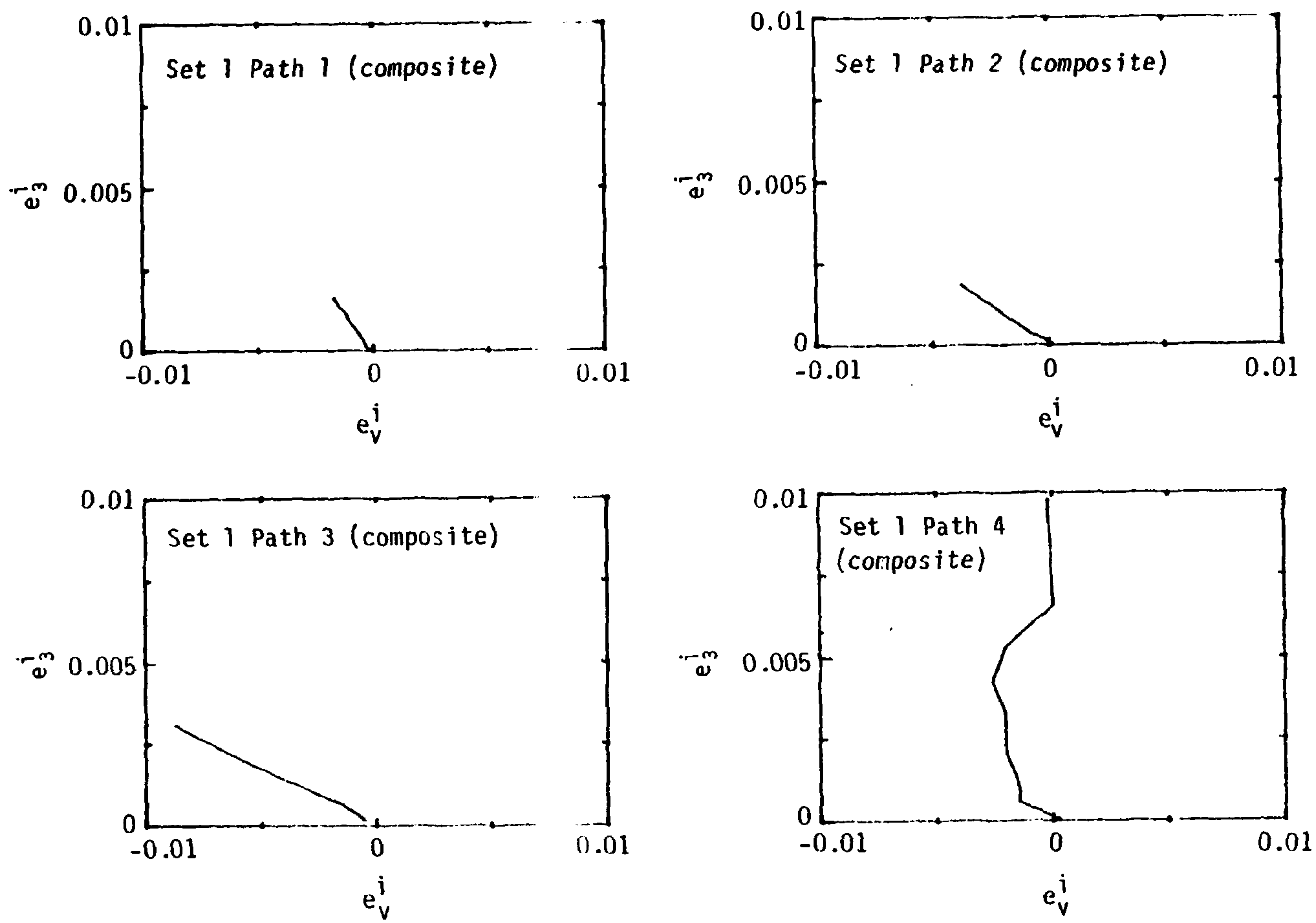

(a) Paths 1 through 4.

Figure 14. e_3^i versus e_v^i, set 1.

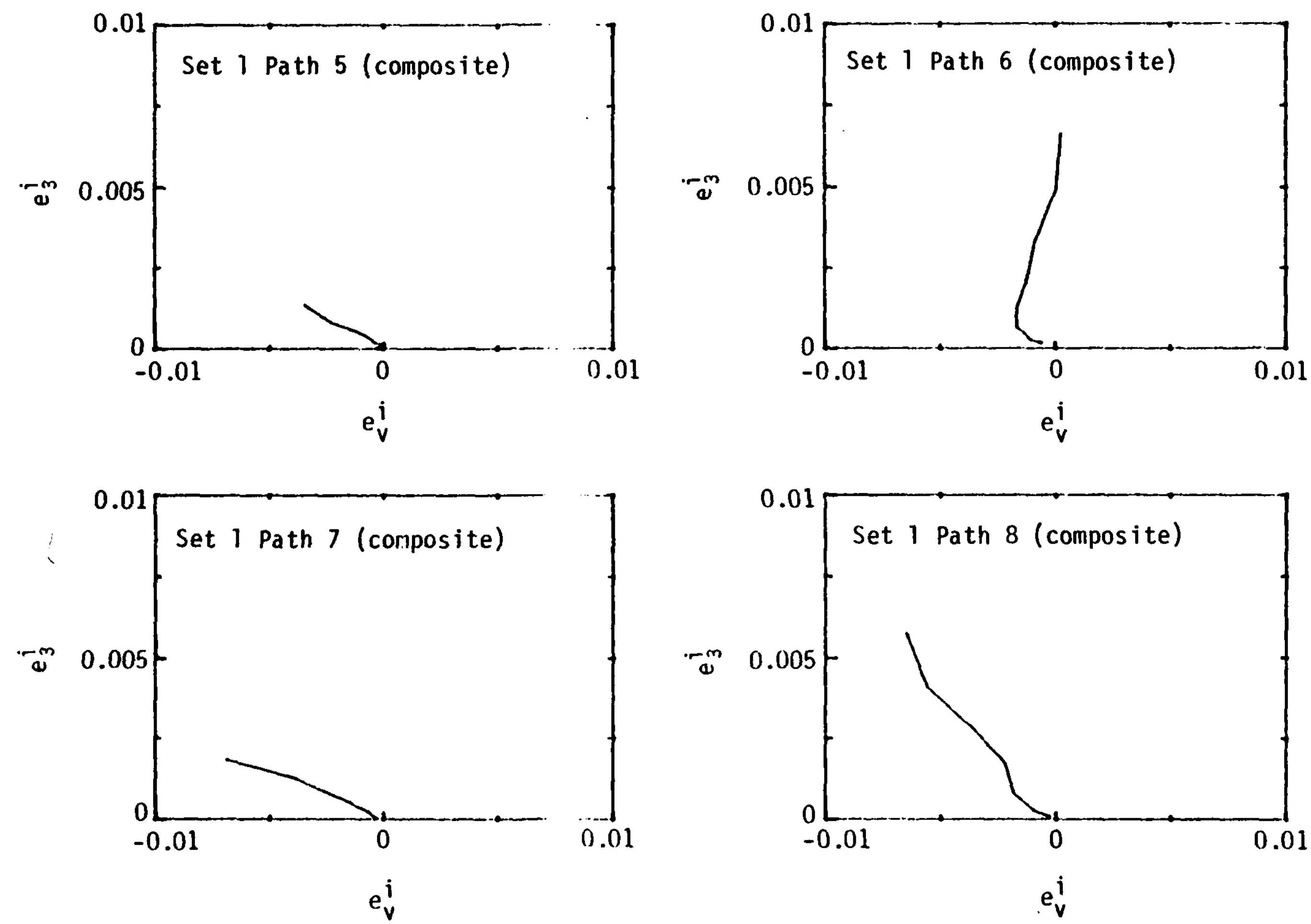

(b) Paths 5 through 8.

Figure 14. Concluded.

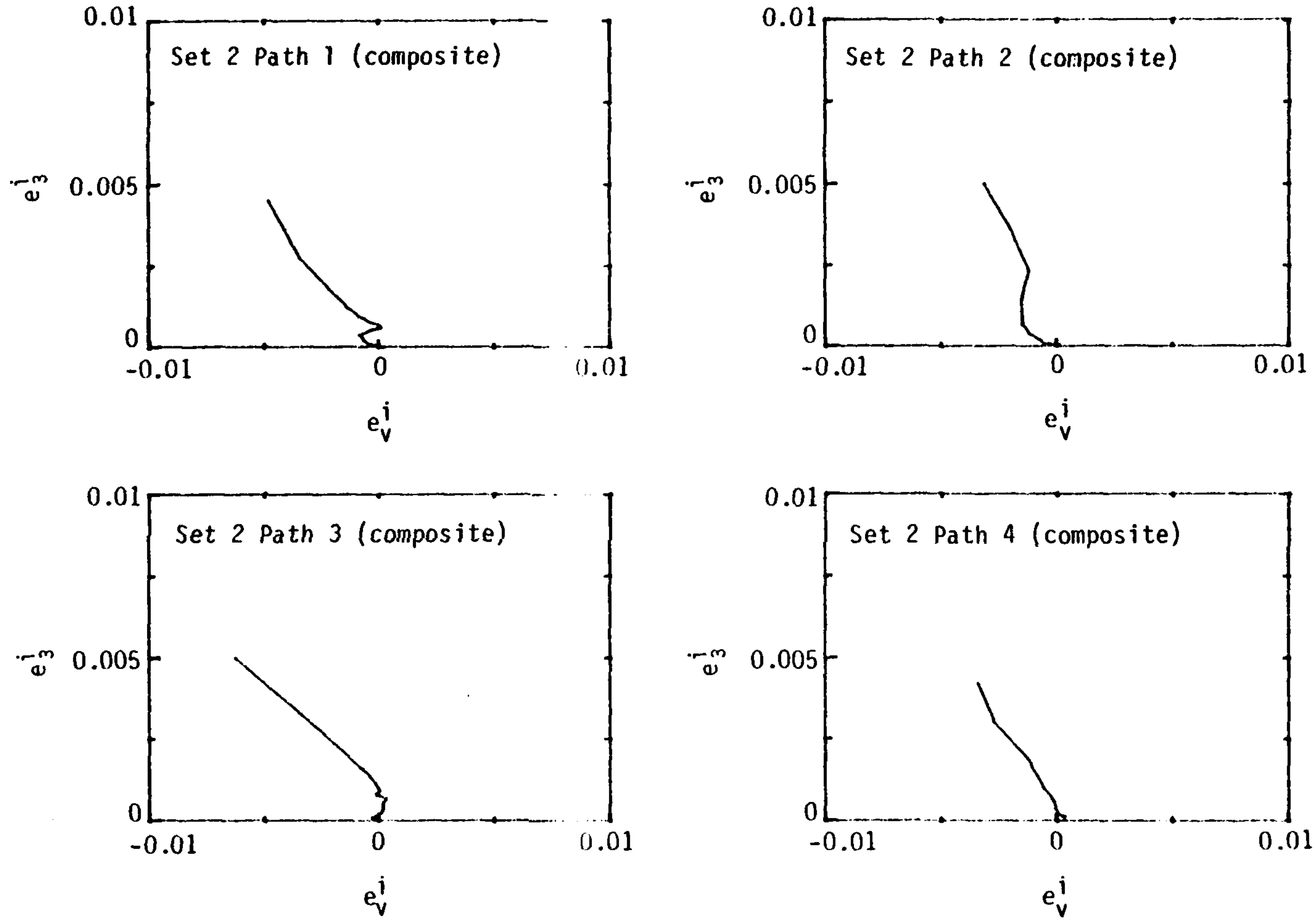

(a) Paths 1 through 4.

Figure 15. e_3^i versus e_v^i, set 2.

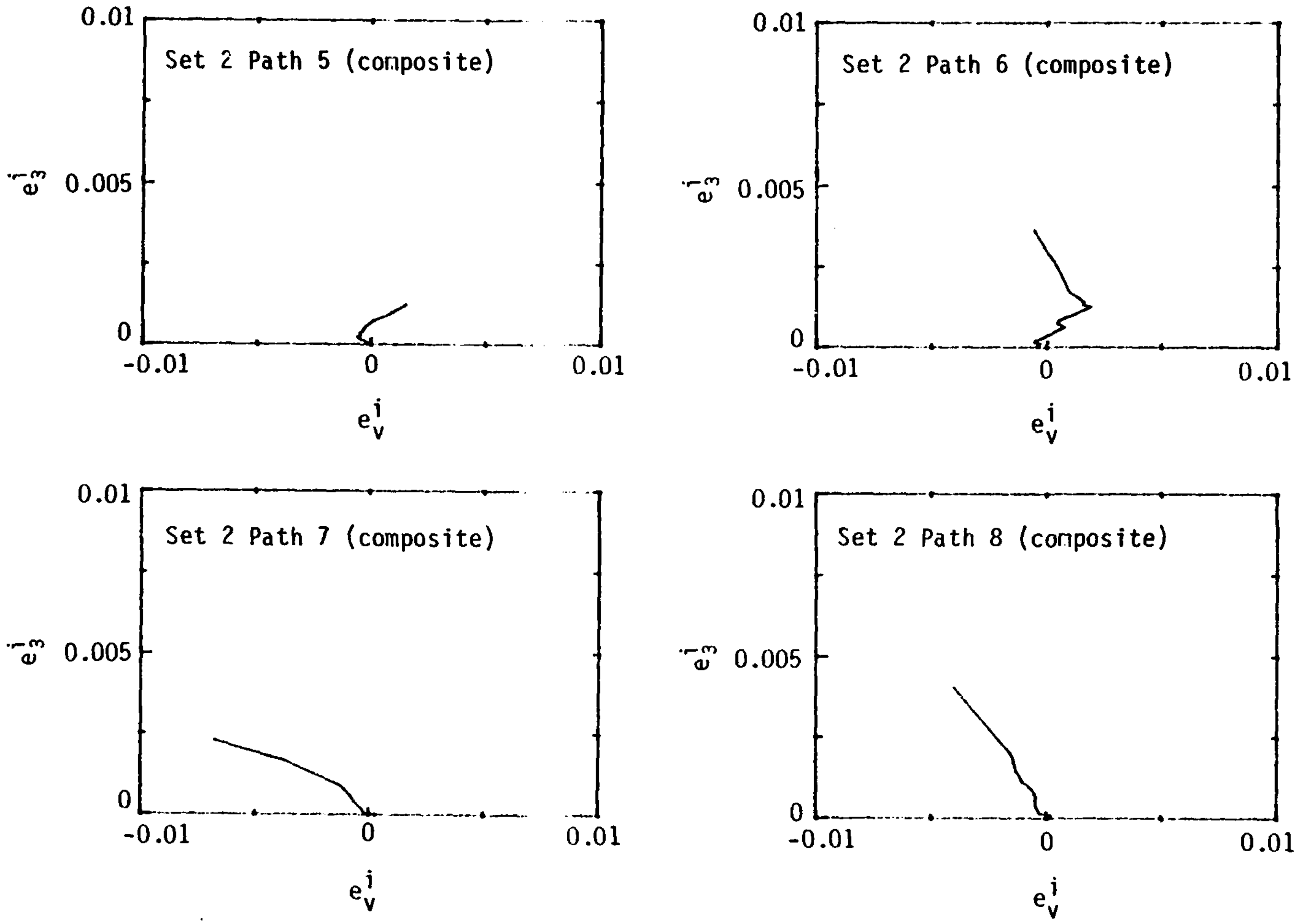

(b) Paths 5 through 8.

Figure 15. Continued.

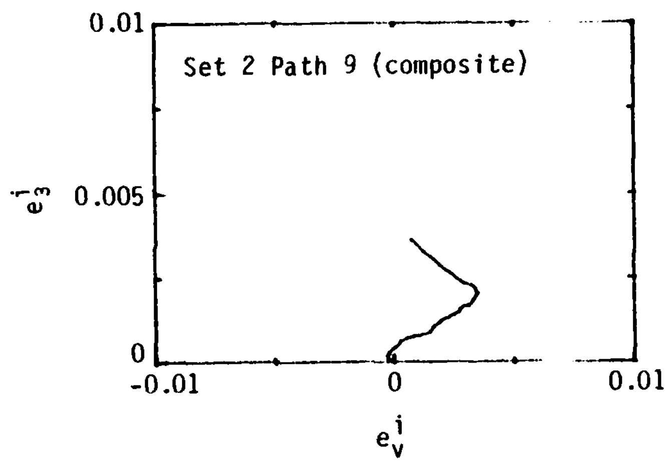

(c) Path 9.

Figure 15. Concluded.

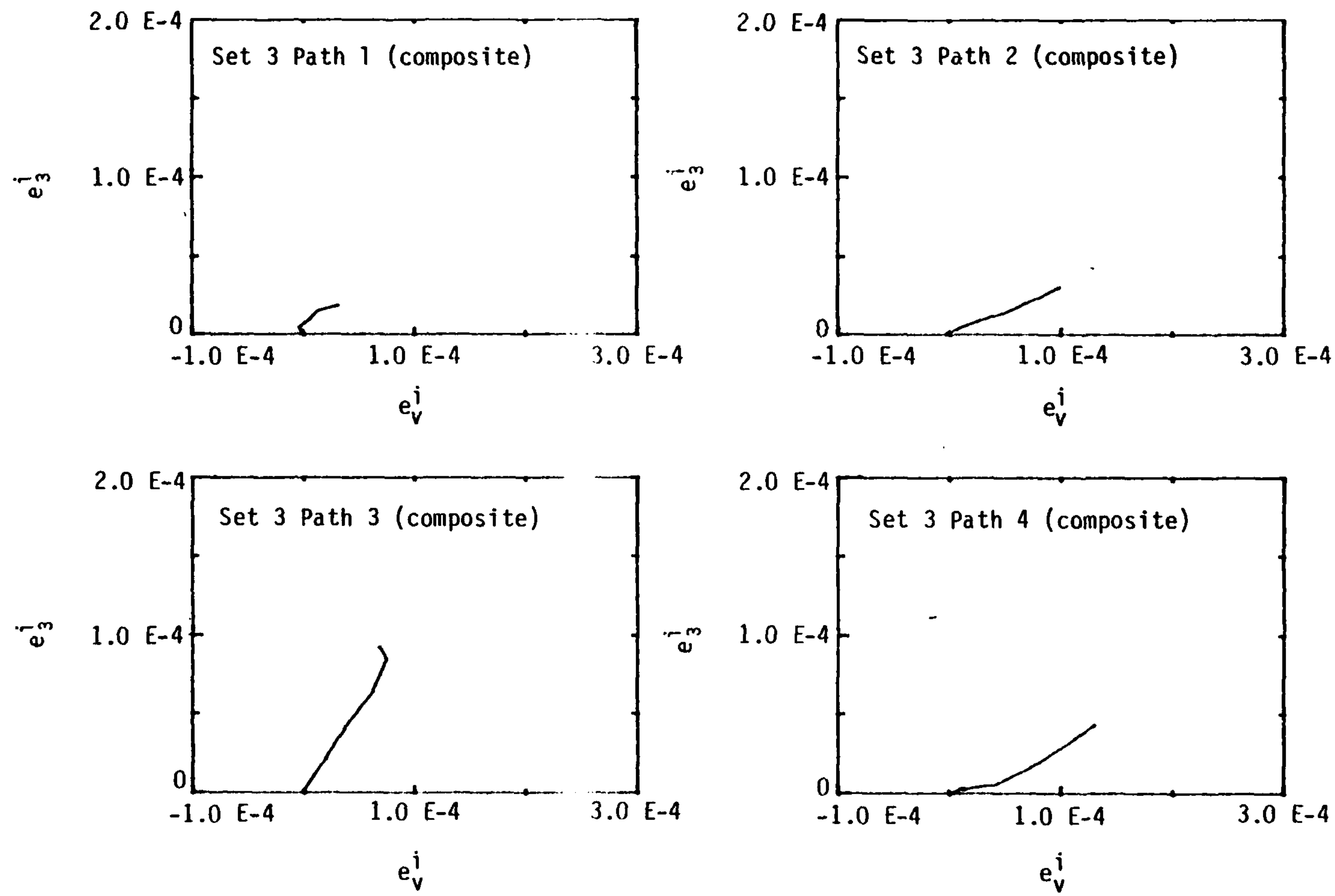

(a) Paths 1 through 4.

Figure 16. e_3^i versus e_v^i, set 3.

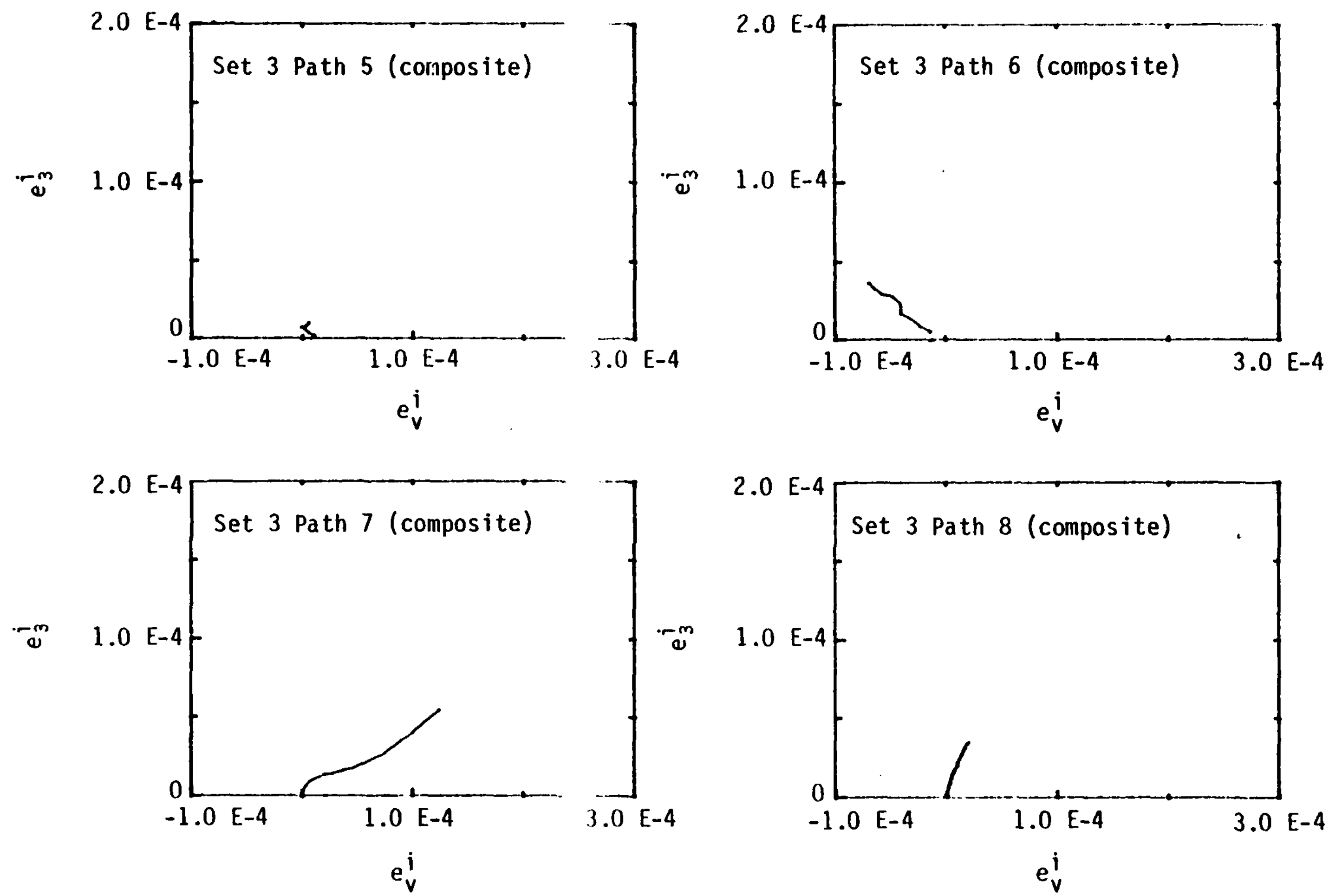

(b) Paths 5 through 8.

Figure 16. Continued.

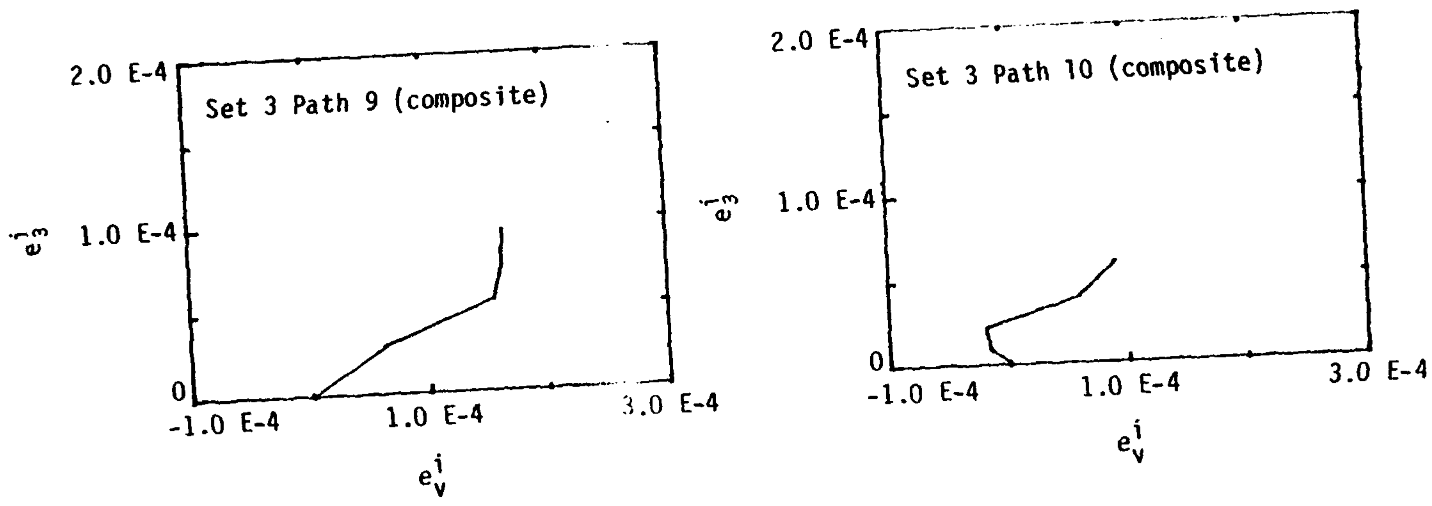

(c) Paths 9 and 10.

Figure 16. Concluded.

The strain invariant plots of e_s^i versus e_v^i show distinct characteristics for the various stress paths. Most of the compression paths indicate a fair amount of negative inelastic volumetric strain. Two exceptions are found in paths 4 and 6 of set 1. Path 4 denotes a hydrostatic load followed by a uniaxial load to failure. Path 6 represents a triaxial stress path with $\sigma_1 = \sigma_2$ and $\sigma_3 = 0.1\sigma_1$. Both paths exhibit large inelastic shear (or deviatoric) strains but relatively small inelastic volumetric strains.

Limit states in terms of these invariants have also been determined. Figure 17 shows limit states in the e_s^i versus e_v^i space; corresponding points are shown in the e_3^i versus e_v^i space in Figure 18. There appears to be no simple relation in terms of the first and second invariants to define the limit state, but the results shown in Figure 18 in terms of the first and third invariants indicate a modest improvement. With the use of all three invariants it may be possible to find a simple strain-based criterion that defines the limit state. It is particularly important that this criterion be accurate for the uniaxial stress test because this test is often used as a standard for evaluating material properties.

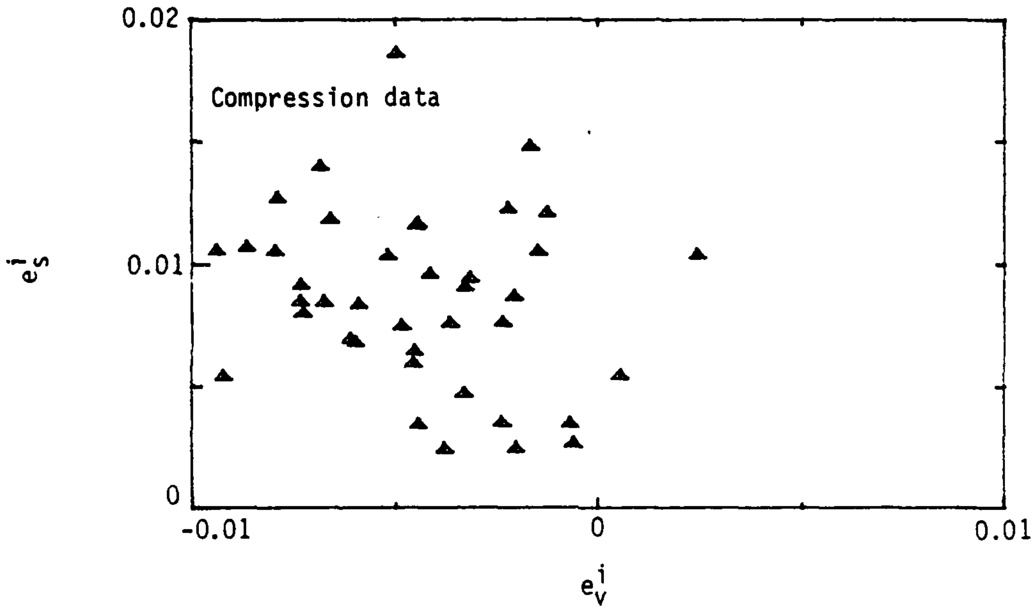

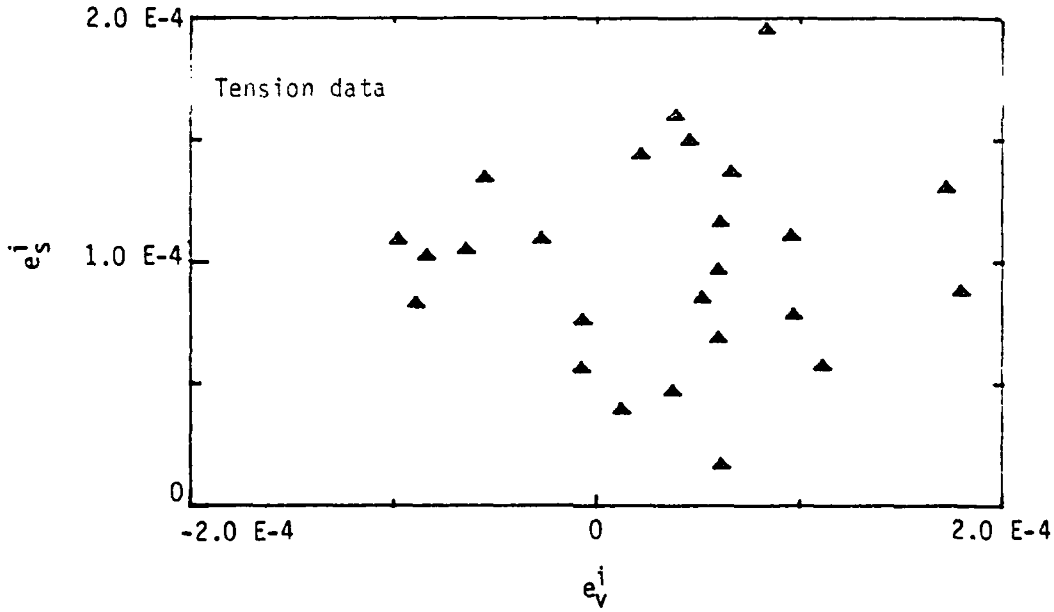

Figure 17. Limit states in terms of e_s^i and e_v^i.

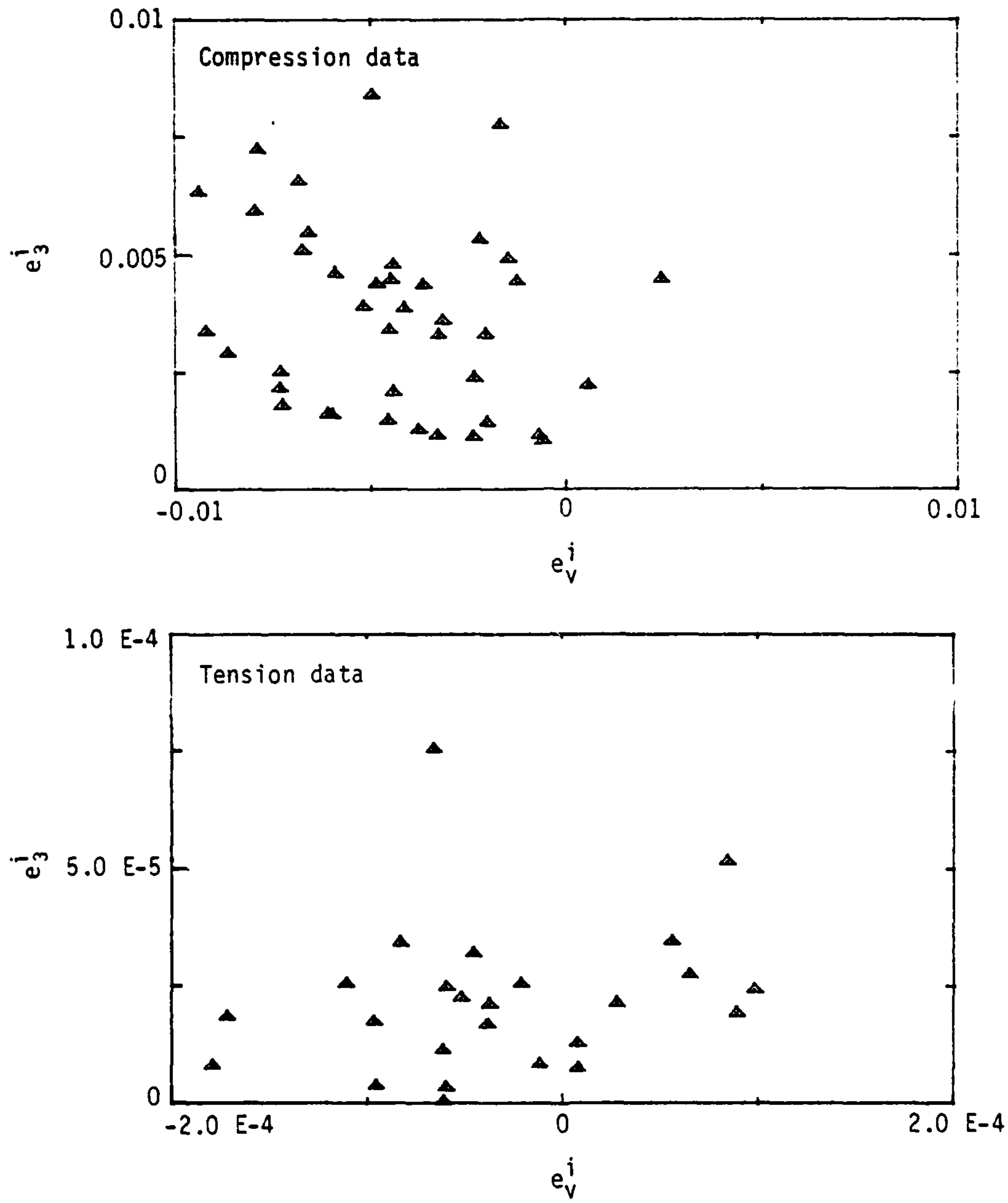

Figure 18. Limit states in terms of e_3^i and e_v^i.

VII. CONCLUSIONS

Except in a few isolated cases, the quality of the experimental data is remarkably good. No deviations from expected concrete behavior were observed for any of the paths, and strain responses in terms of prescribed stress appear to be smoothly varying functions. These results should provide a good base for evaluating the application of constitutive models to weak concrete.

Although these data cover a significant range of concrete behavior, it must be emphasized that no data of a comparable comprehensive nature exist for other regimes that involve strain softening, general cycling paths, and multidimensional tensile paths. The apparatus used in the NMSU tests could be used to provide the experimental capability for obtaining data in these regimes with a minor modification to provide displacement-controlled heads. Such data are necessary if constitutive models are to be verified for applications that involve large inelastic deformations.

A linear relationship between a form of the third invariant and the mean normal pressure represents the limit state very well in the L-P space. Currently, limit states are not represented well by a simple relationship in which strain invariants are used. However, there are indications that alternate combinations of invariants will be successful. Additional work in this area could lead to the development of plasticity algorithms that are as useful for frictional materials as for metals.

REFERENCES

1. Traina, L. A., Experimental Stress-Strain Behavior of a Low Strength Concrete Under Multiaxial States of Stress, AFWL-TR-82-92, Air Force Weapons Laboratory, Kirtland Air Force Base, New Mexico, December 1982.

2. Lade, P. V., "Three-Parameter Failure Criterion for Concrete," Journal of the Engineering Mechanics Division, ASE, 108:850-863, 1982.

3. Schreyer, H. L., "A Third-Invariant Plasticity Theory for Frictional Materials," Journal of Structural Mechanics, June 1983.

4. Green, S. J., and Swanson, S. R., Static Constitutive Relations for Concrete, AFWL-TR-72-244, Air Force Weapons Laboratory, Kirtland Air Force Base, New Mexico, April 1983.

APPENDIX A

STRESS-STRAIN CURVES

This appendix contains the original stress-strain data for the compression stress paths of sets 1 and 2. The tension data are not included because no adjustments were made to them. The original tension data, which are the same as the adjusted data, are presented in Appendix B. The stress-strain (σ-ε) plots in Appendix A are followed by mean normal pressure-volumetric strain (P-e_v) plots.

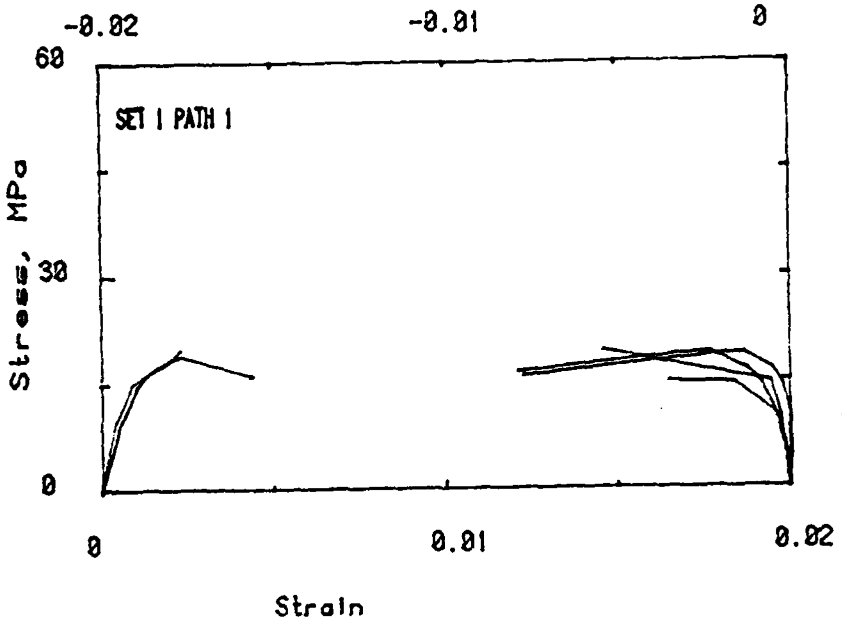

-0.02
-0.01
0
60
SET 1 PATH 1
Stress, MPa
30
0
0
0.01
0.02
Strain

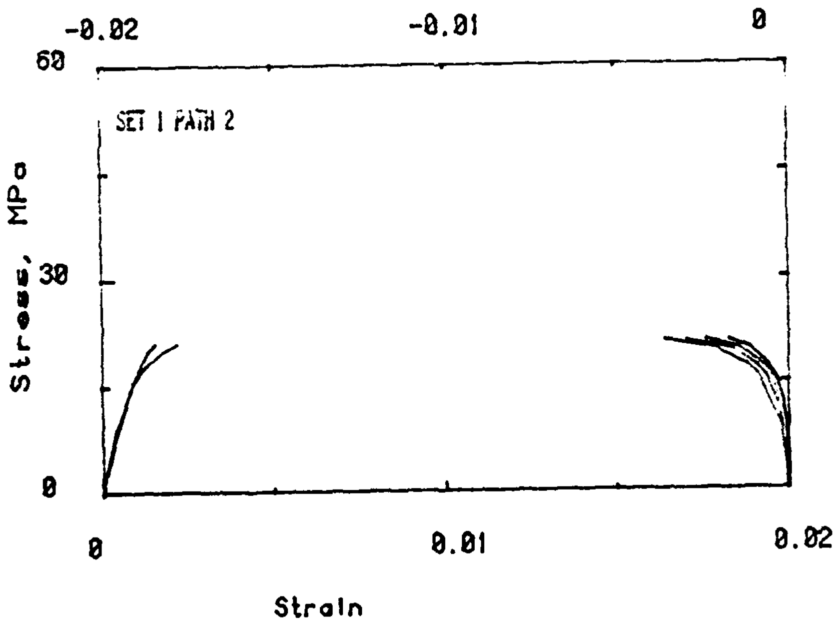

-0.02
-0.01
0
60
SET 1 PATH 2
Stress, MPa
30
0
0
0.01
0.02
Strain

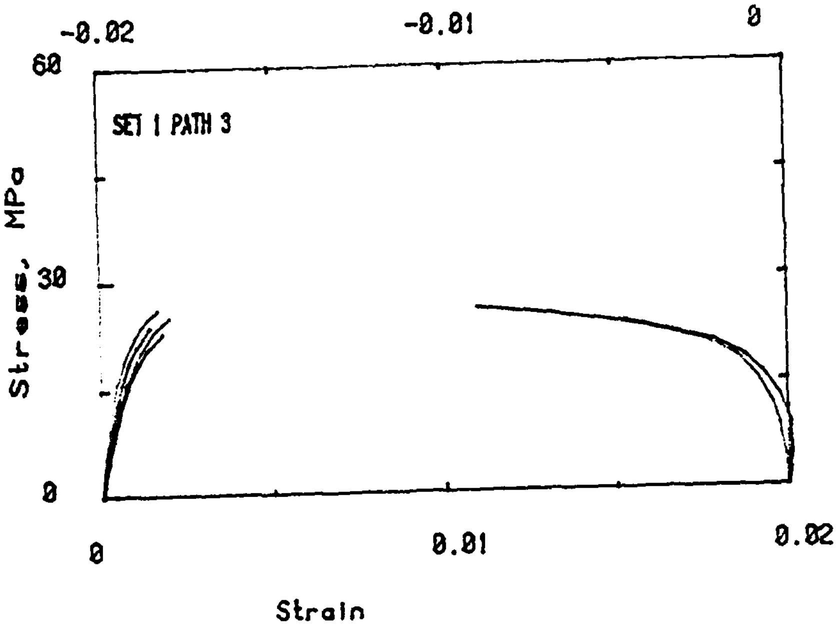
-0.02
-0.01
0
60
SET 1 PATH 3
Stress, MPa
30
0
0
0.01
0.02
Strain

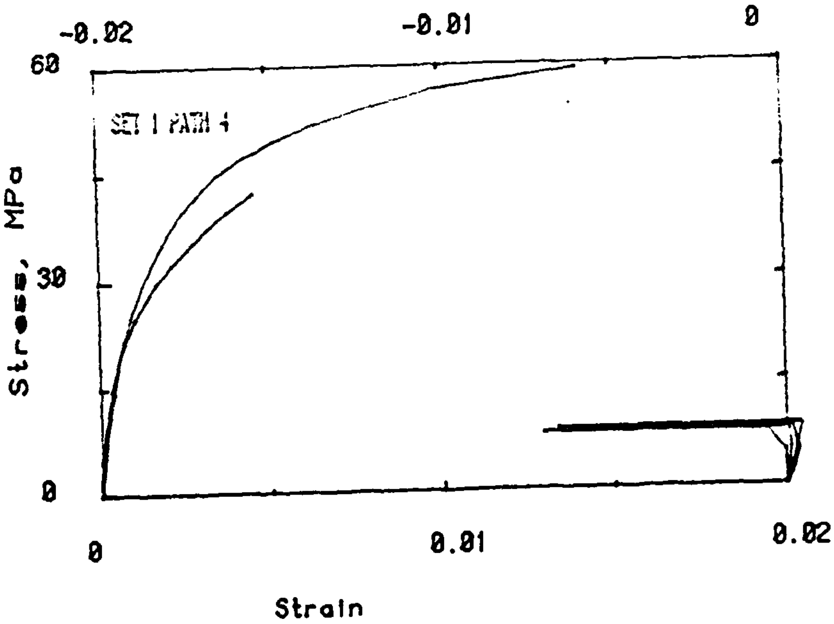
-0.02
-0.01
0
60
SET 1 PATH 4
Stress, MPa
30
0
0
0.01
0.02
Strain

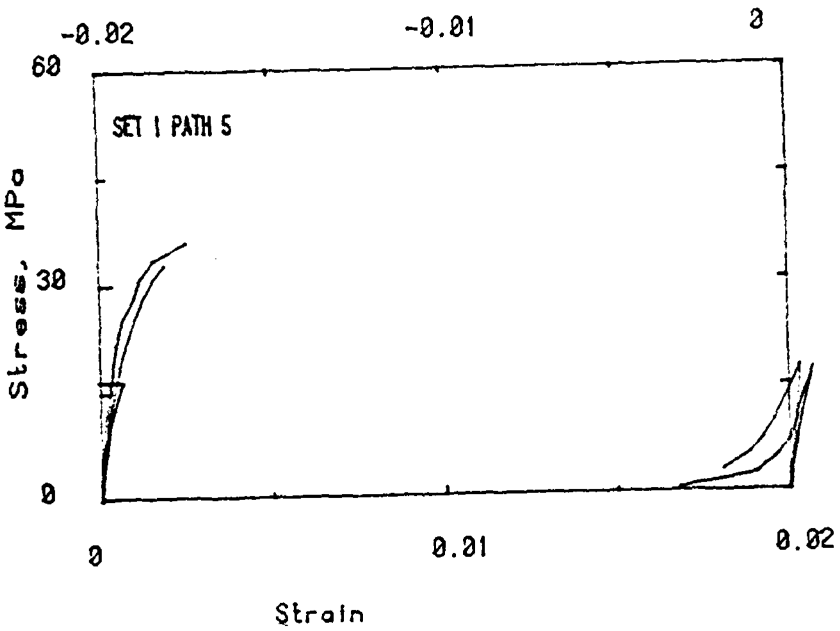

-0.02
-0.01
0
60
SET 1 PATH 5
Stress, MPa
30
0
0
0.01
0.02
Strain

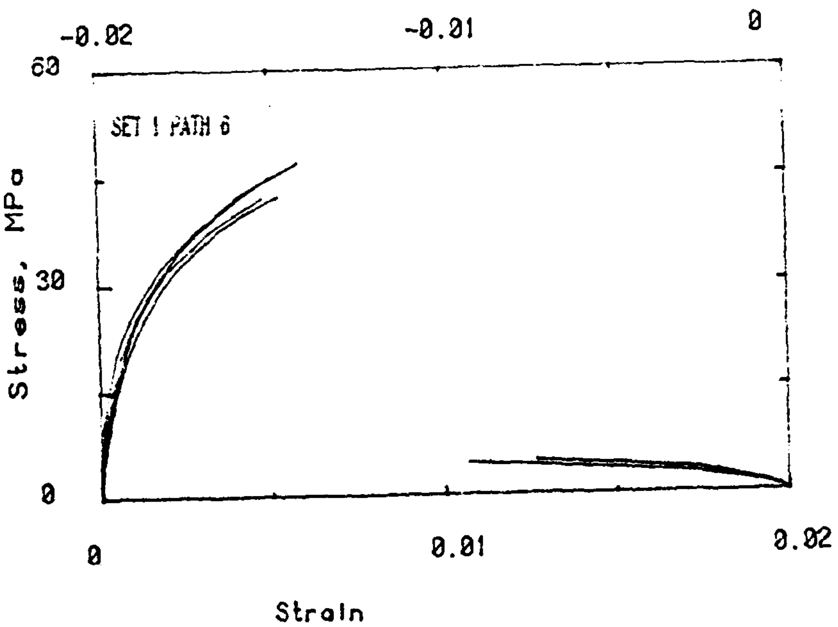

-0.02
-0.01
0
60
SET 1 PATH 6
Stress, MPa
30
0
0
0.01
0.02
Strain

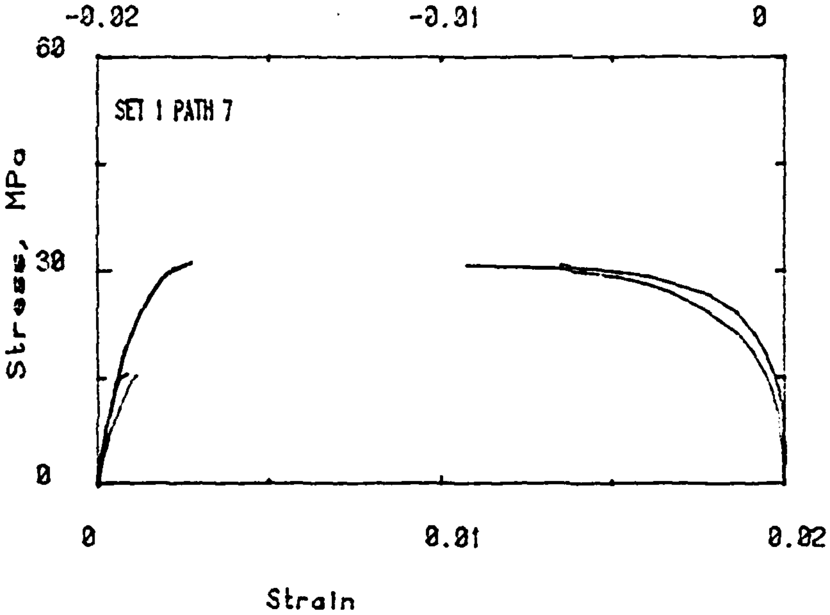
-0.02
-0.01
0
60
30
0
SET 1 PATH 7
Stress, MPa
0
0.01
0.02
Strain

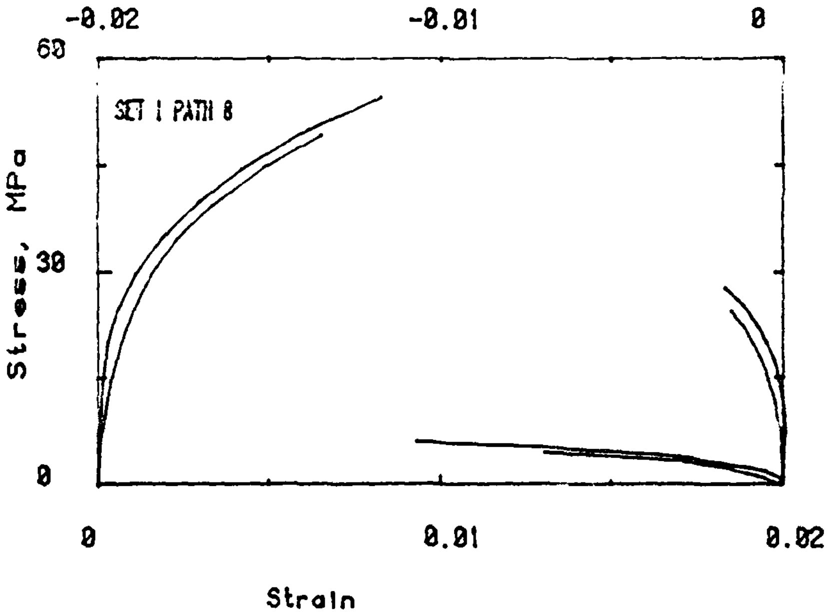
-0.02
-0.01
0
60
30
0
SET 1 PATH 8
Stress, MPa
0
0.01
0.02
Strain

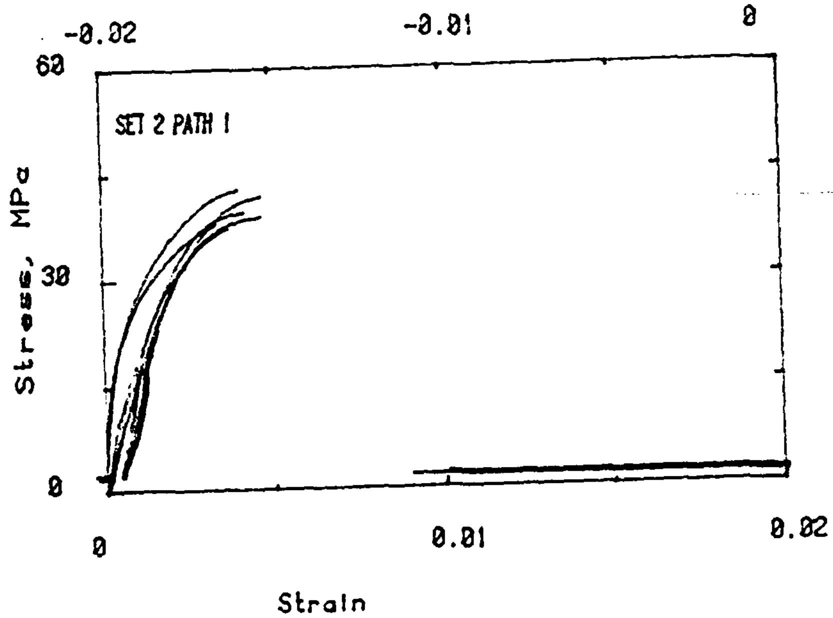
-0.02
-0.01
0
60
SET 2 PATH 1
Stress, MPa
30
0
0
0.01
0.02
Strain

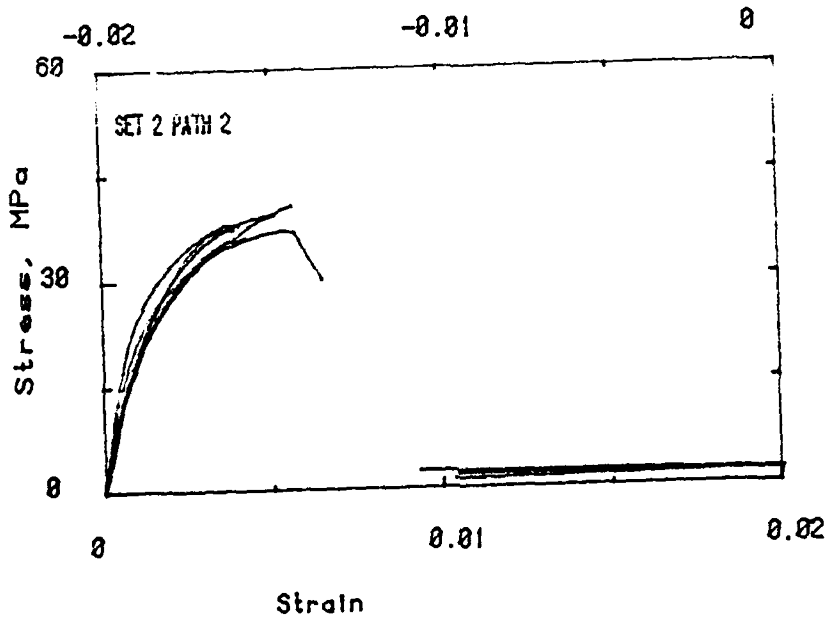
-0.02
-0.01
0
60
SET 2 PATH 2
Stress, MPa
30
0
0
0.01
0.02
Strain

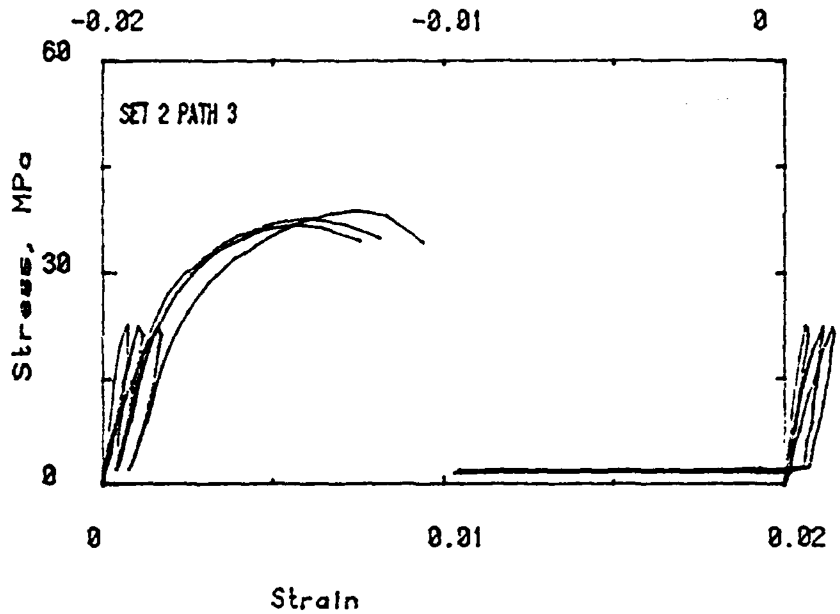

-0.02
-0.01
0
60
SET 2 PATH 3
Stress, MPa
30
0
0
0.01
0.02
Strain

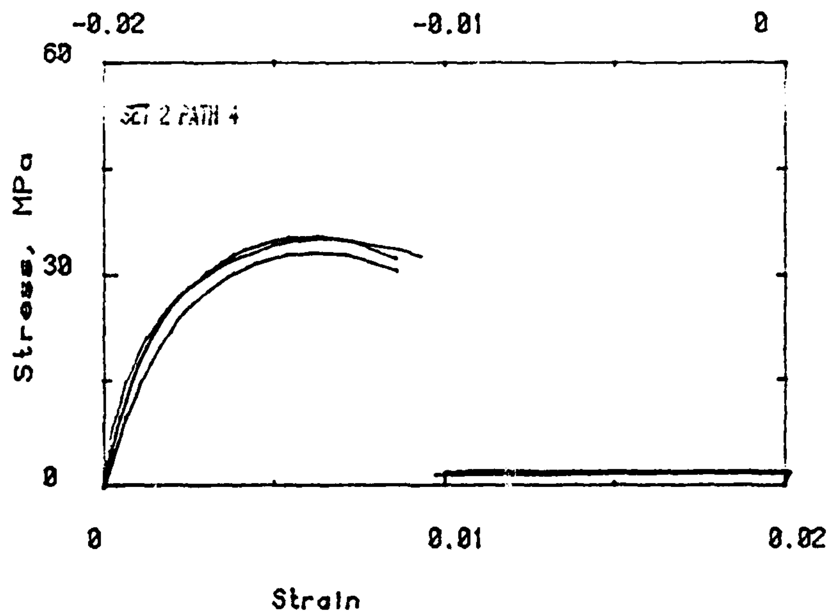

-0.02
-0.01
0
60
SET 2 PATH 4
Stress, MPa
30
0
0
0.01
0.02
Strain

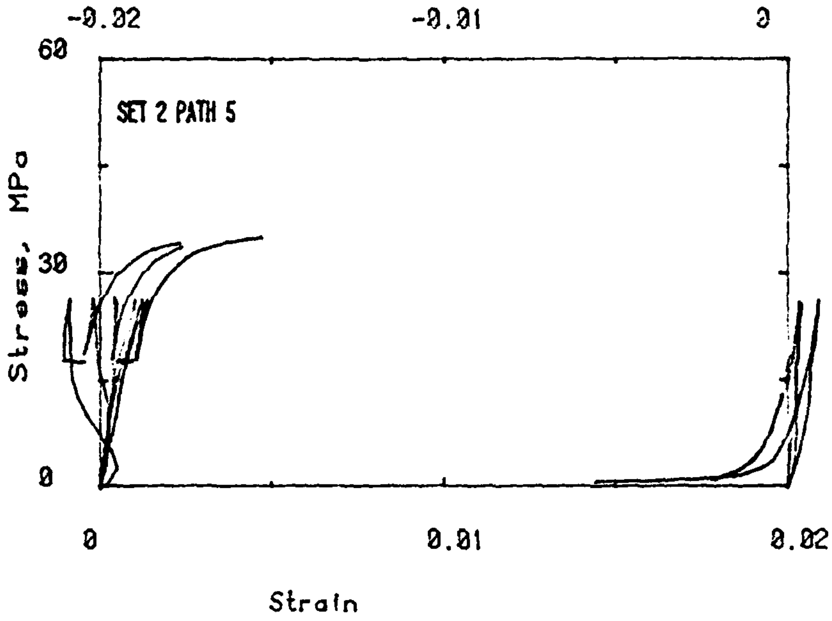

-0.02
-0.01
0
60
SET 2 PATH 5
Stress, MPa
30
0
0
0.01
0.02
Strain

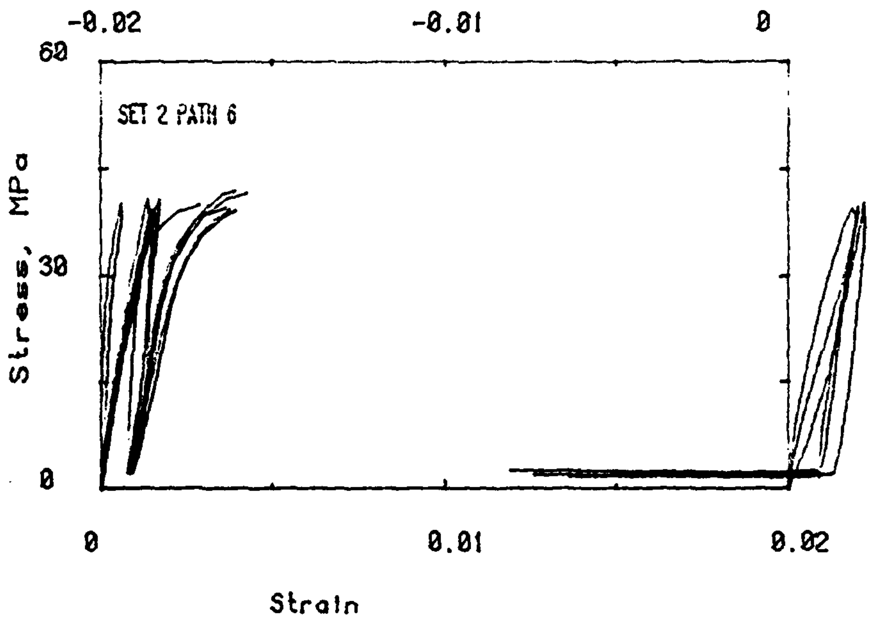

-0.02
-0.01
0
60
SET 2 PATH 6
Stress, MPa
30
0
0
0.01
0.02
Strain

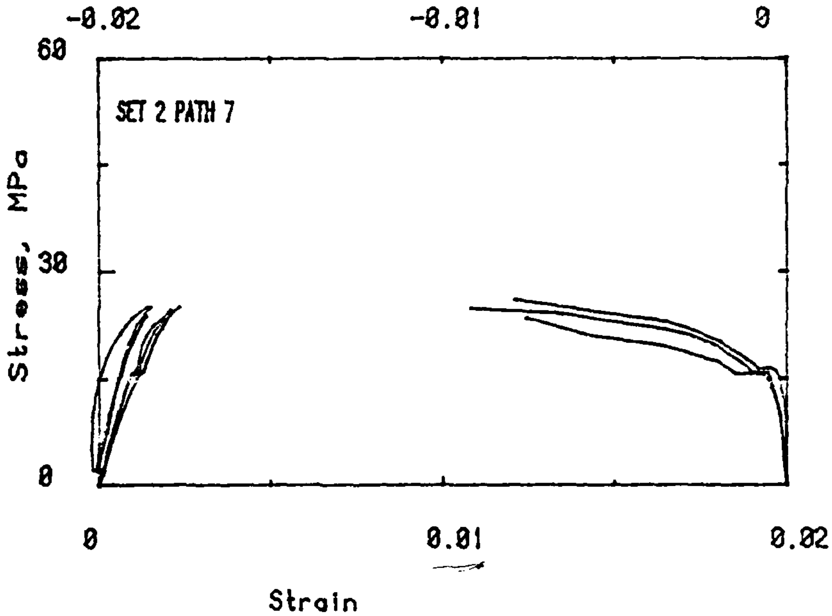

-0.02
-0.01
0
60
SET 2 PATH 7
Stress, MPa
30
0
0
0.01
0.02
Strain

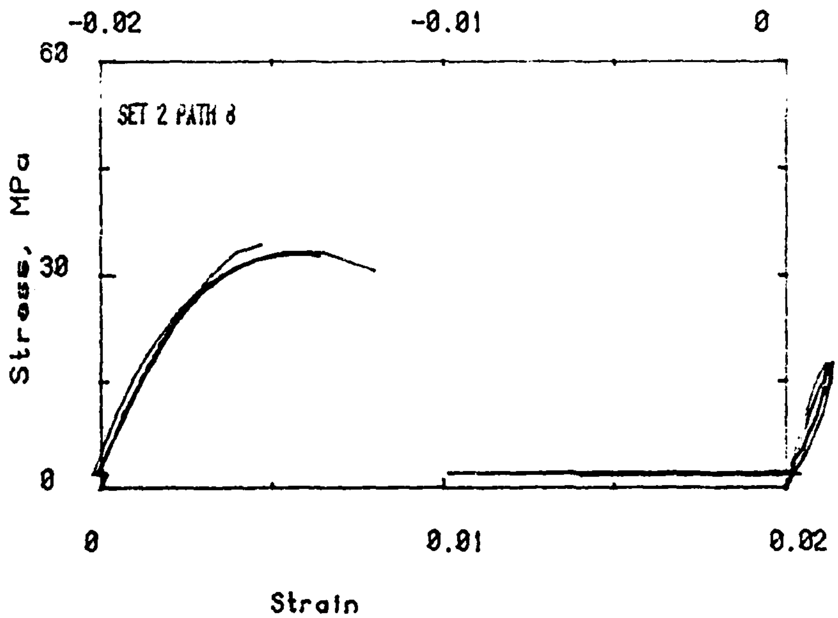

-0.02
-0.01
0
60
SET 2 PATH 8
Stress, MPa
30
0
0
0.01
0.02
Strain

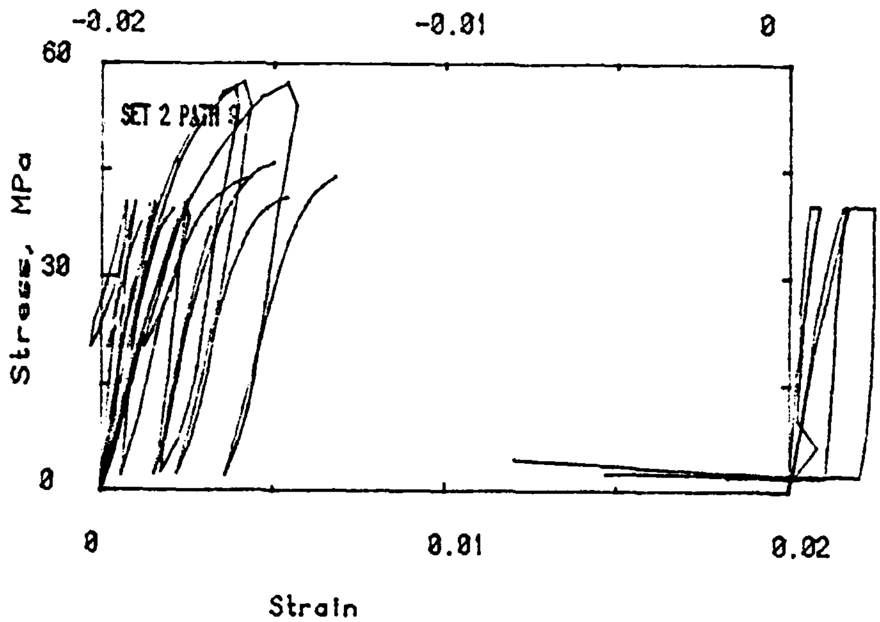
-0.02
-0.01
0
60
SET 2 PATH 9
Stress, MPa
30
0
0
0.01
0.02
Strain

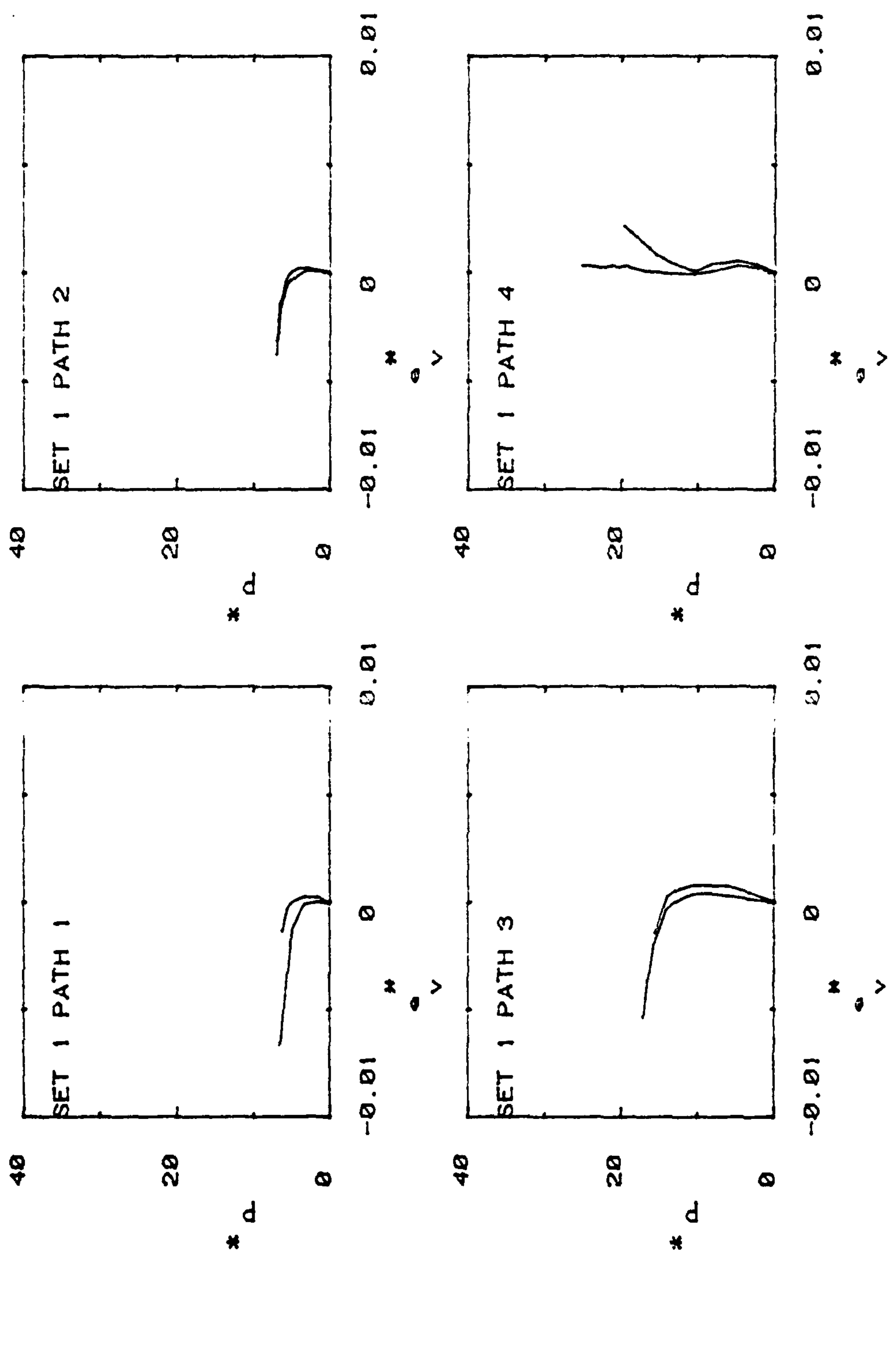
SET 1 PATH 1
SET 1 PATH 2
SET 1 PATH 3
SET 1 PATH 4
40
20
0
p*
-0.01
0
0.01
v*

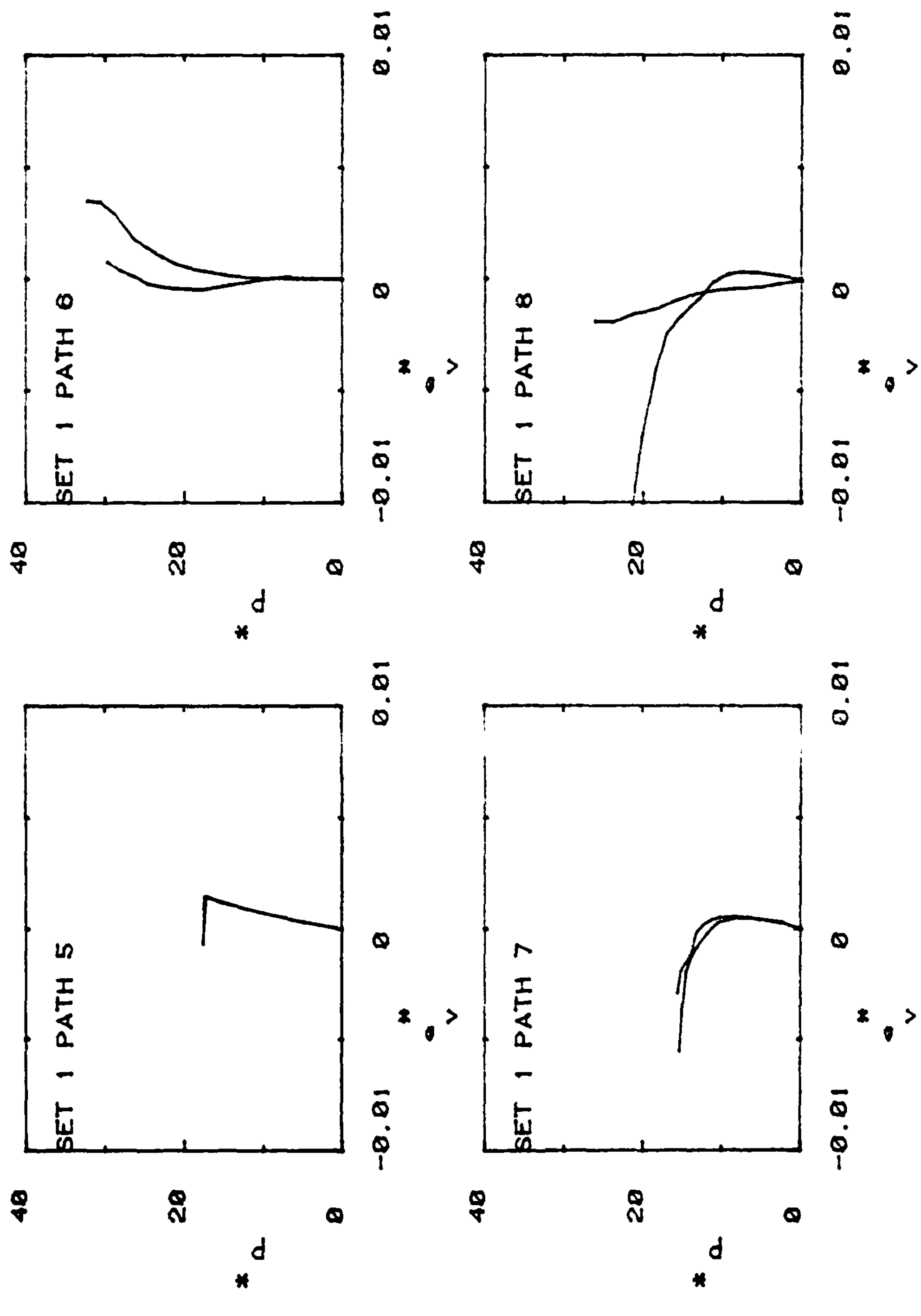
SET 1 PATH 5
SET 1 PATH 6
SET 1 PATH 7
SET 1 PATH 8
p*
v*
40
20
0
-0.01
0
0.01

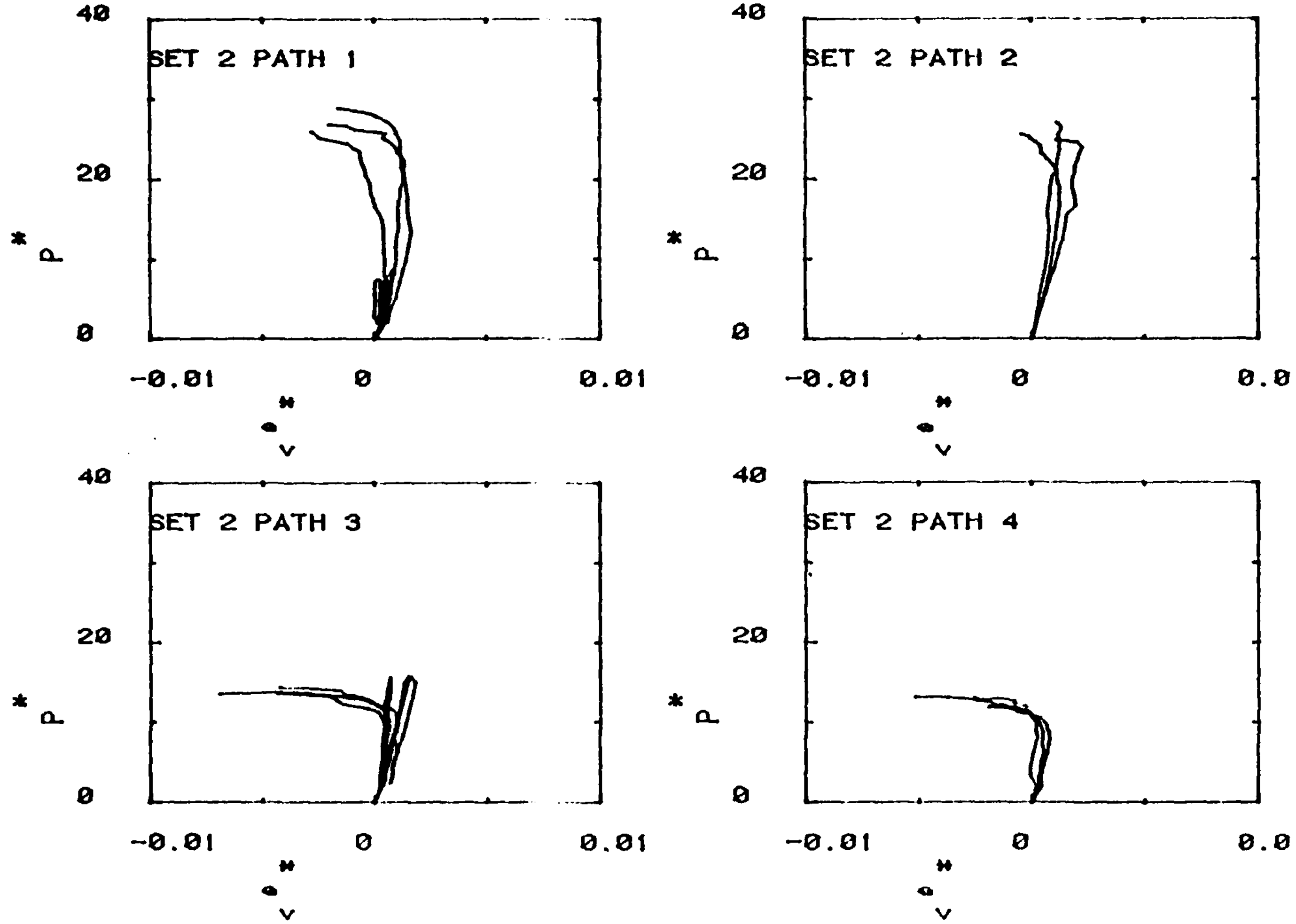
SET 2 PATH 1
SET 2 PATH 2
SET 2 PATH 3
SET 2 PATH 4
40
20
0
-0.01
0
0.01
P^*
ϵ_v^*

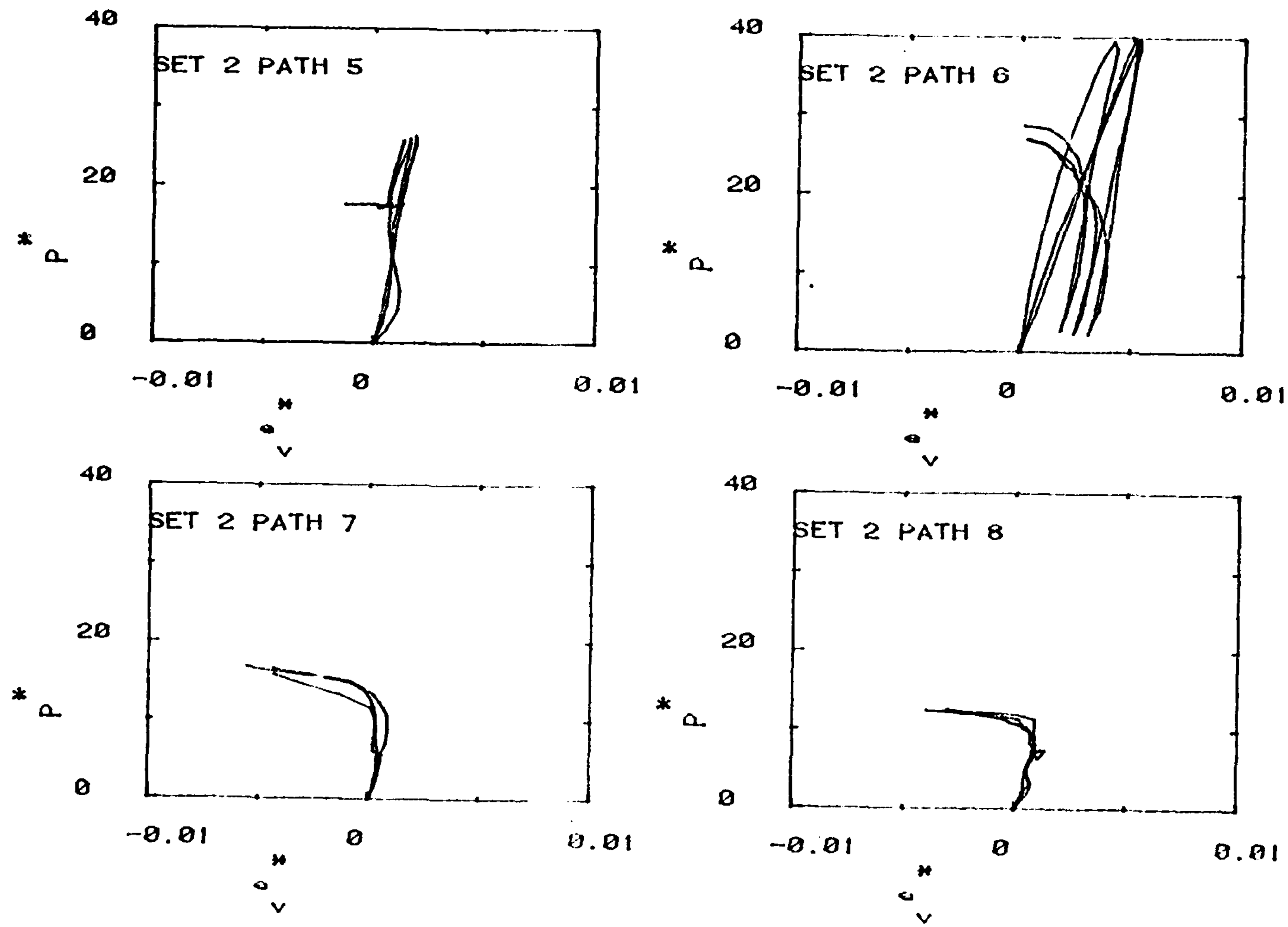
SET 2 PATH 5
SET 2 PATH 6
SET 2 PATH 7
SET 2 PATH 8
40
20
0
-0.01
0
0.01
P*
e*v

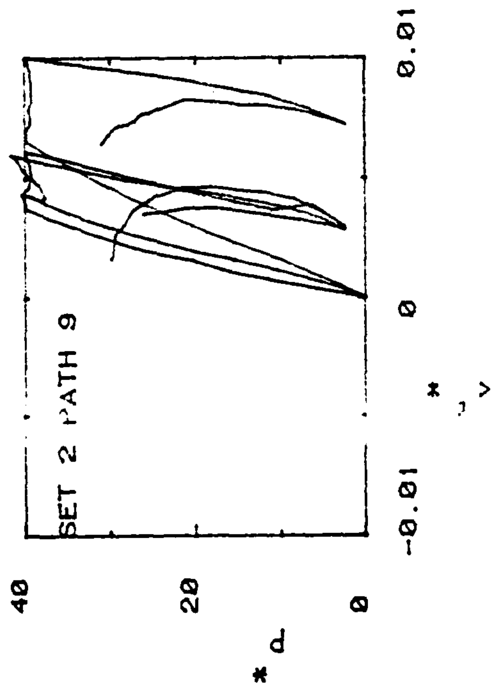
SET 2 PATH 9
40
20
0
-0.01
0
0.01
p*
v*

APPENDIX B

ADJUSTED STRESS-STRAIN CURVES WITH COMPOSITE PLOTS

Adjusted stress-strain curves with composite curves overlaid are presented in this appendix. Curves for tension specimens eliminated from consideration in the construction of the composite curves are marked with an X. The mean normal pressure versus volumetric strain curves also appear in this appendix.

Contents	Page

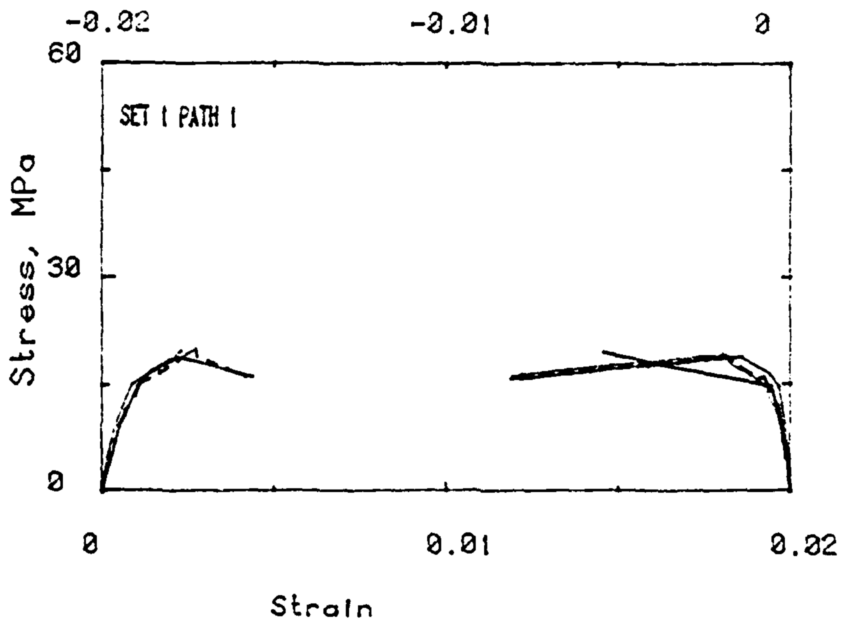
-0.02
-0.01
0
60
SET 1 PATH 1
Stress, MPa
30
0
0
0.01
0.02
Strain

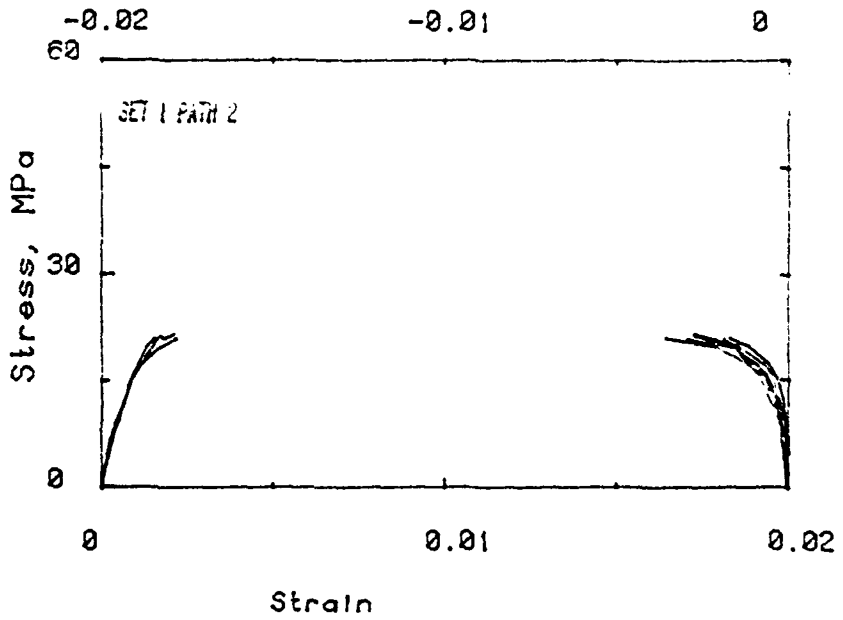
-0.02
-0.01
0
60
SET 1 PATH 2
Stress, MPa
30
0
0
0.01
0.02
Strain

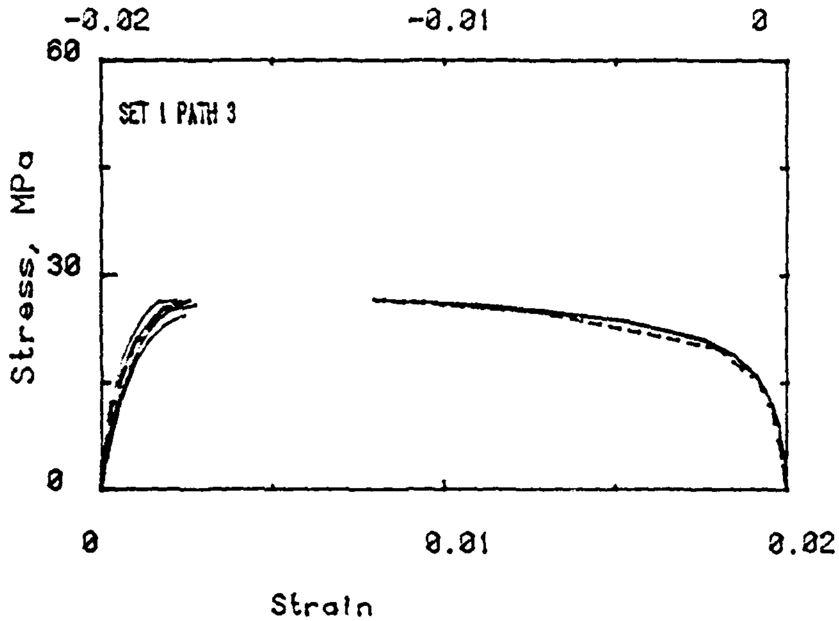
-0.02
-0.01
0
60
SET 1 PATH 3
Stress, MPa
30
0
0
0.01
0.02
Strain

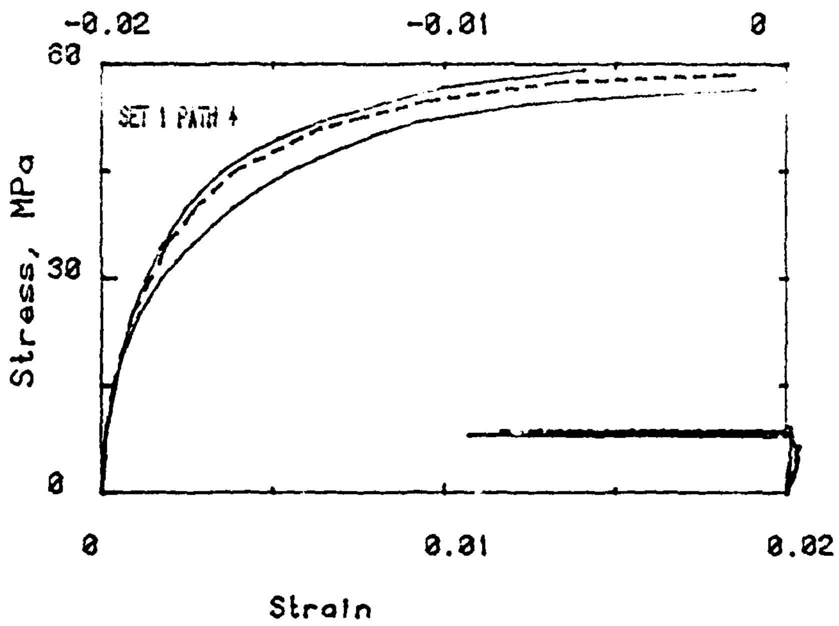
-0.02
-0.01
0
60
SET 1 PATH 4
Stress, MPa
30
0
0
0.01
0.02
Strain

AD-A129 716 REDUCED EXPERIMENTAL STRESS-STRAIN RESULTS FOR A LOW-STRENGTH CONCRETE UN..(U) NEW MEXICO ENGINEERING RESEARCH INST ALBUQUERQUE L A TRAINA ET AL. MAY 83

2/2

UNCLASSIFIED AFWL-TR-83-3 F29601-81-C-0013 F/G 11/2 NL

END
DATE
FILMED
7 83
DTIC

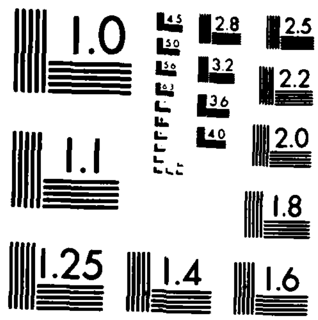

MICROCOPY RESOLUTION TEST CHART
NATIONAL BUREAU OF STANDARDS-1963-A

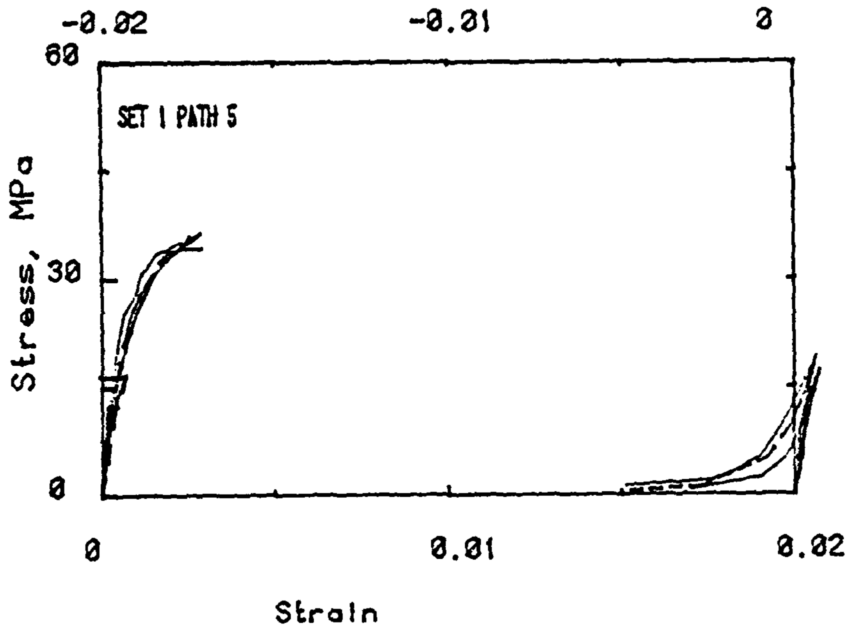

-0.02
-0.01
0
60
SET 1 PATH 5
Stress, MPa
30
0
0
0.01
0.02
Strain

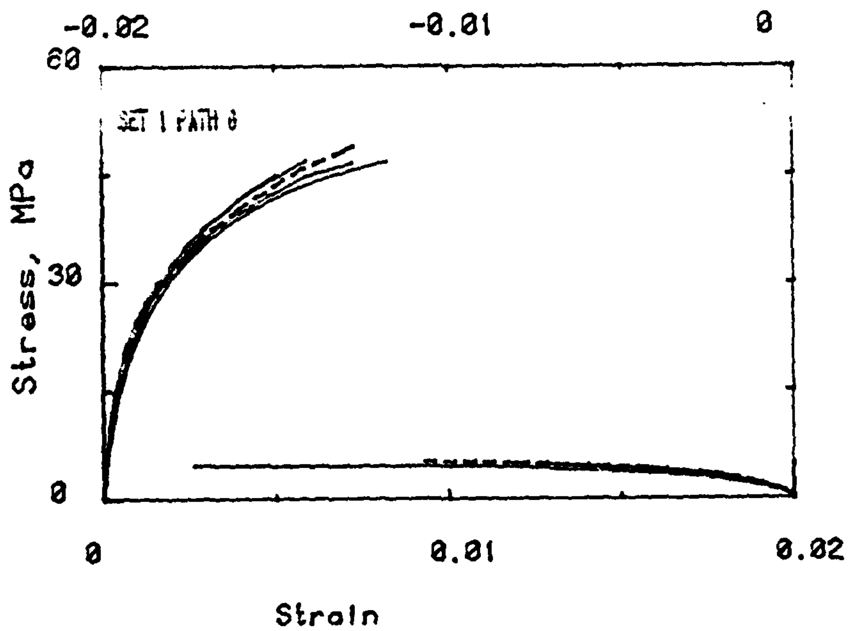

-0.02
-0.01
0
60
SET 1 PATH 6
Stress, MPa
30
0
0
0.01
0.02
Strain

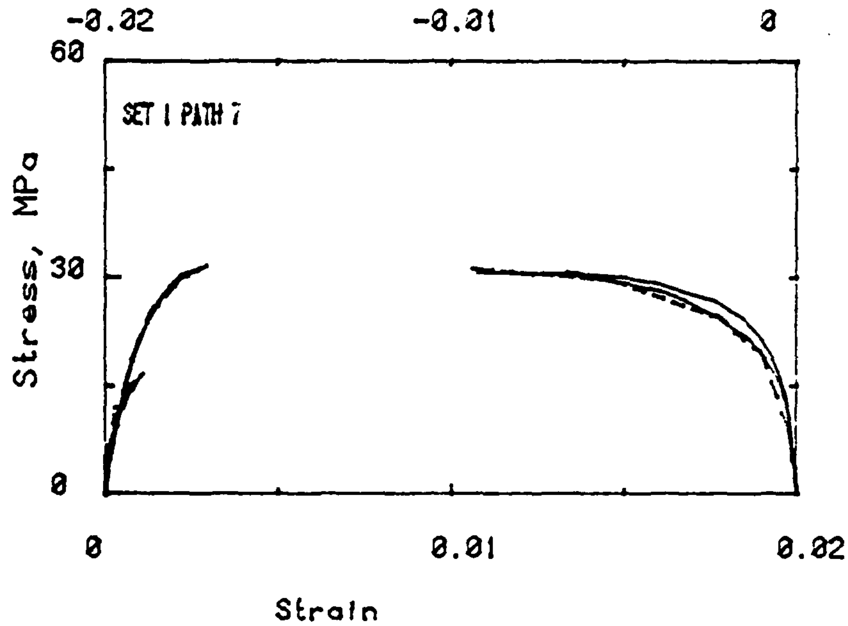

-0.02
-0.01
0
60
SET 1 PATH 7
Stress, MPa
30
0
0
0.01
0.02
Strain

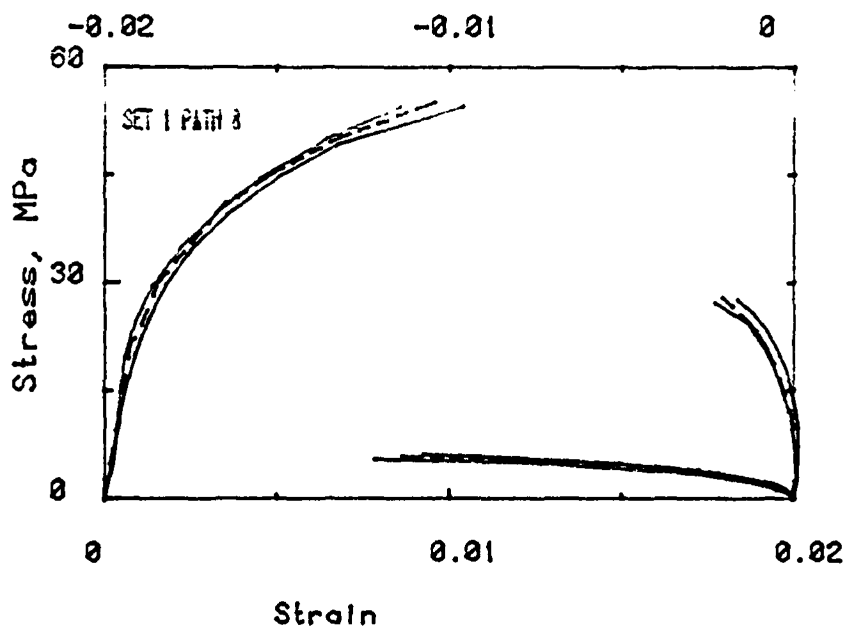

-0.02
-0.01
0
60
SET 1 PATH 8
Stress, MPa
30
0
0
0.01
0.02
Strain

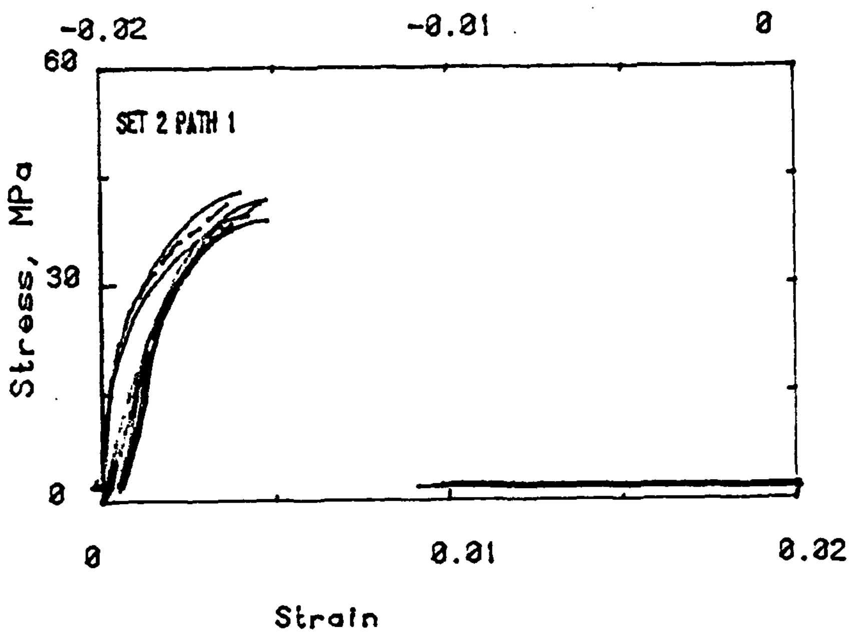
-0.02
-0.01
0
60
SET 2 PATH 1
Stress, MPa
30
0
0
0.01
0.02
Strain

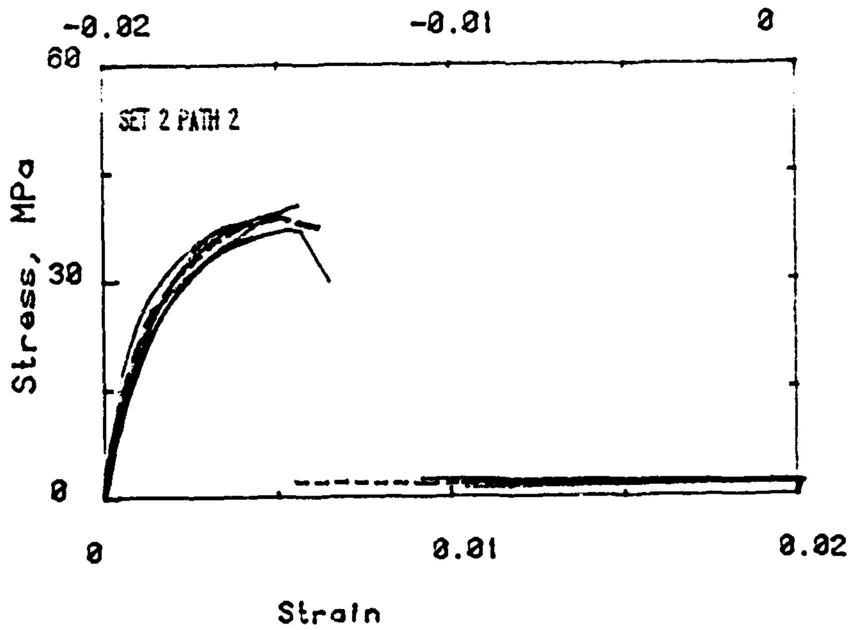
-0.02
-0.01
0
60
SET 2 PATH 2
Stress, MPa
30
0
0
0.01
0.02
Strain

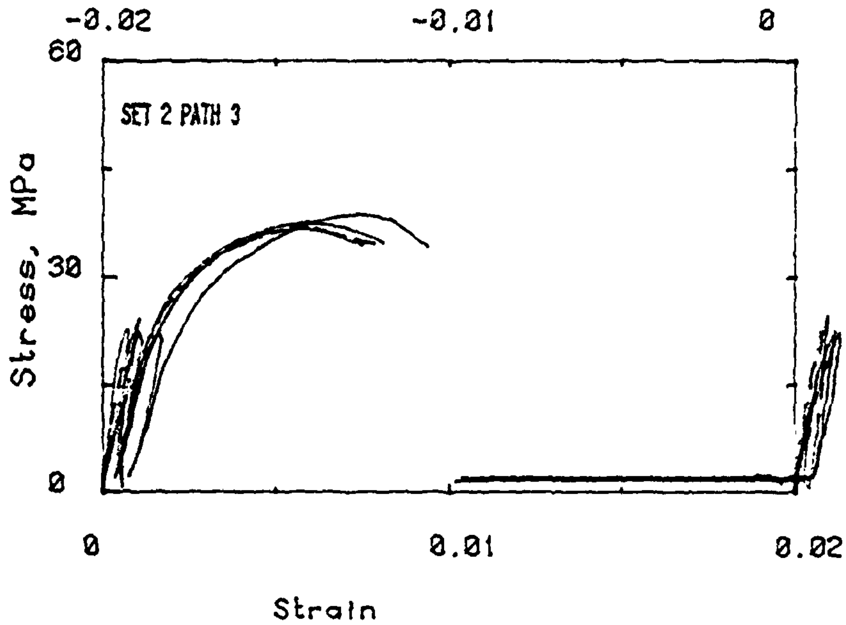
-0.02
-0.01
0
60
SET 2 PATH 3
Stress, MPa
30
0
0
0.01
0.02
Strain

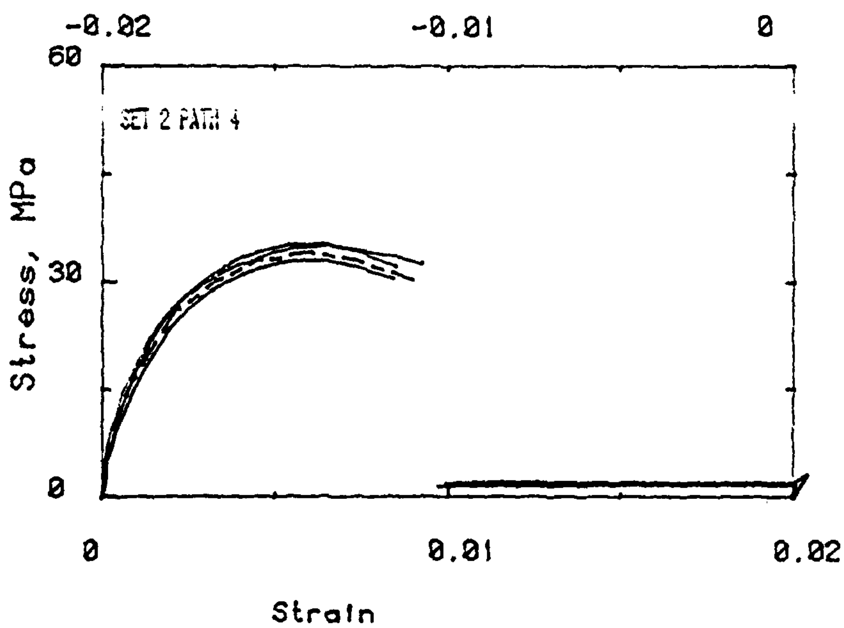
-0.02
-0.01
0
60
SET 2 PATH 4
Stress, MPa
30
0
0
0.01
0.02
Strain

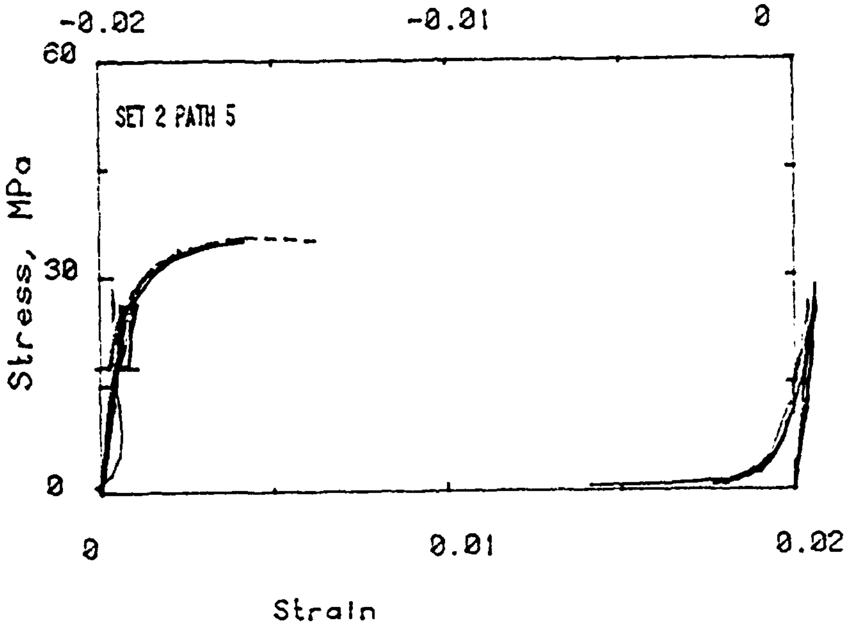

-0.02
-0.01
0
60
SET 2 PATH 5
Stress, MPa
30
0
0
0.01
0.02
Strain

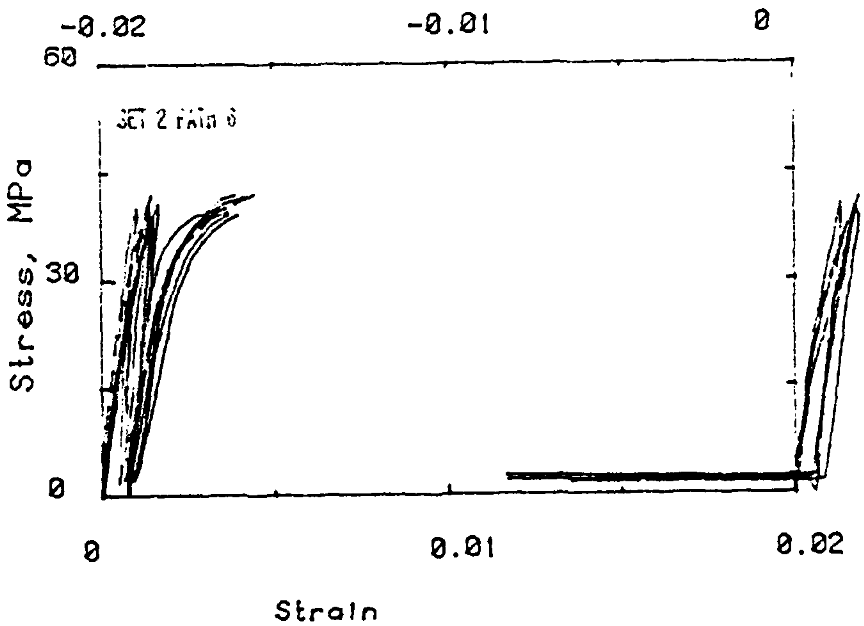

-0.02
-0.01
0
60
Stress, MPa
30
0
0
0.01
0.02
Strain

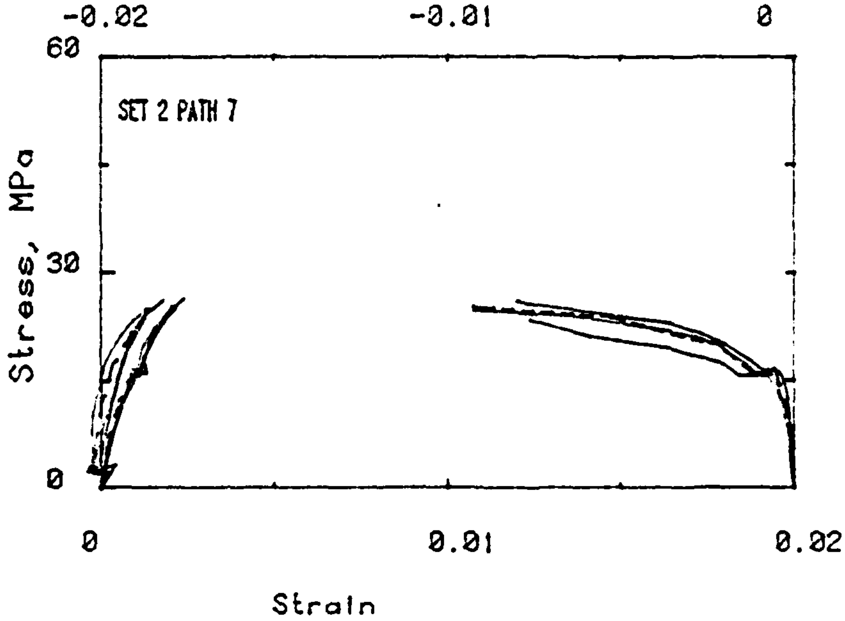
-0.02
-0.01
0
60
30
0
SET 2 PATH 7
Stress, MPa
0
0.01
0.02
Strain

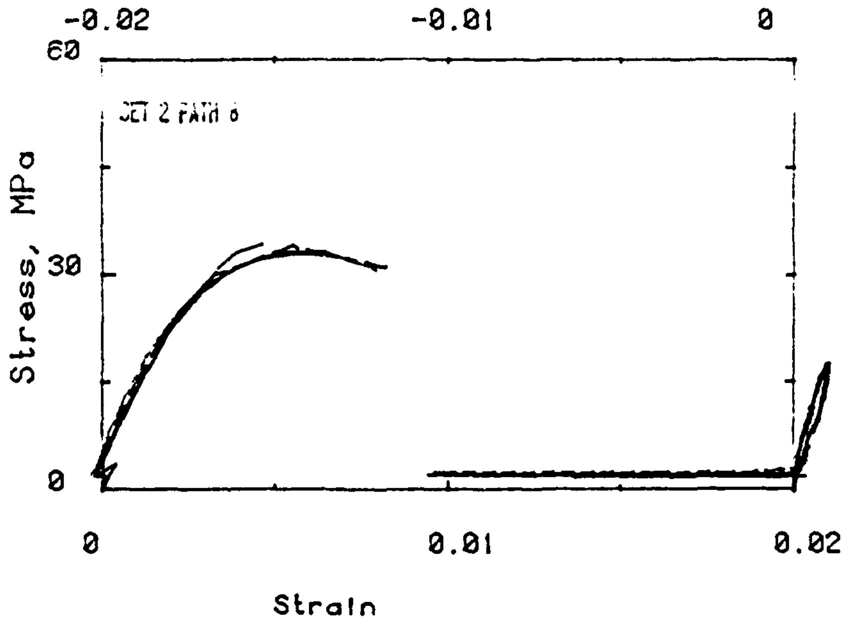
-0.02
-0.01
0
60
30
0
Stress, MPa
0
0.01
0.02
Strain

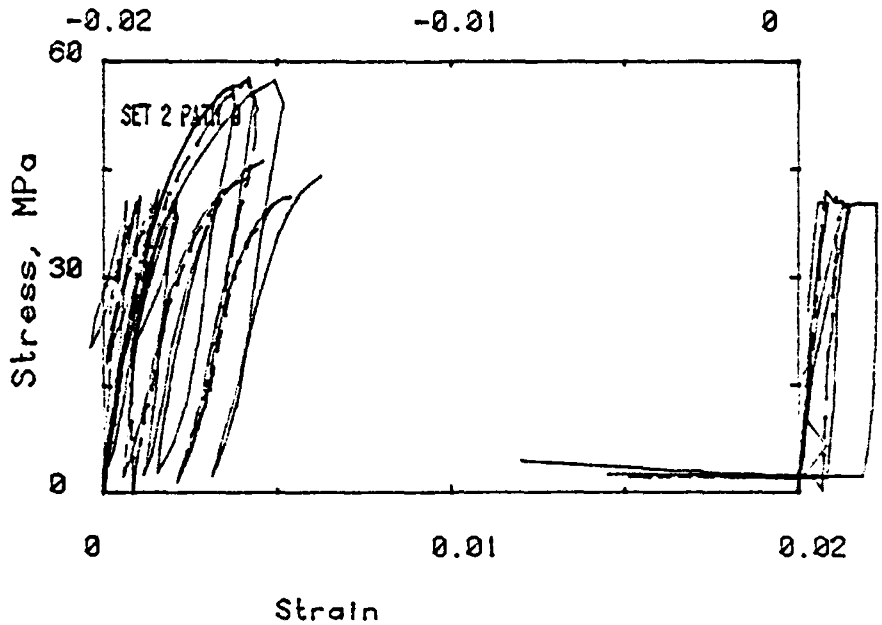

-0.02
-0.01
0
60
SET 2 PATH 8
Stress, MPa
30
0
0
0.01
0.02
Strain

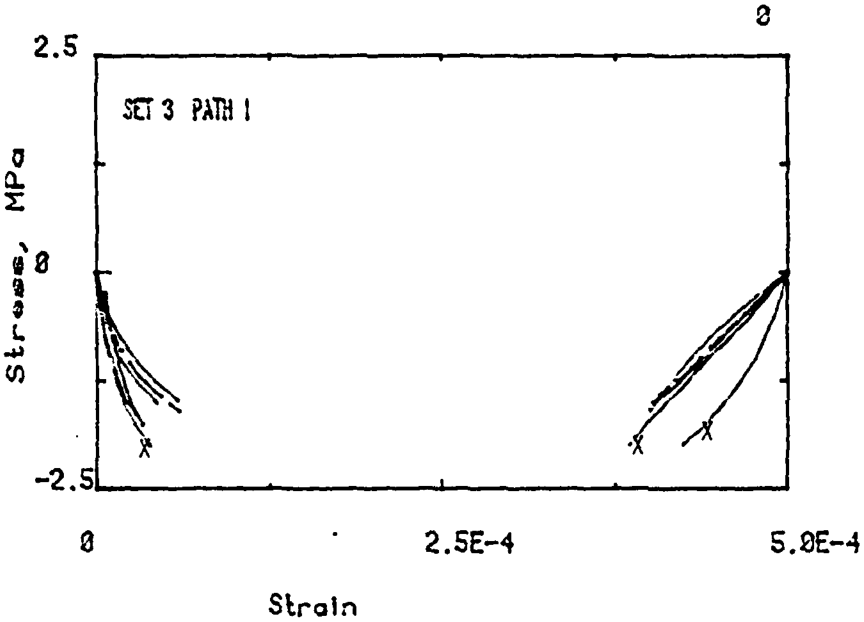

0
2.5
SET 3 PATH 1
Stress, MPa
0
-2.5
0
2.5E-4
5.0E-4
Strain

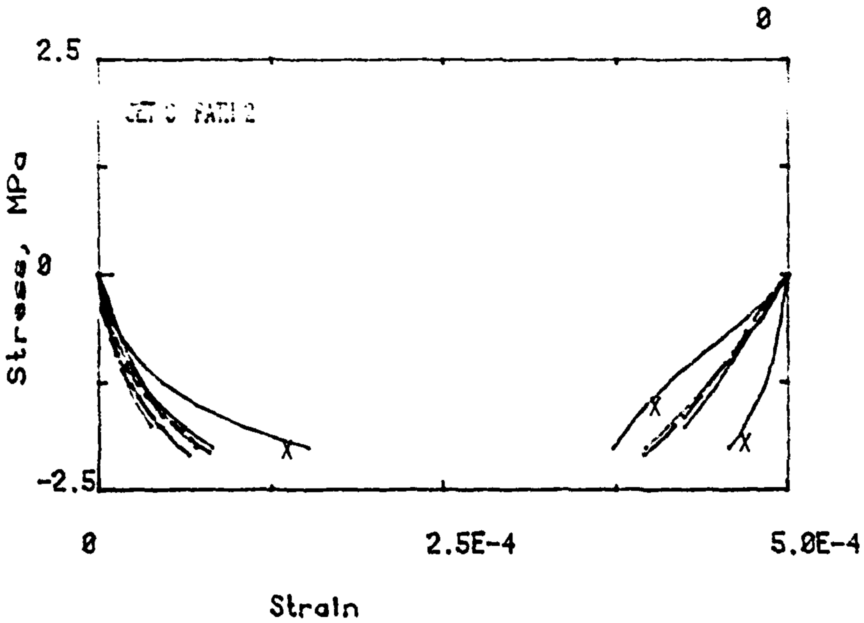

0
2.5
Stress, MPa
0
-2.5
0
2.5E-4
5.0E-4
Strain

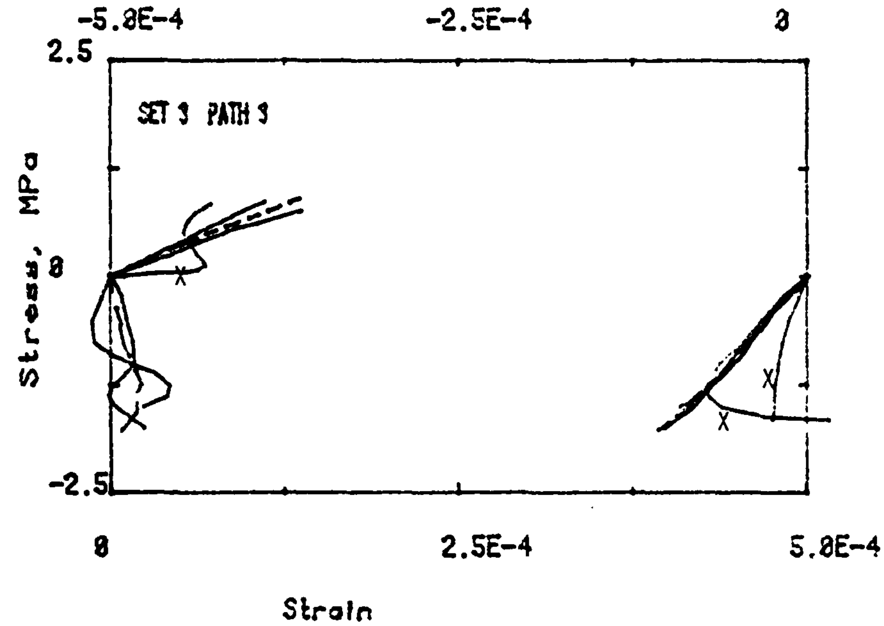
-5.0E-4
-2.5E-4
0
2.5
SET 3 PATH 3
Stress, MPa
0
-2.5
0
2.5E-4
5.0E-4
Strain

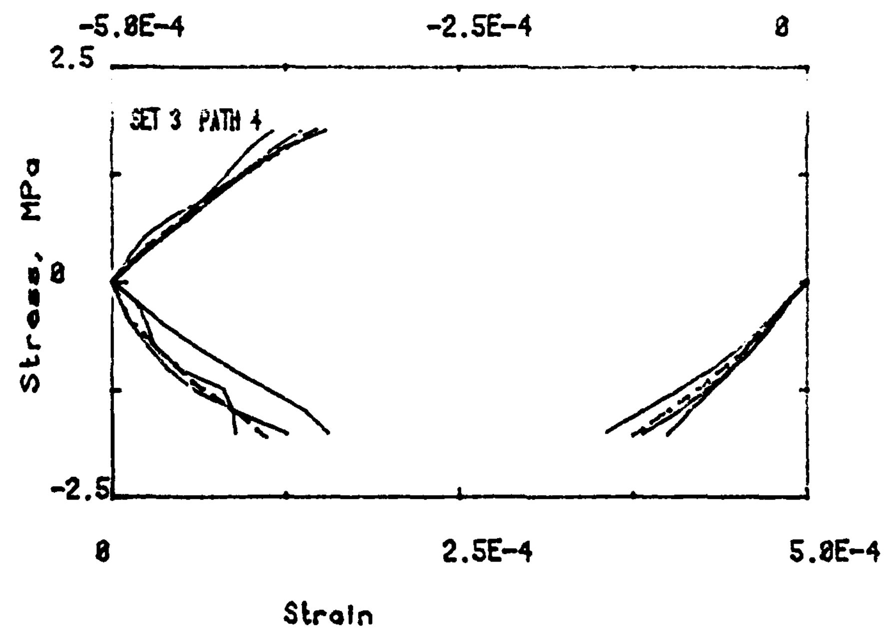
-5.0E-4
-2.5E-4
0
2.5
SET 3 PATH 4
Stress, MPa
0
-2.5
0
2.5E-4
5.0E-4
Strain

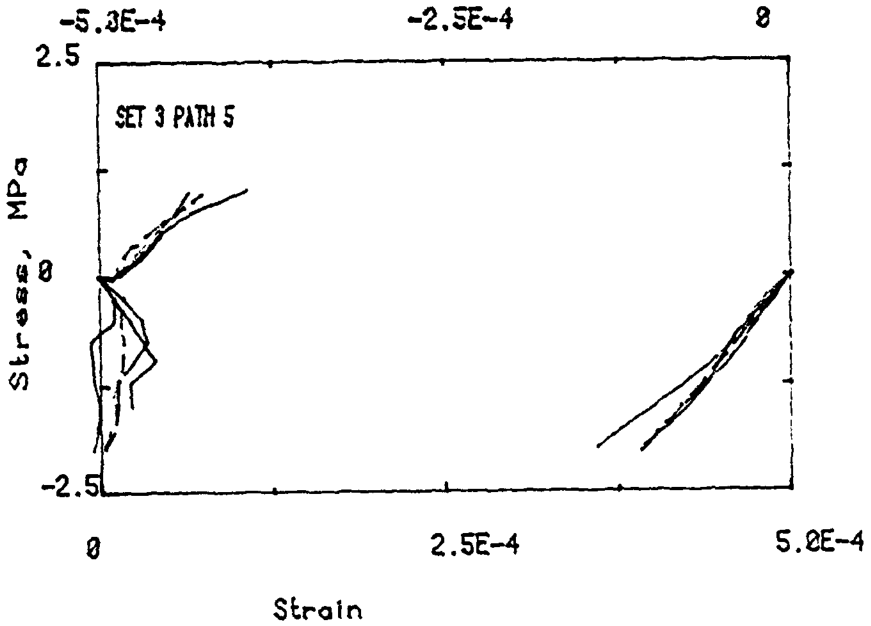
-5.0E-4
-2.5E-4
0
2.5
SET 3 PATH 5
Stress, MPa
0
-2.5
0
2.5E-4
5.0E-4
Strain

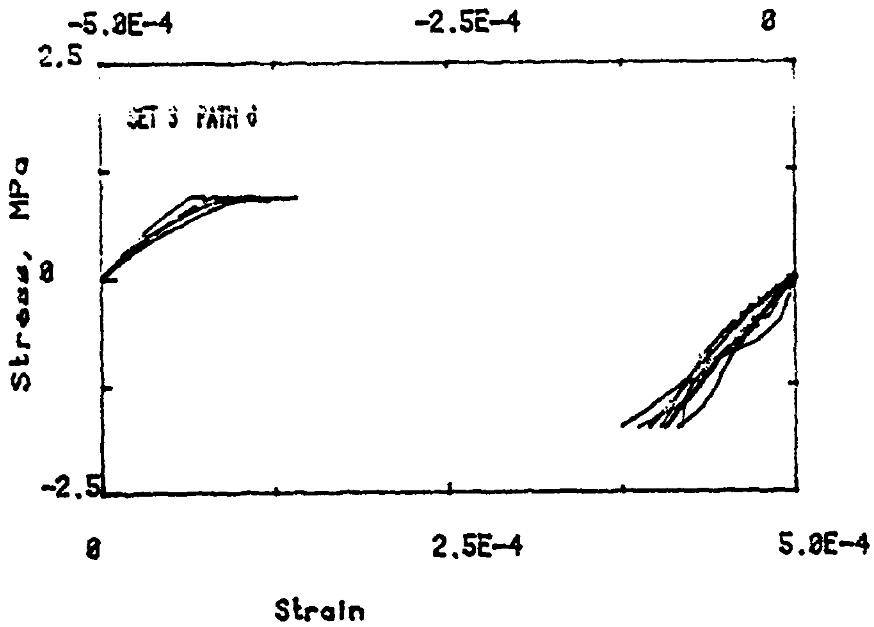
-5.0E-4
-2.5E-4
0
2.5
Stress, MPa
0
-2.5
0
2.5E-4
5.0E-4
Strain

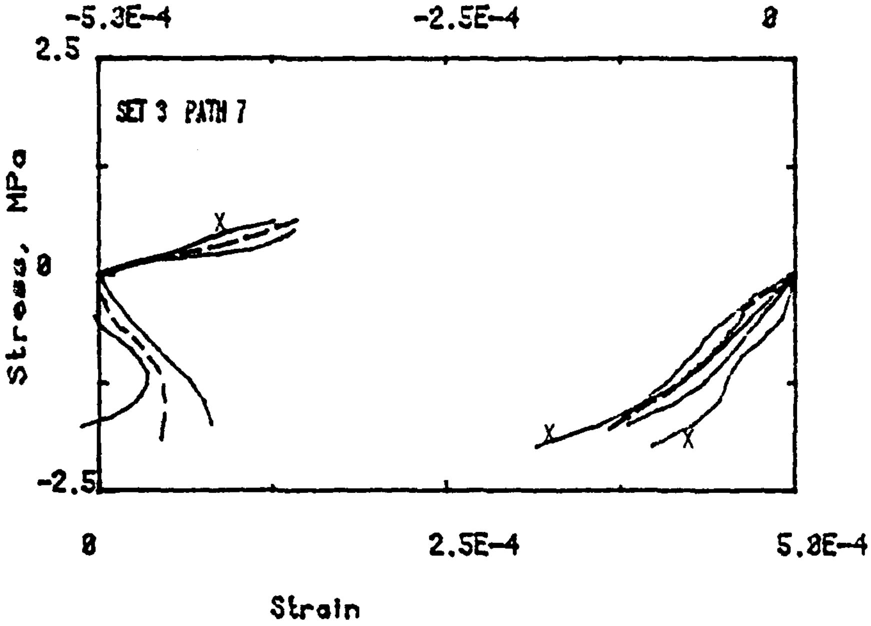
-5.3E-4
-2.5E-4
0
2.5
SET 3 PATH 7
Stress, MPa
0
-2.5
0
2.5E-4
5.0E-4
Strain

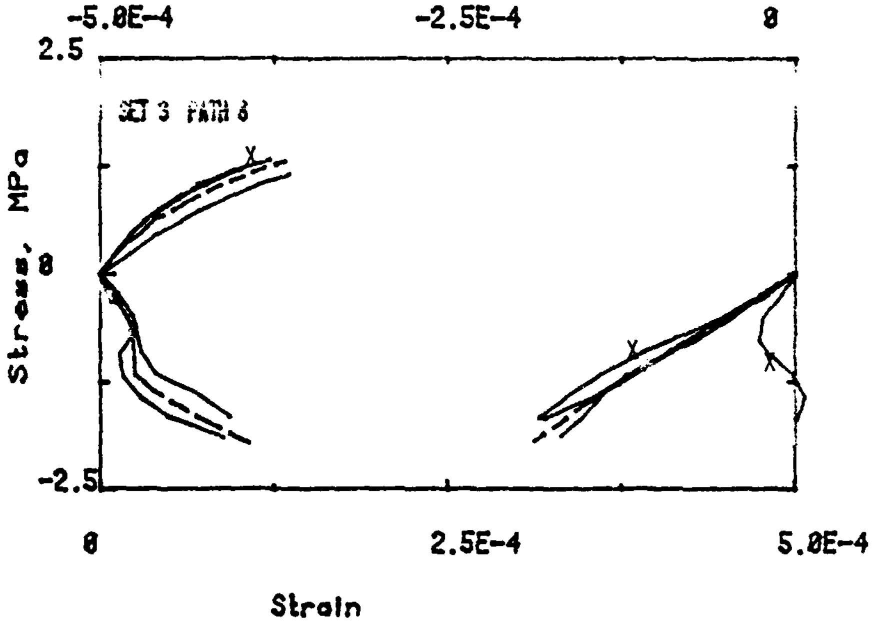
-5.0E-4
-2.5E-4
0
2.5
SET 3 PATH 8
Stress, MPa
0
-2.5
0
2.5E-4
5.0E-4
Strain

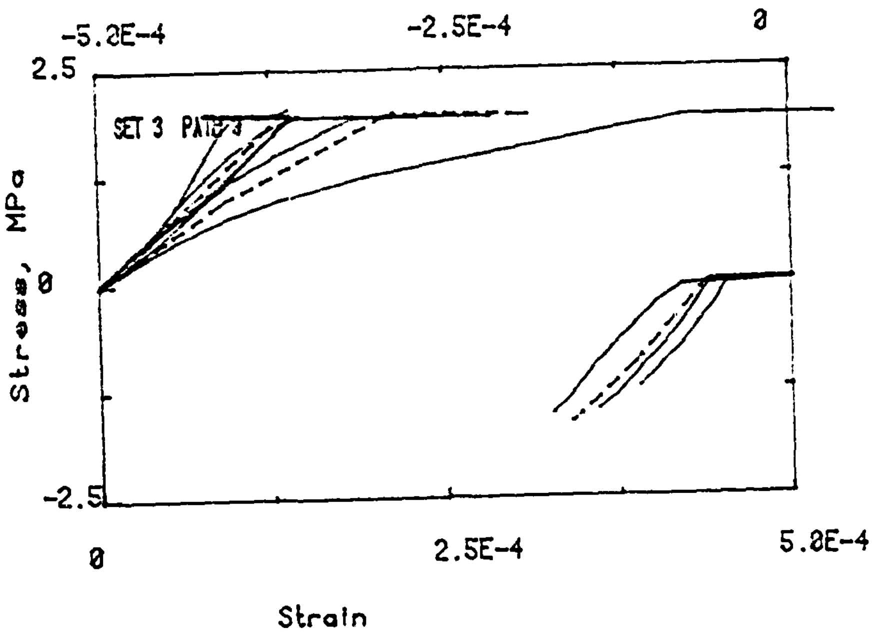
-5.0E-4
-2.5E-4
0
2.5
SET 3 PATH 3
Stress, MPa
0
-2.5
0
2.5E-4
5.0E-4
Strain

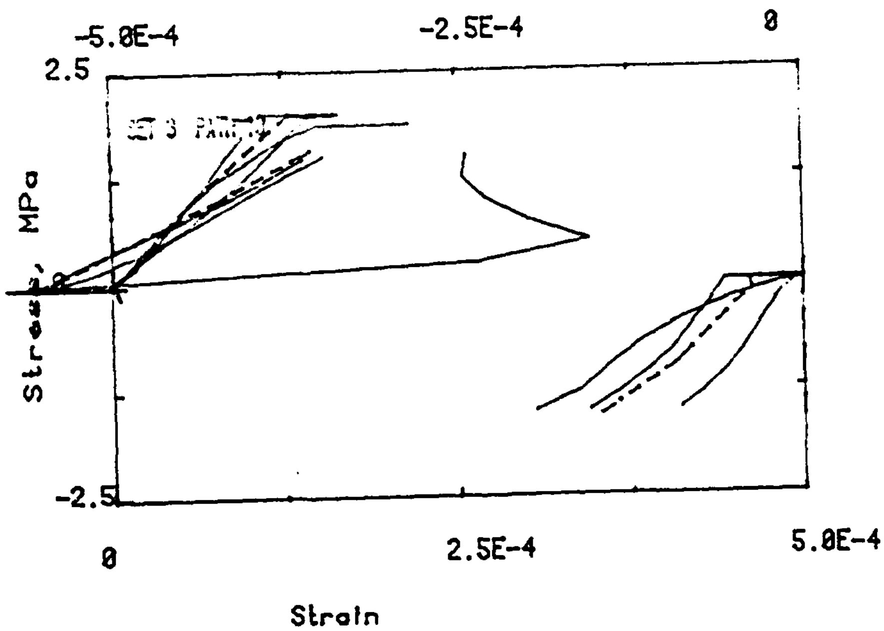
-5.0E-4
-2.5E-4
0
2.5
Stress, MPa
-2.5
0
2.5E-4
5.0E-4
Strain

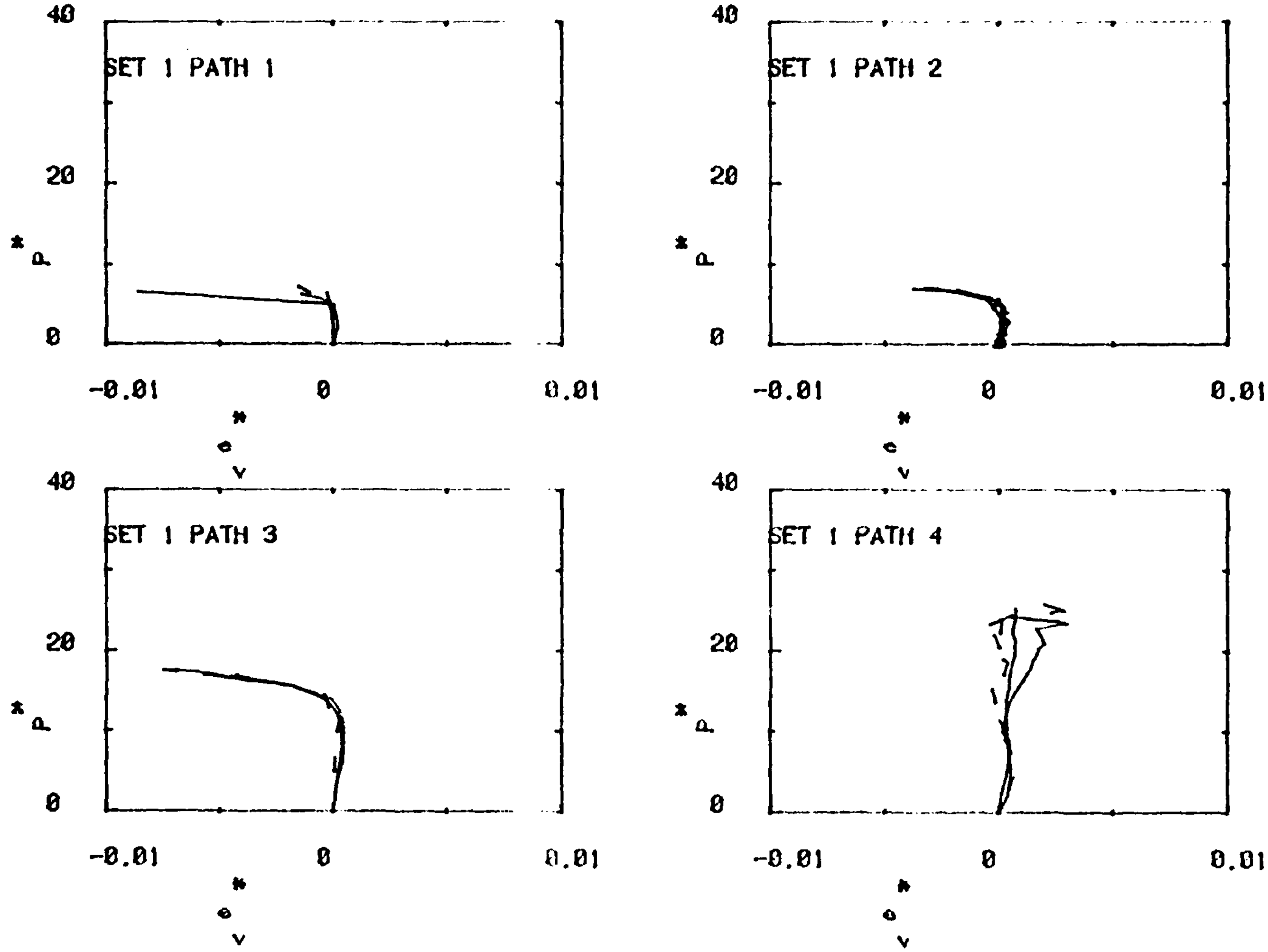
SET 1 PATH 1
SET 1 PATH 2
SET 1 PATH 3
SET 1 PATH 4
40
20
0
-0.01
0
0.01
p*
e*v

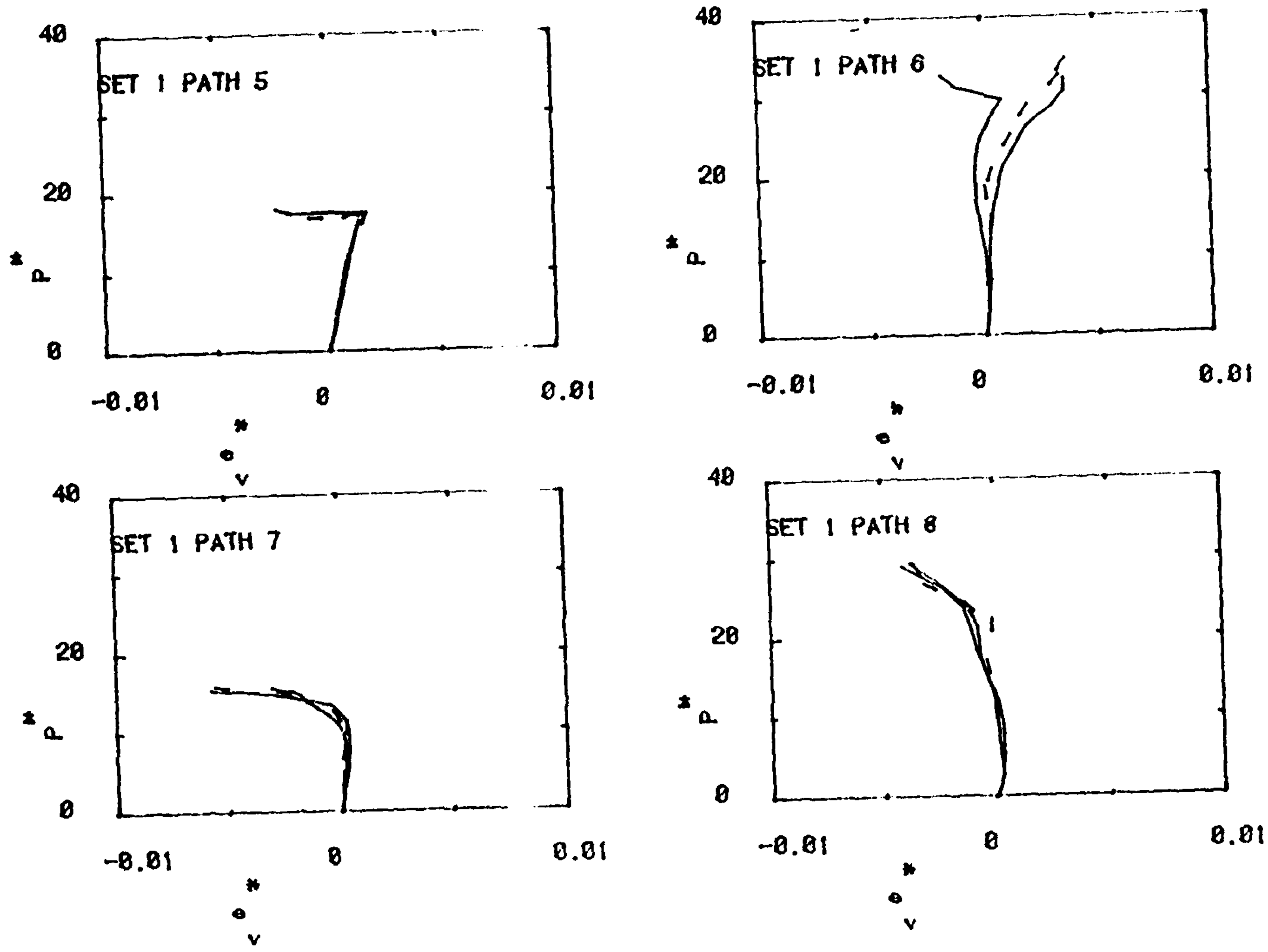
SET 1 PATH 5
SET 1 PATH 6
SET 1 PATH 7
SET 1 PATH 8
40
20
0
-0.01
0
0.01
p*
e*v

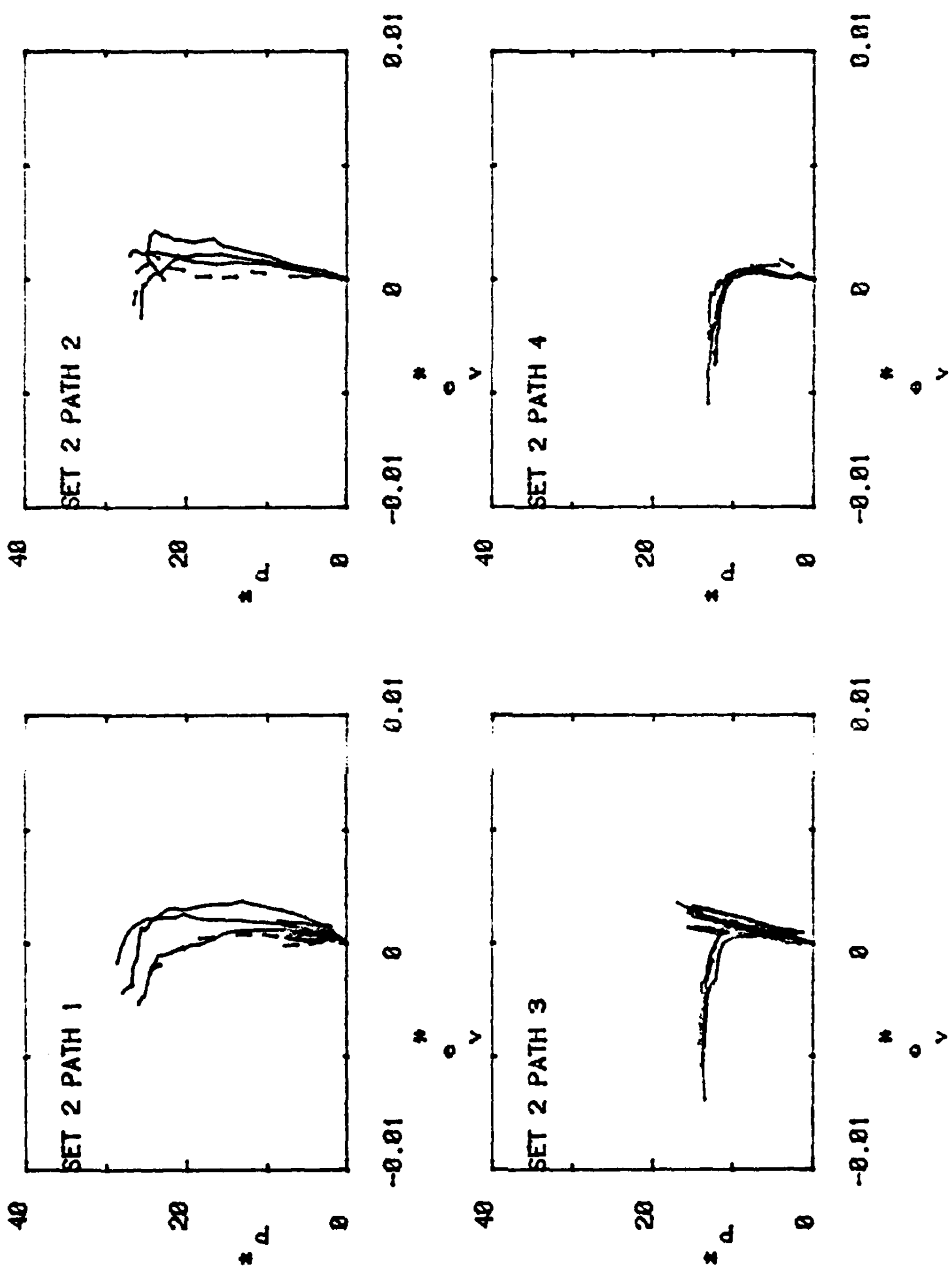
SET 2 PATH 1
SET 2 PATH 2
SET 2 PATH 3
SET 2 PATH 4
40
20
0
-0.01
0
0.01

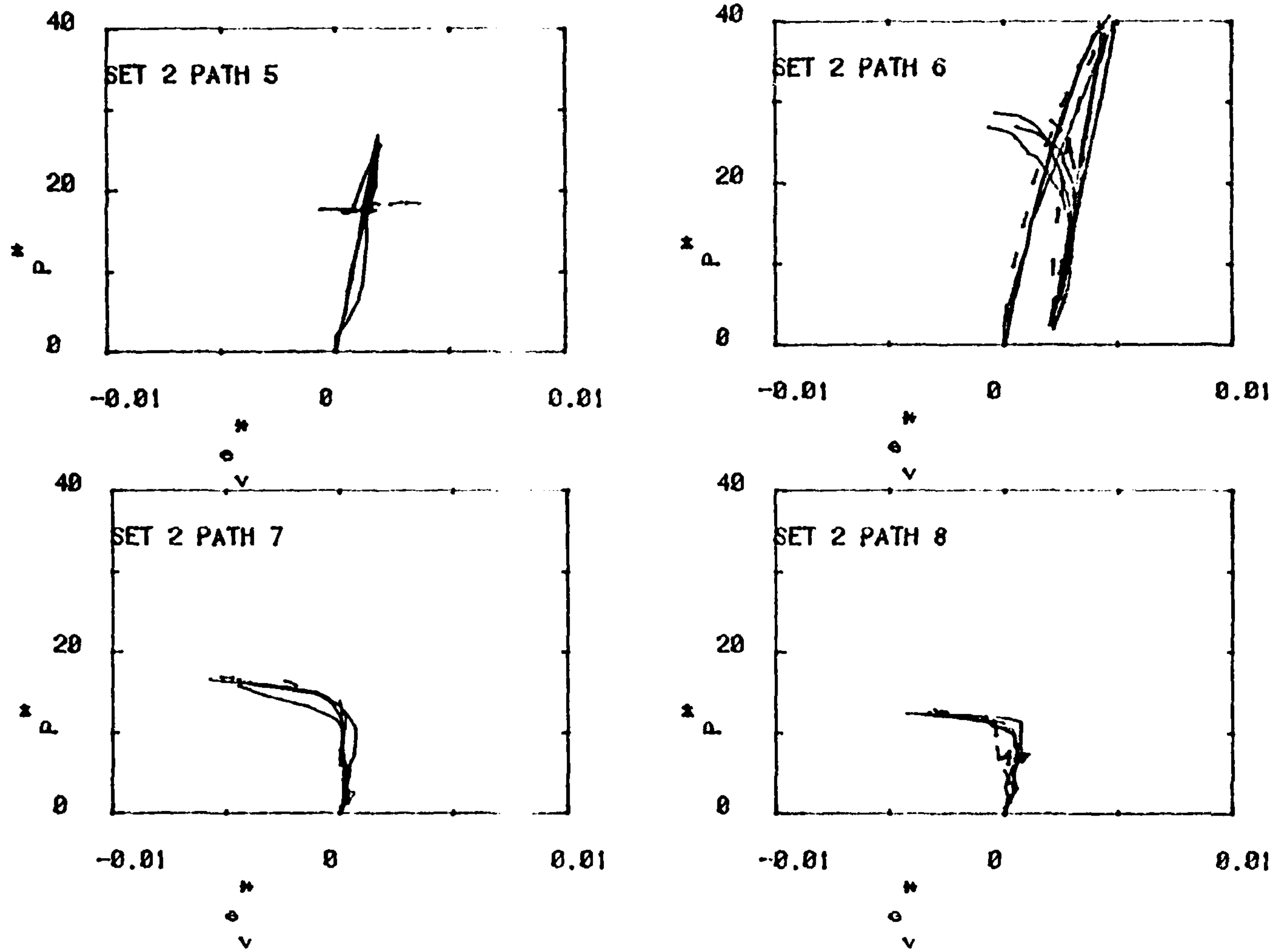
SET 2 PATH 5
SET 2 PATH 6
SET 2 PATH 7
SET 2 PATH 8
40
20
0
-0.01
0
0.01
p*
ve*

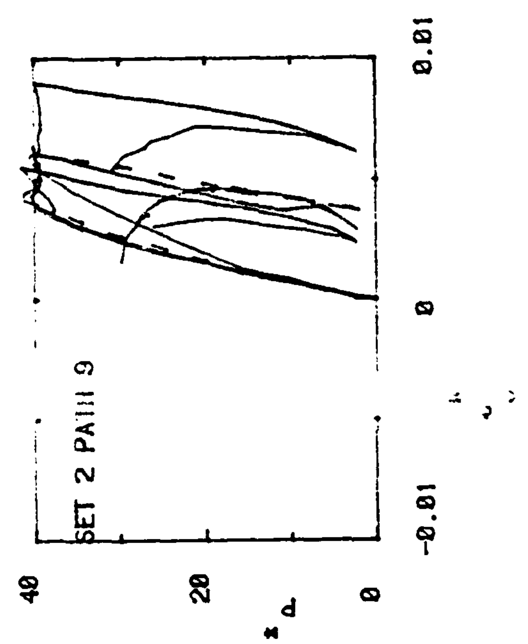
SET 2 PATH 9
40
20
0
-0.01
0
0.01

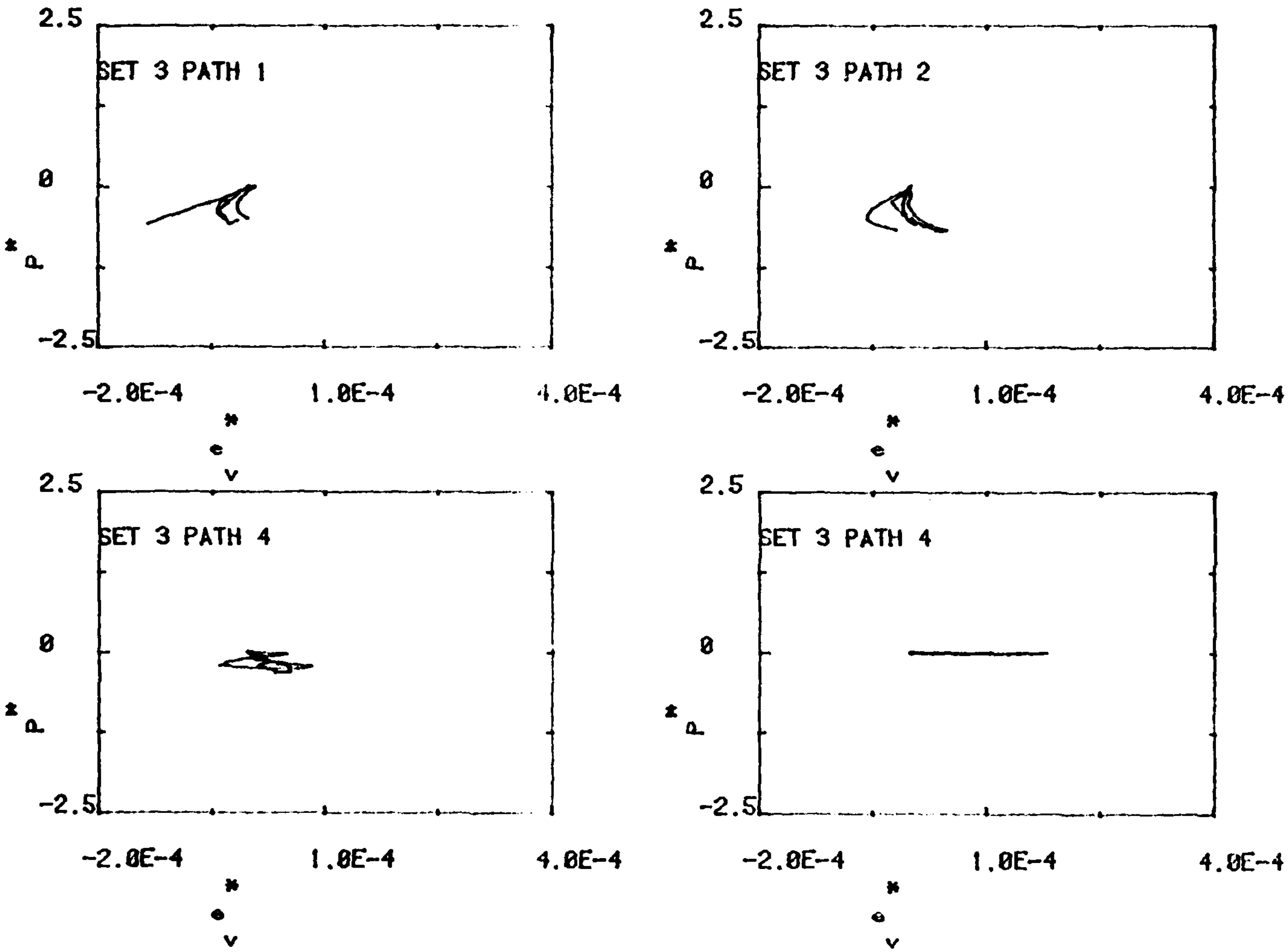

SET 3 PATH 1
SET 3 PATH 2
SET 3 PATH 4
SET 3 PATH 4
2.5
0
-2.5
p*
-2.0E-4
1.0E-4
4.0E-4
ev*

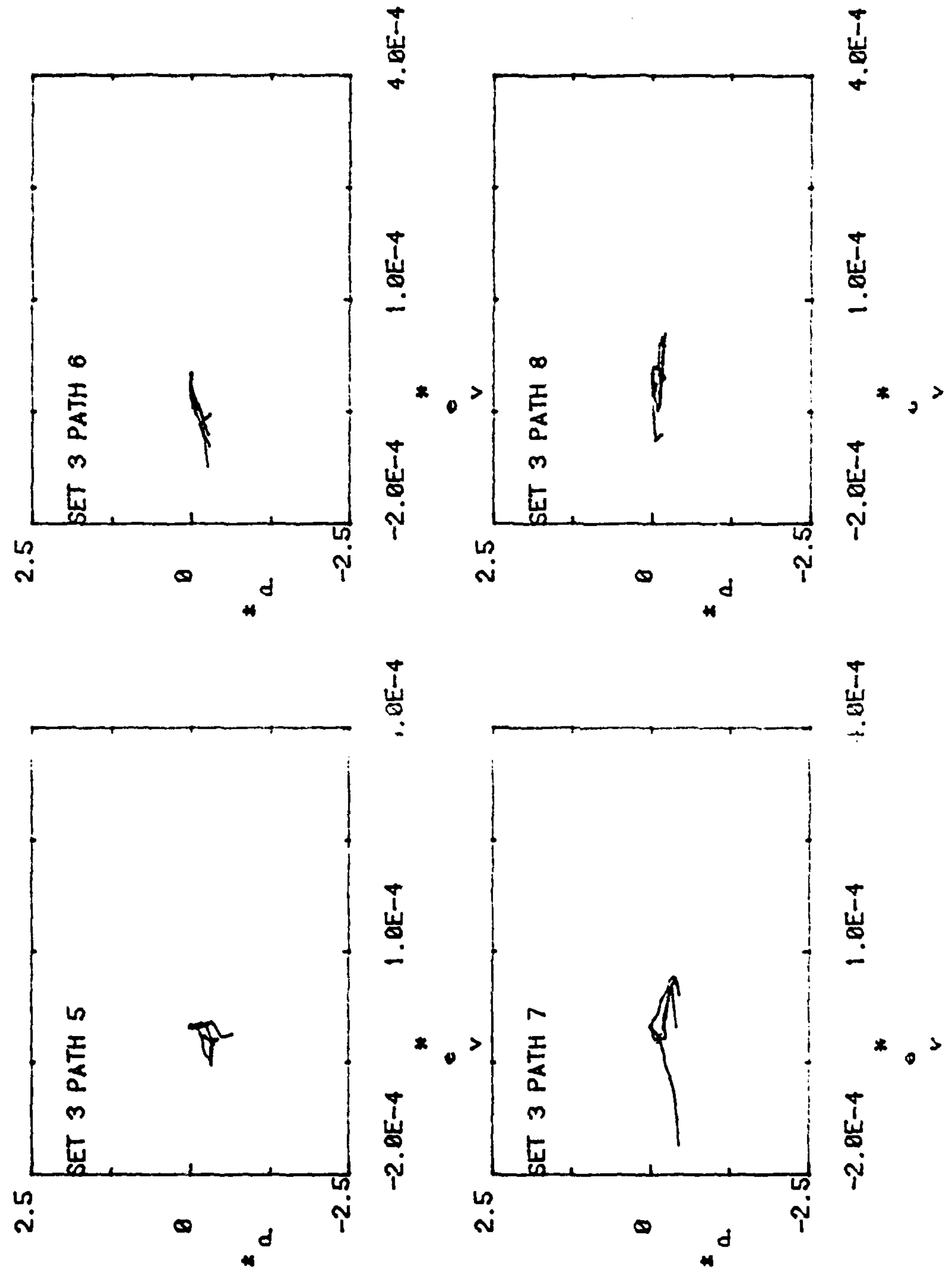

SET 3 PATH 5
SET 3 PATH 6
SET 3 PATH 7
SET 3 PATH 8
2.5
0
-2.5
-2.0E-4
1.0E-4
4.0E-4

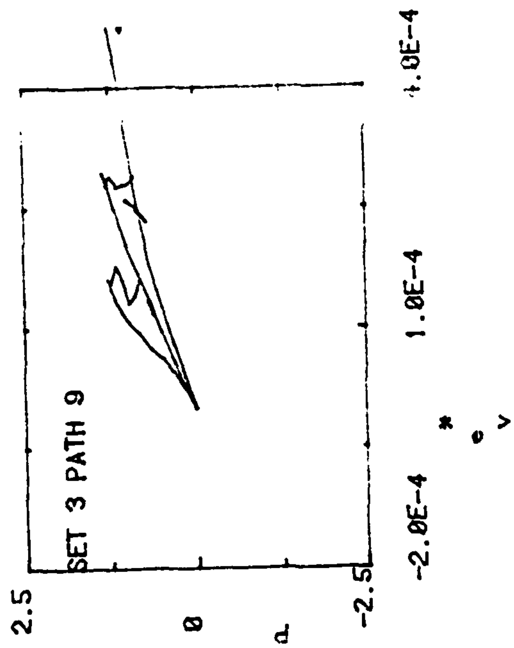
SET 3 PATH 9
2.5
0
-2.5
-2.0E-4
1.0E-4
4.0E-4

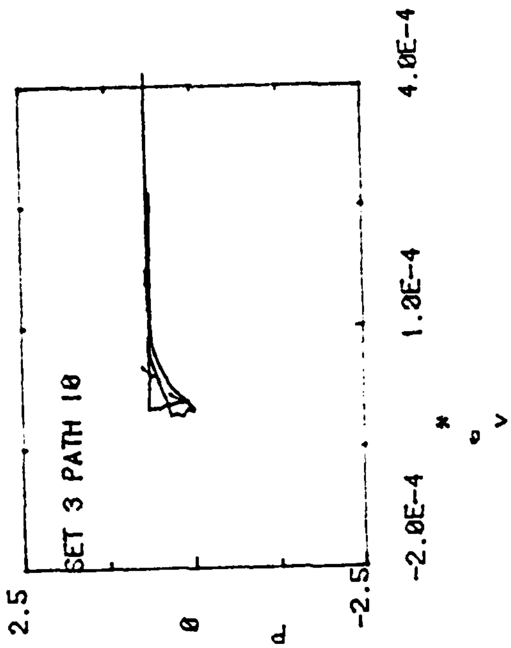
SET 3 PATH 10
2.5
0
-2.5
-2.0E-4
1.0E-4
4.0E-4

APPENDIX C

LOADING PATHS AND COMPOSITE CURVES IN TERMS OF INELASTIC STRAIN INVARIANTS

This appendix contains all of the paths plotted in two strain-invariant spaces. The composite curves constructed from the σ-ε paths and plotted in the strain-invariant spaces are superimposed on their respective experimental curves.

Contents | Page

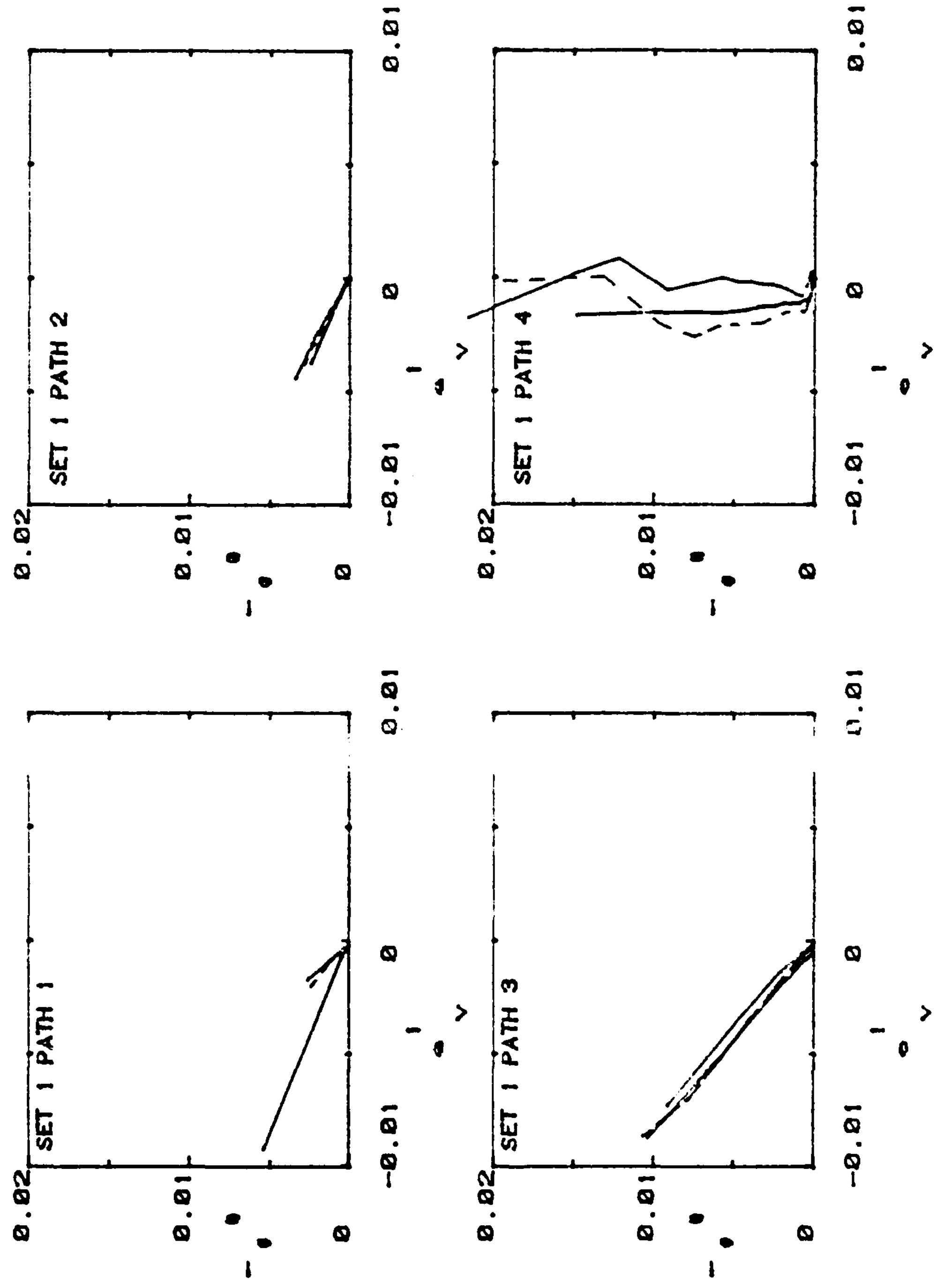
SET 1 PATH 1
SET 1 PATH 2
SET 1 PATH 3
SET 1 PATH 4
0.02
0.01
0
-0.01
0.01

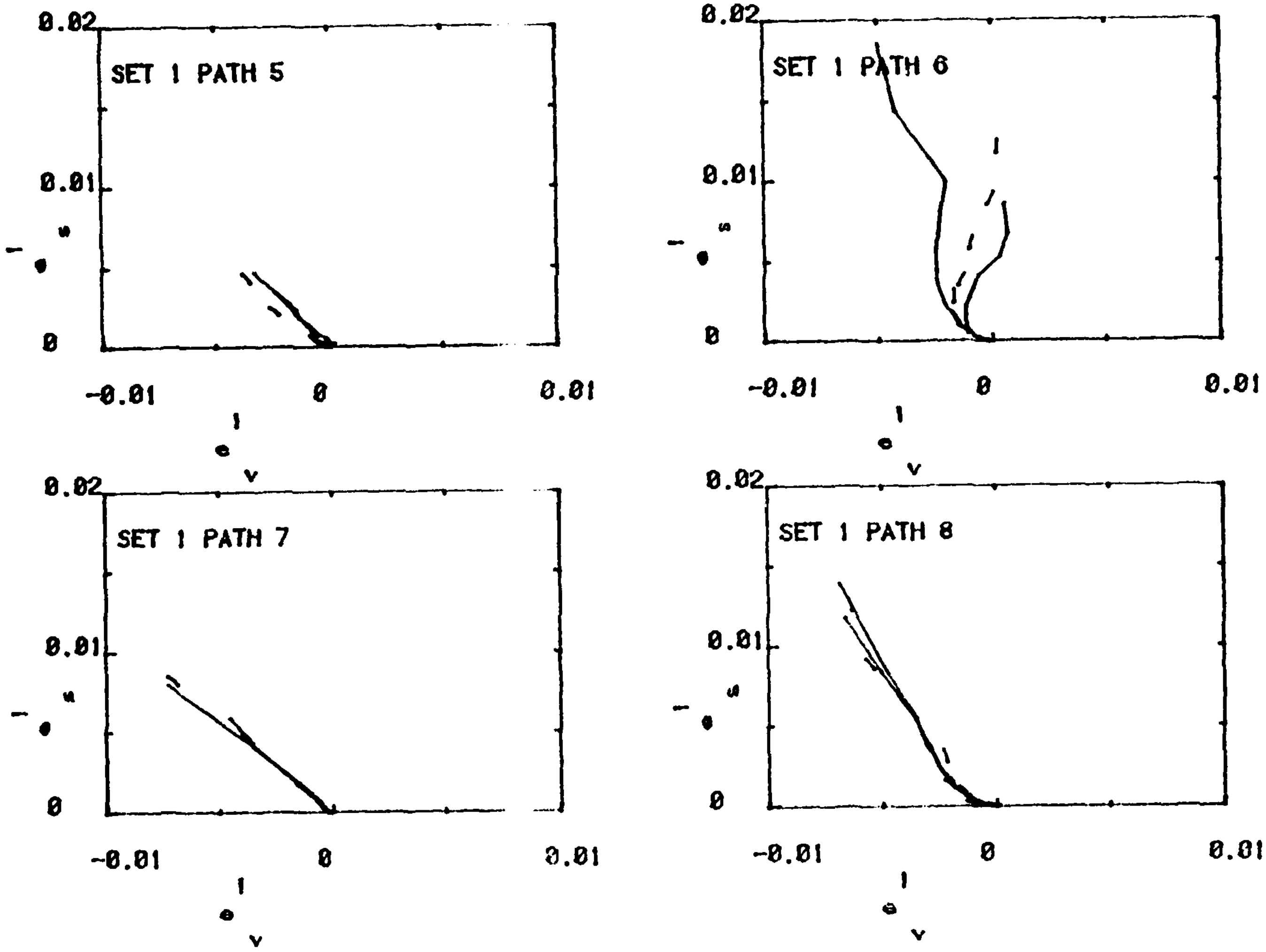
SET 1 PATH 5
SET 1 PATH 6
SET 1 PATH 7
SET 1 PATH 8
0.02
0.01
0
-0.01
0
0.01

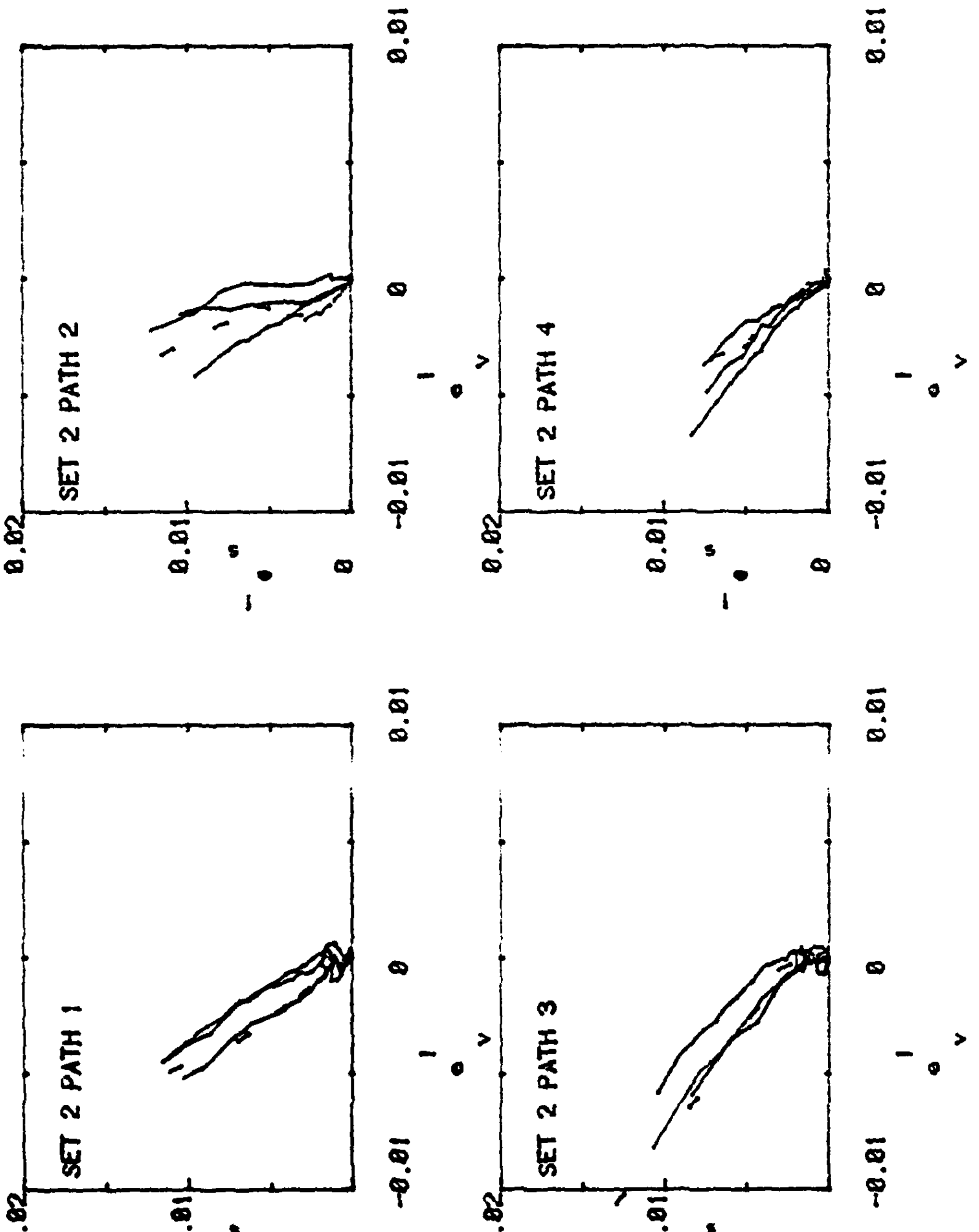
SET 2 PATH 1
SET 2 PATH 2
SET 2 PATH 3
SET 2 PATH 4
0.02
0.01
0
-0.01
0
0.01

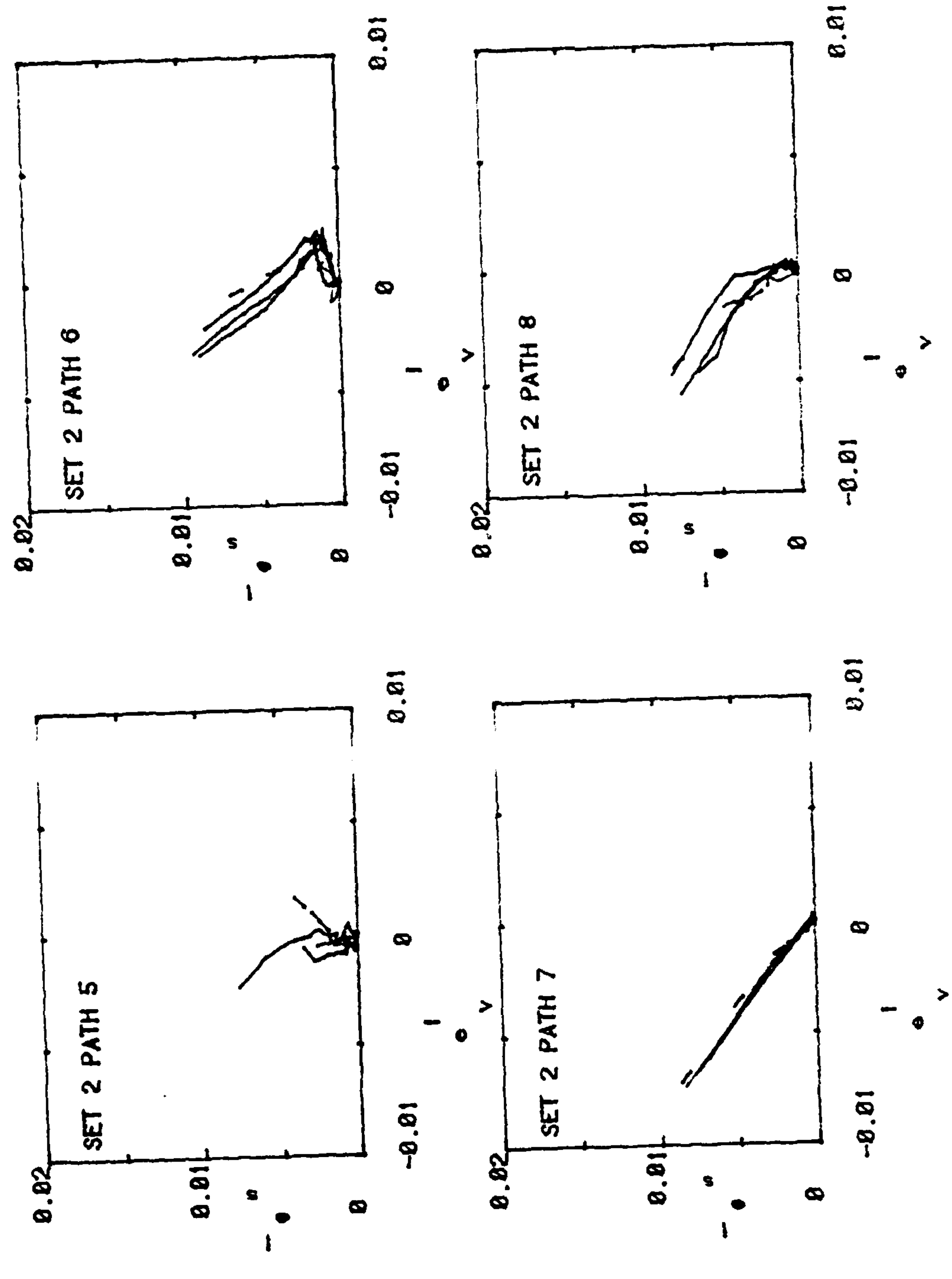
SET 2 PATH 5
SET 2 PATH 6
SET 2 PATH 7
SET 2 PATH 8
0.02
0.01
0
-0.01

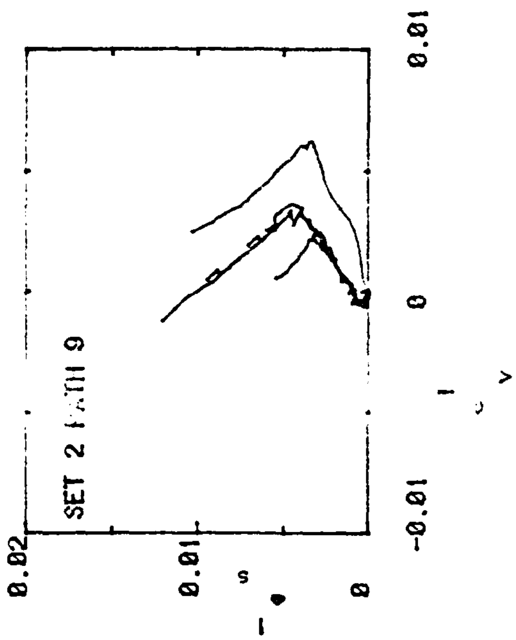
SET 2 PATH 9
0.02
0.01
0
-0.01
0
0.01

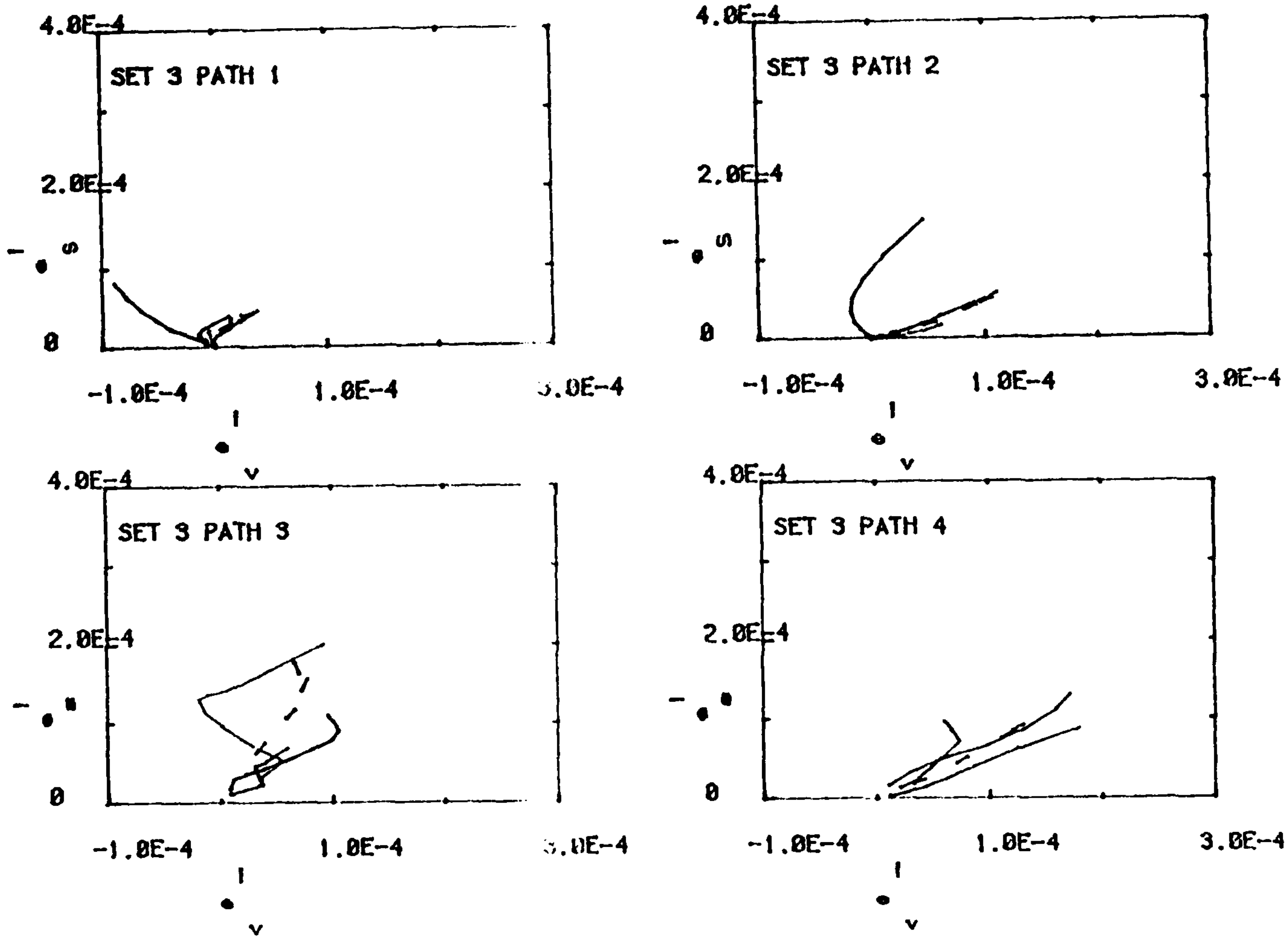

SET 3 PATH 1
SET 3 PATH 2
SET 3 PATH 3
SET 3 PATH 4
4.0E-4
2.0E-4
0
-1.0E-4
1.0E-4
3.0E-4

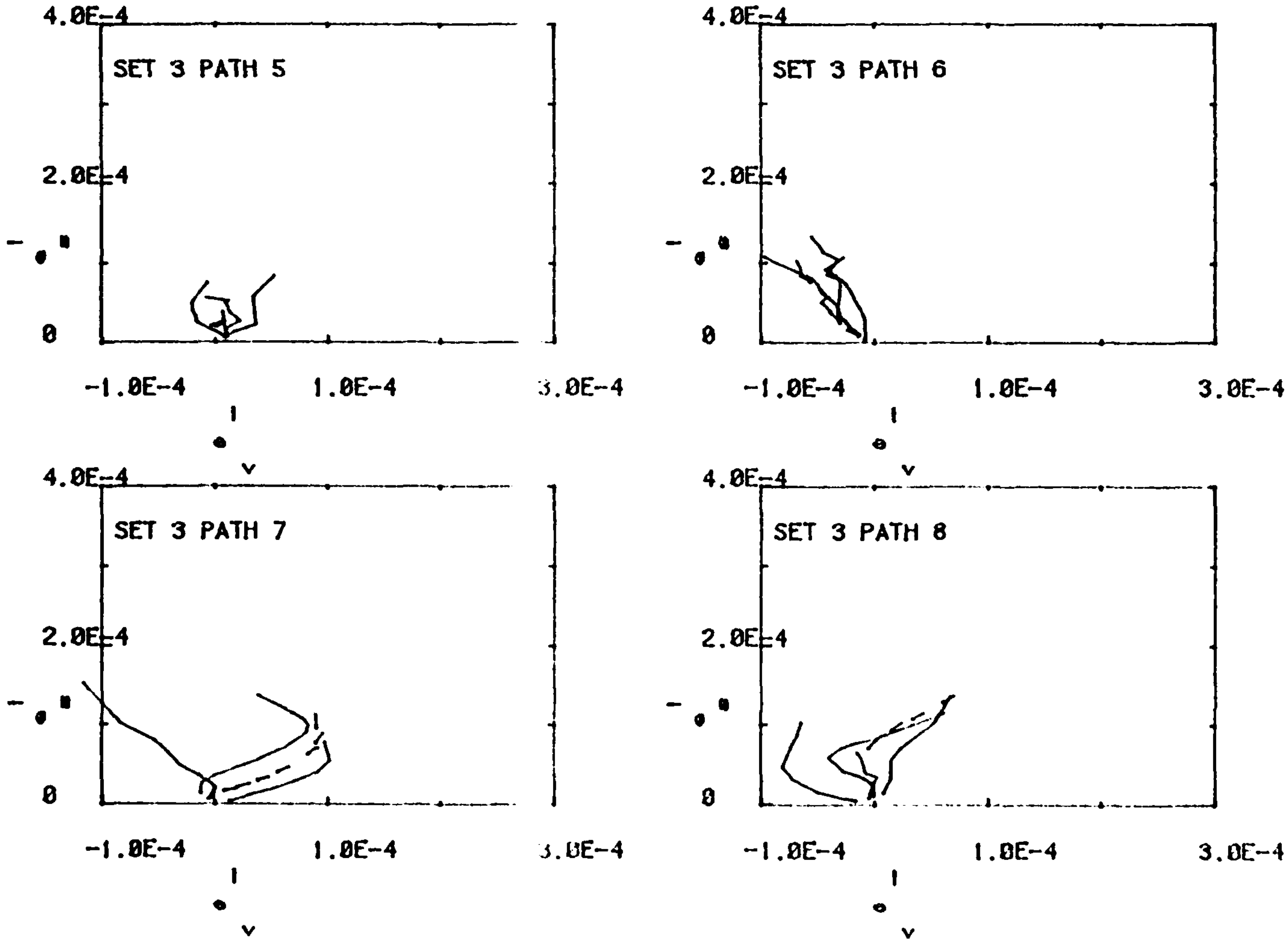
SET 3 PATH 5
SET 3 PATH 6
SET 3 PATH 7
SET 3 PATH 8
4.0E-4
2.0E-4
0
-1.0E-4
1.0E-4
3.0E-4

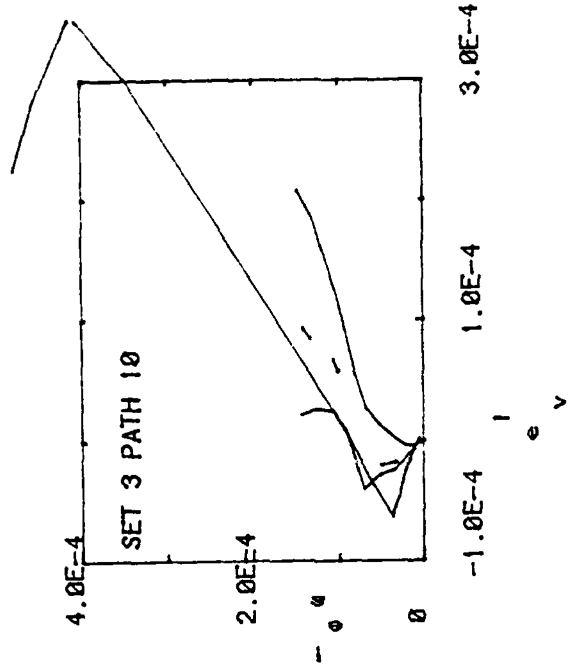
SET 3 PATH 10
4.0E-4
2.0E-4
0
-1.0E-4
1.0E-4
3.0E-4

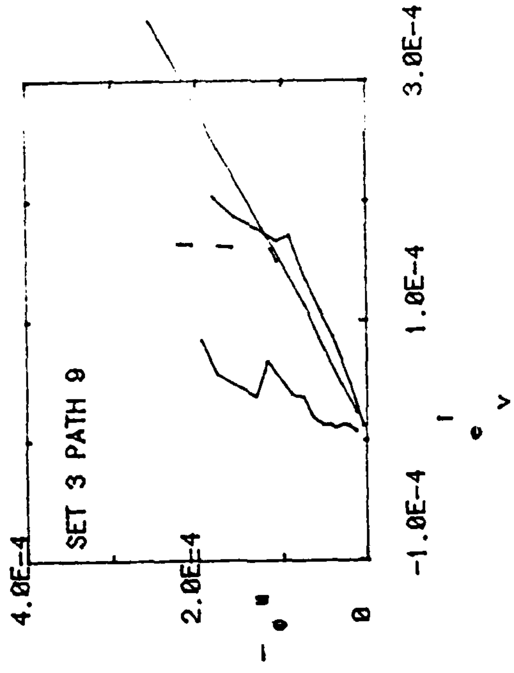
SET 3 PATH 9
4.0E-4
2.0E-4
0
-1.0E-4
1.0E-4
3.0E-4

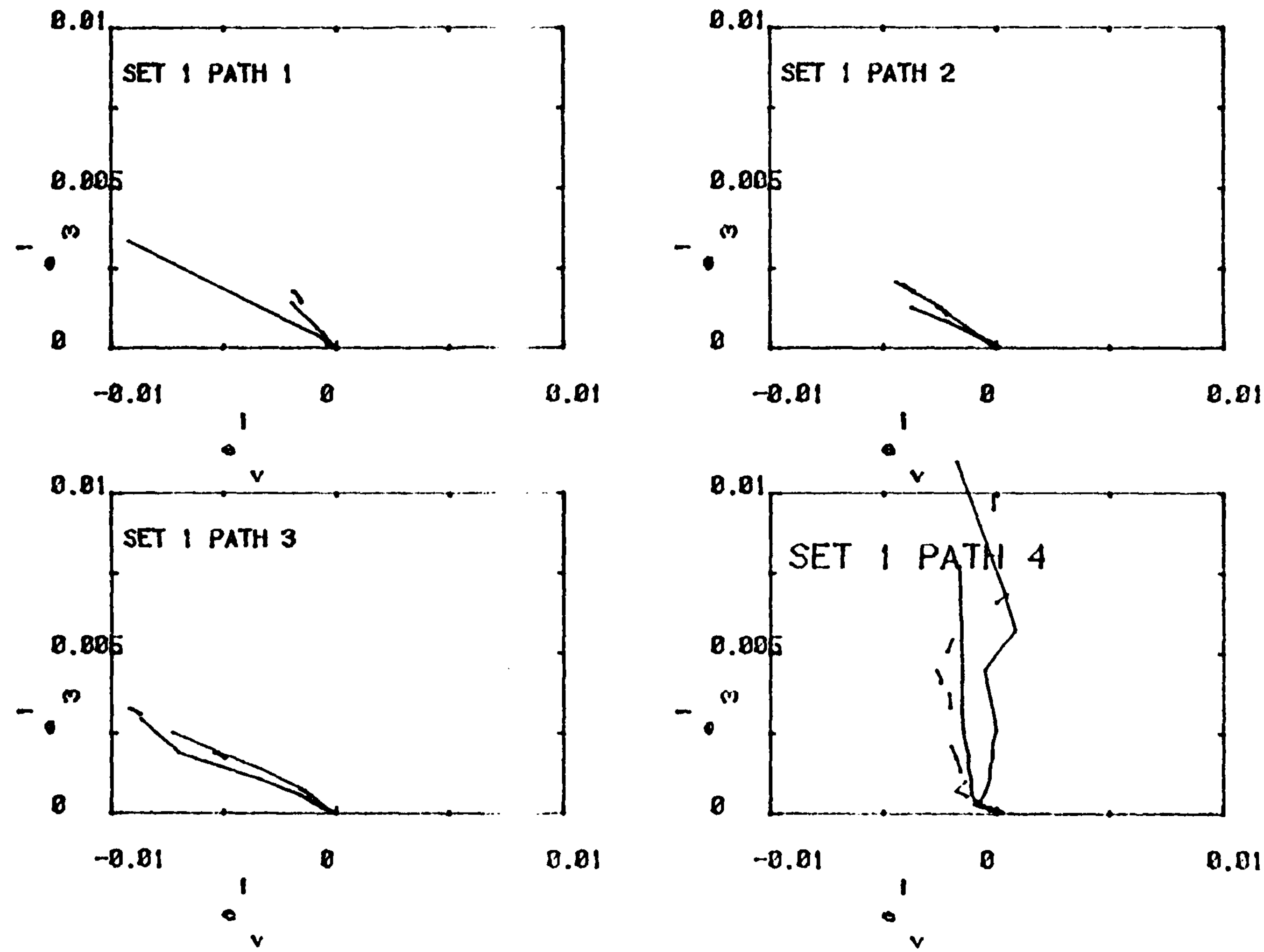
SET 1 PATH 1
SET 1 PATH 2
SET 1 PATH 3
SET 1 PATH 4
0.01
0.005
0
-0.01
0.01
$-\epsilon_3$
$-\epsilon_v$

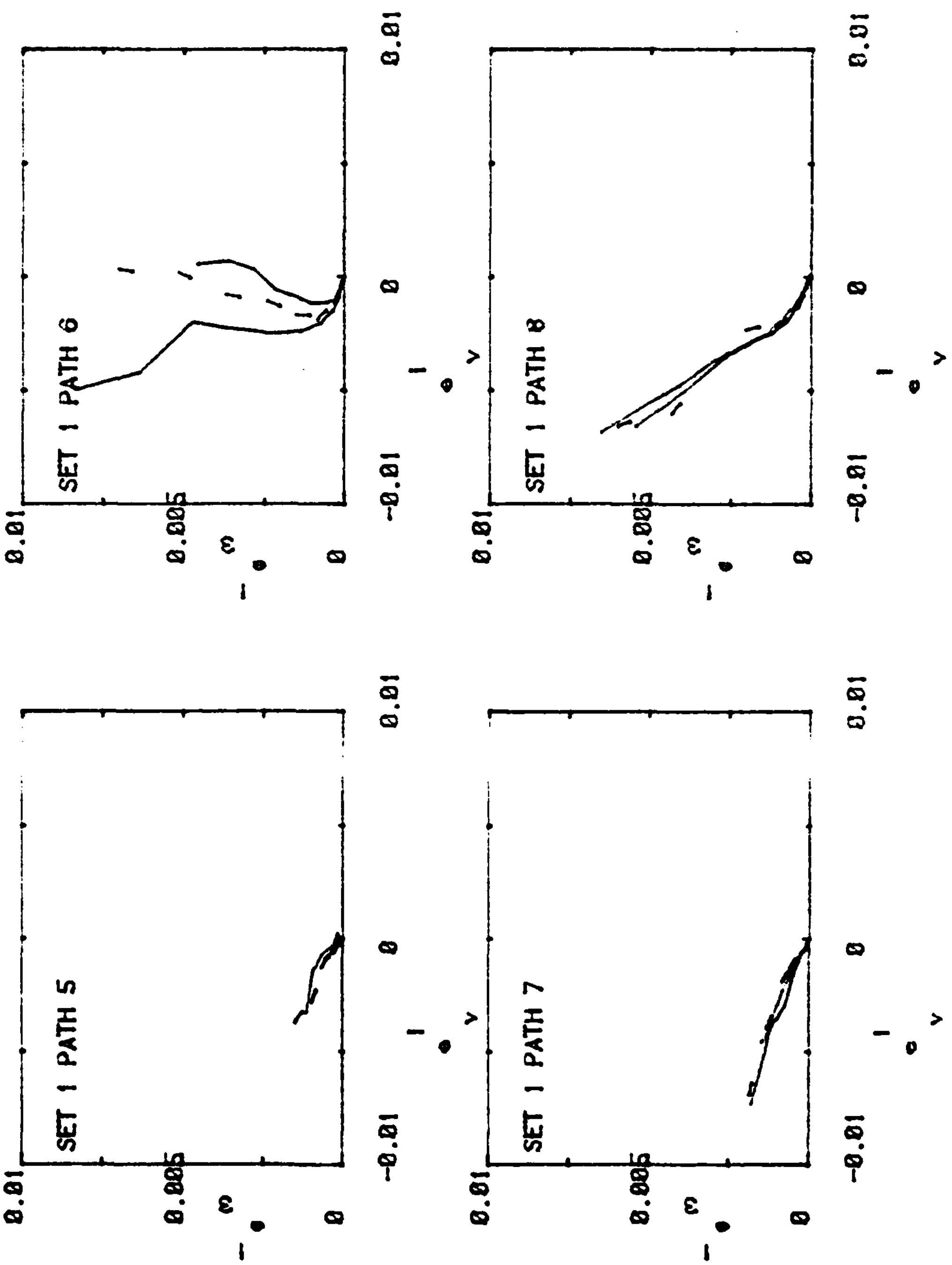

SET 1 PATH 5
SET 1 PATH 6
SET 1 PATH 7
SET 1 PATH 8

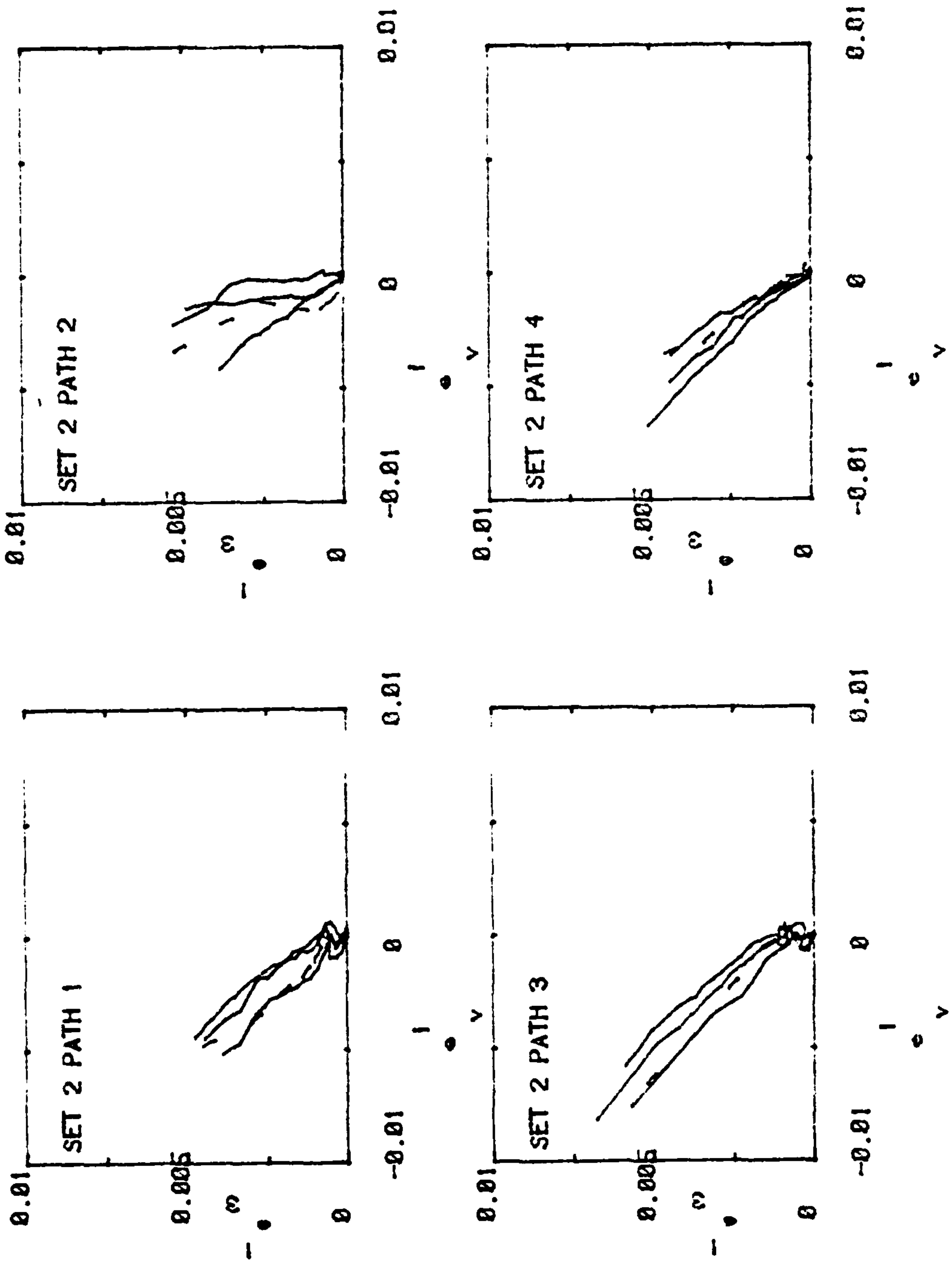
SET 2 PATH 1
SET 2 PATH 2
SET 2 PATH 3
SET 2 PATH 4
0.01
0.005
0
-0.01
0
0.01
$-e_3$
$-e_v$

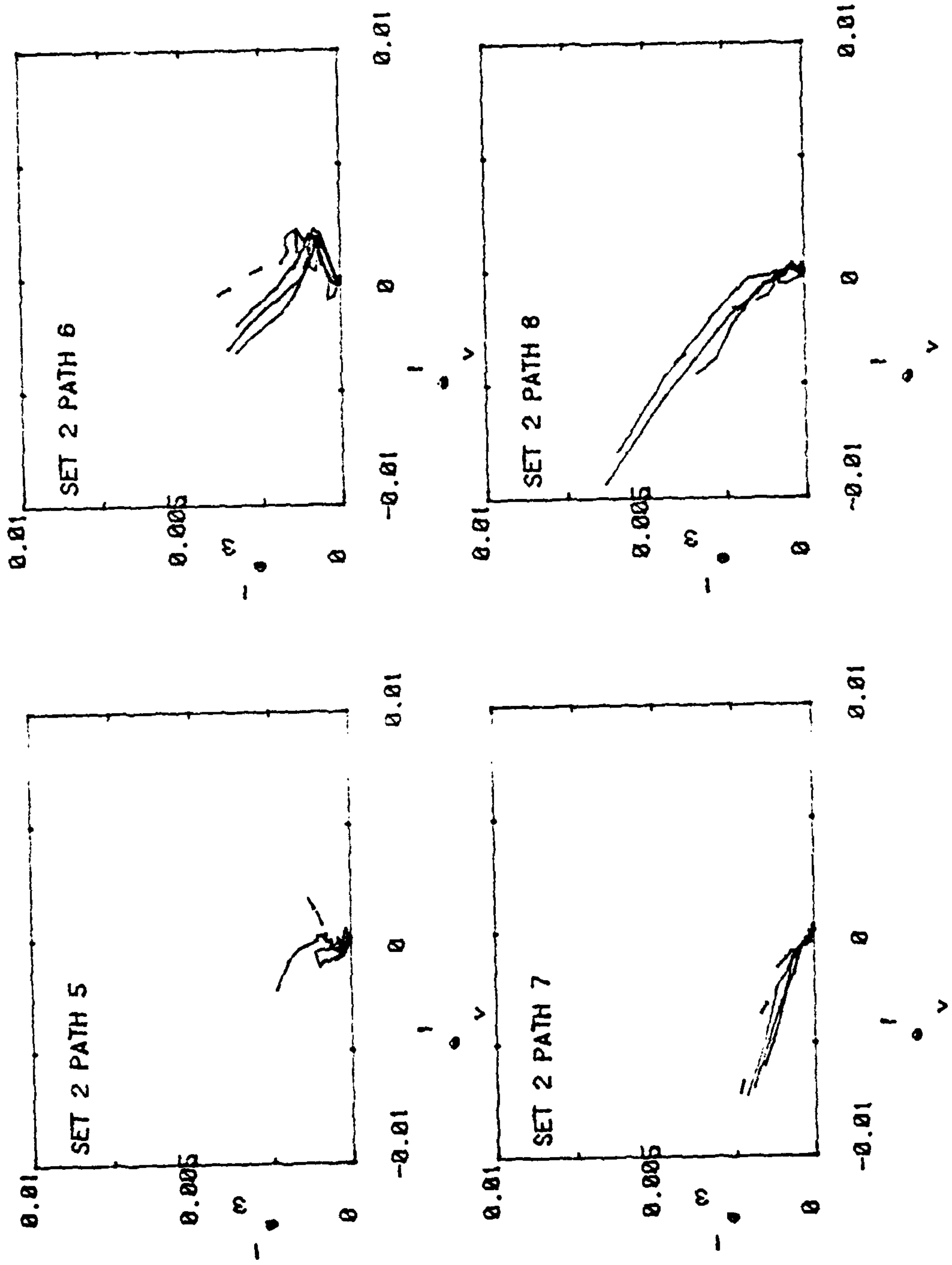
SET 2 PATH 5
SET 2 PATH 6
SET 2 PATH 7
SET 2 PATH 8
0.01
0.005
0
-0.01

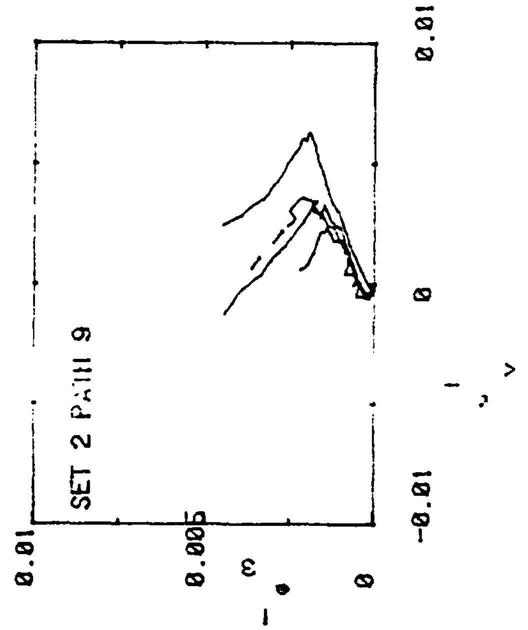
SET 2 PATH 9
0.01
0.005
0
-0.01
0
0.01

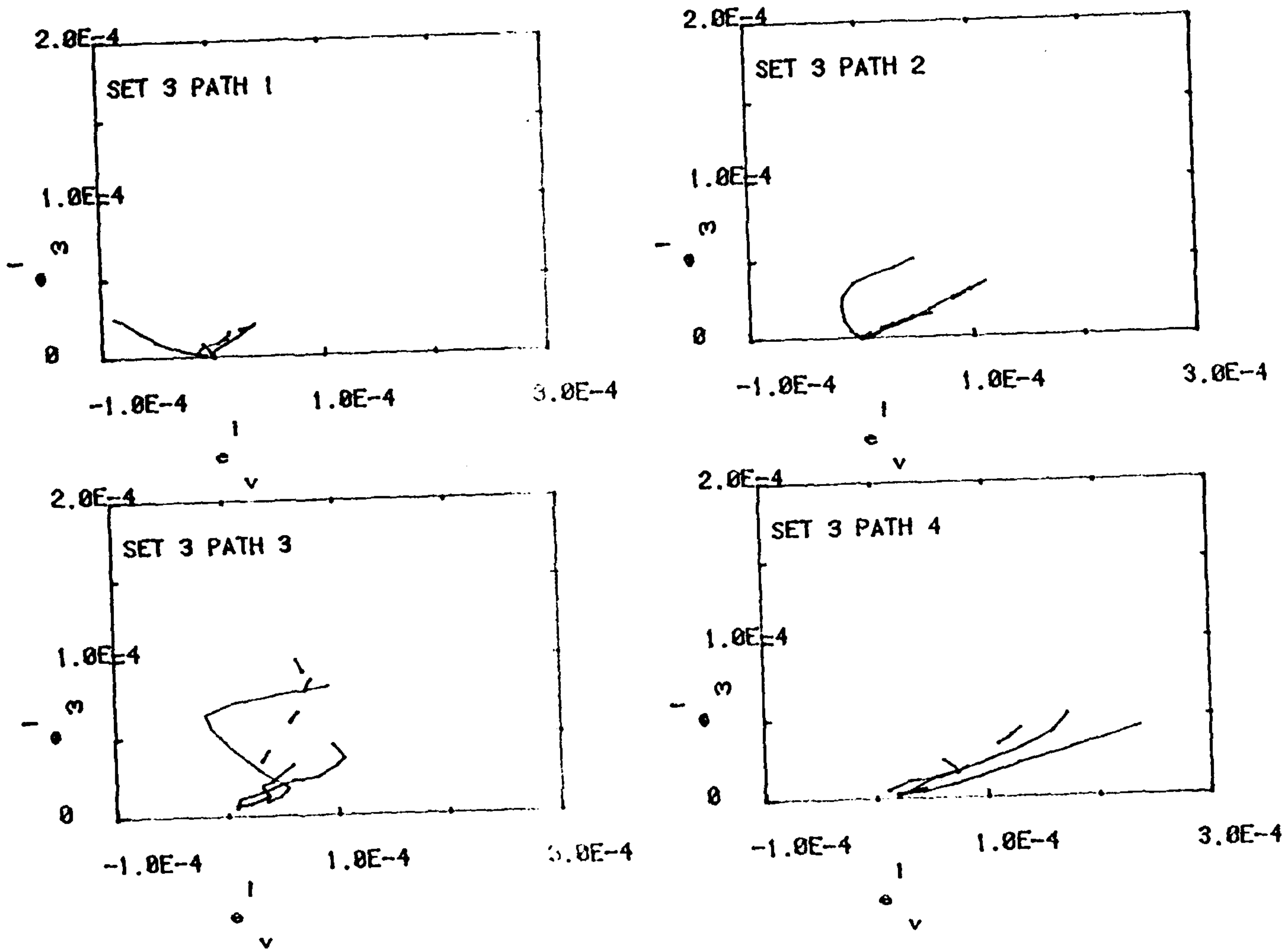
SET 3 PATH 1
SET 3 PATH 2
SET 3 PATH 3
SET 3 PATH 4
2.0E-4
1.0E-4
0
-1.0E-4
1.0E-4
3.0E-4

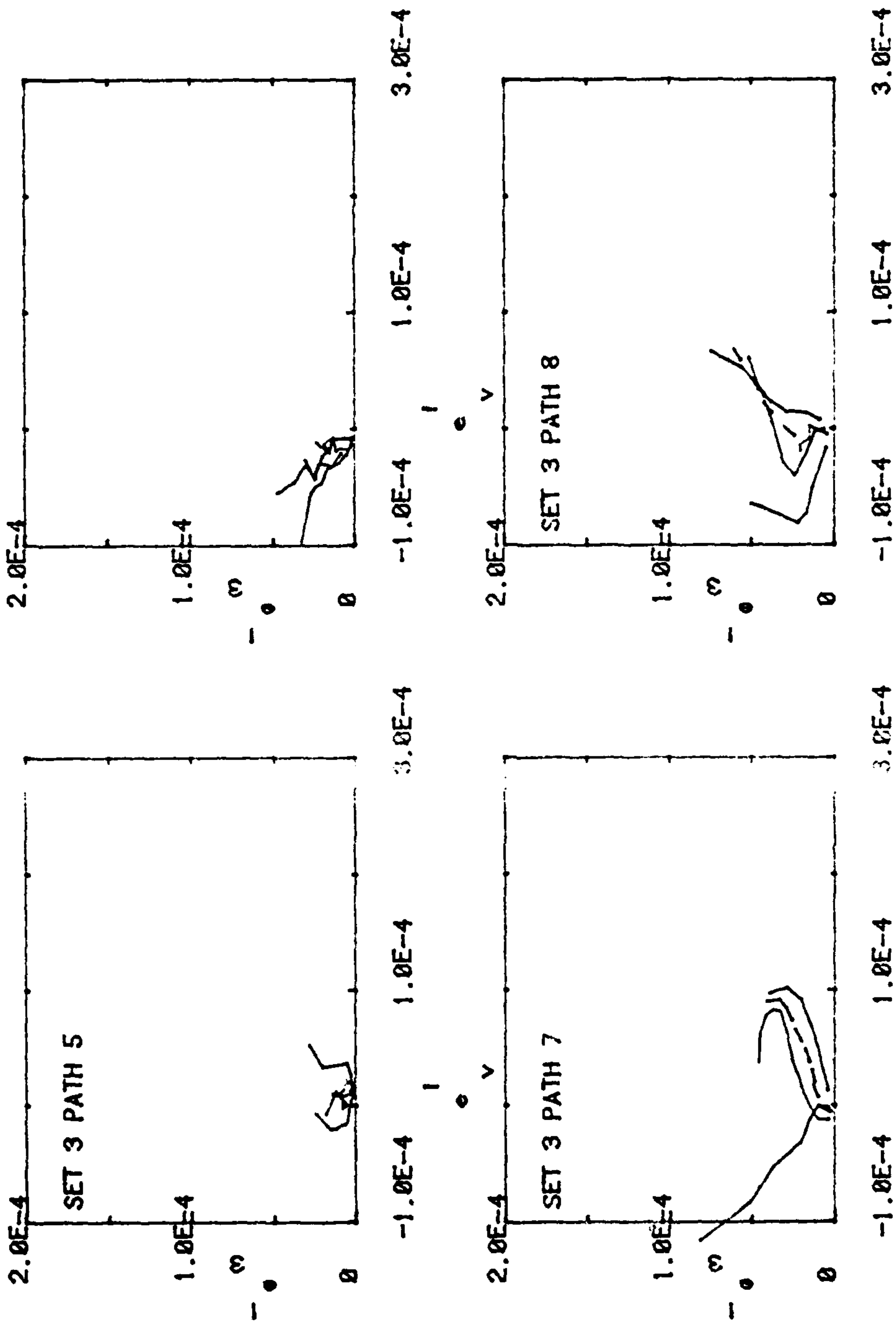

SET 3 PATH 5
SET 3 PATH 7
SET 3 PATH 8
2.0E-4
1.0E-4
0
-1.0E-4
1.0E-4
3.0E-4

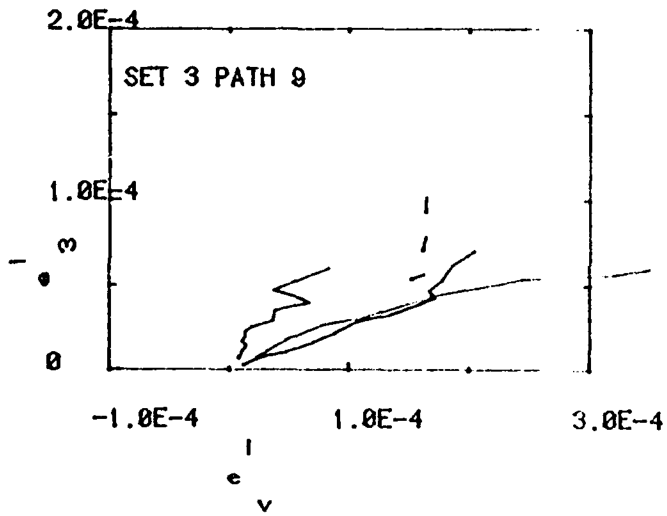

SET 3 PATH 9
2.0E-4
1.0E-4
0
-1.0E-4
1.0E-4
3.0E-4

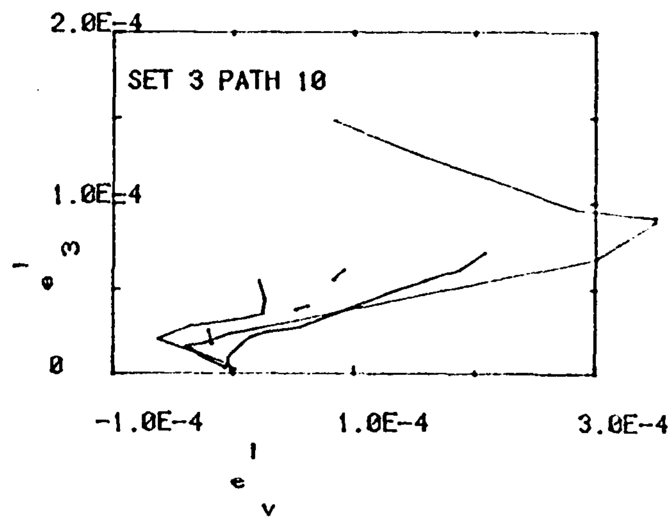

SET 3 PATH 10
2.0E-4
1.0E-4
0
-1.0E-4
1.0E-4
3.0E-4

ATE

LMED